

Is there chaos out there?

Analysis of complex dynamics in plankton
communities

Elisa Benincà

Thesis committee

Thesis supervisors

Prof. dr. Marten Scheffer
Professor of Aquatic Ecology and Water Quality Management
Wageningen University, The Netherlands

Prof. dr. Jef Huisman
Professor of Aquatic Microbiology
University of Amsterdam, The Netherlands

Thesis co-supervisors

Dr. Klaus Jöhnk
Senior Research Scientist
CSIRO Land and Water, Australia

Dr. ir. Egbert H. van Nes
Assistant professor, Aquatic Ecology and Water Quality Management Group
Wageningen University, The Netherlands

Other members

Prof. dr. ir. Johan Grasman
Wageningen University, The Netherlands

Prof. dr. Jack Middelburg
NIOO-KNAW, The Netherlands

Prof. dr. Sergio Rinaldi
Politecnico di Milano, Italy

Prof. dr. Franjo Weissing
University of Groningen, The Netherlands

This research was conducted under the auspices of the graduate research school SENSE.

Is there chaos out there?

Analysis of complex dynamics in plankton
communities

Elisa Benincà

Thesis:

Submitted in fulfillment of the requirements for the degree of doctor
at Wageningen University
by the authority of the Rector Magnificus
Prof. Dr. M.J. Kropff
in the presence of the
Thesis Committee appointed by the Academic Board
to be defended in public
on Monday December 6th 2010
at 1:30 p.m. in the Aula

Elisa Benincà

Is there chaos out there? Analysis of complex dynamics in plankton communities,
169 pages.

Thesis Wageningen University, Wageningen, NL (2010).

With references, with summaries in English, Dutch and Italian.

ISBN 978-90-8585-812-6

Cover: Guido Romeijn
Photo: Randolph Femmer, life.nbio.gov.

Contents

1	Introduction	1
1.1	The enigma of population oscillations	1
1.2	The discovery of chaos: Lorenz’s famous cup of coffee	1
1.3	What is chaos?	2
1.3.1	Definition of chaos and the “butterfly effect”	2
1.3.2	Strange attractors: patterns of chaos in phase space	2
1.3.3	A measure of chaos: the Lyapunov exponent	5
1.3.4	Deterministic chaos versus stochasticity	6
1.4	Chaos in ecology	7
1.5	Thesis outline	9
2	Chaos in a long-term experiment with a plankton community	11
2.1	Introduction	12
2.2	The mesocosm experiment dataset	12
2.3	Methods	14
2.3.1	Methods summary	14
2.3.2	Experimental set-up	14
2.3.3	Data treatment	15
2.3.4	Predictability	15
2.3.5	Lyapunov exponents	16
2.4	Data analysis	17
2.5	Discussion	21
3	Coupled predator-prey oscillations in a chaotic food web	23
3.1	Introduction	23
3.2	Theory	26
3.3	Material and methods	27
3.3.1	Long-term experiment	27
3.3.2	Alternations in species dominance	29
3.3.3	Wavelet analysis	29
3.4	Results	30
3.4.1	Theoretical predictions	30
3.4.2	Experimental analysis	32

3.4.3	Comparison between theoretical predictions and experimental data	35
3.5	Discussion	36
4	Interannual variability in species composition explained as seasonally entrained chaos	39
4.1	Introduction	39
4.2	Methods	42
4.2.1	Model description	42
4.2.2	Parameterization	43
4.2.3	Assessment of complex dynamics	44
4.3	Results	46
4.4	Discussion	50
4.4.1	Interannual variability as an intrinsic property	50
4.4.2	Comparison with empirical data	51
4.4.3	The role of seasonality and productivity	52
5	Resonance of plankton communities to temperature fluctuations	55
5.1	Introduction	56
5.2	Predator-prey model	58
5.3	The paradox of enrichment	59
5.4	Adding noise	59
5.4.1	White Noise	61
5.4.2	Red noise	61
5.5	Resonance and the power spectrum of red noise	62
5.6	Time scales of plankton populations and temperature fluctuations	64
5.7	Discussion	69
6	Afterthoughts	73
6.1	Is there chaos out there?	73
6.2	Limits to prediction	75
6.3	Methodological considerations	77
6.4	The challenge ahead	78
	Appendices	79
A	Supplementary information to chapter 2	81
A.1	Materials and methods of the mesocosm experiment	81
A.2	Earlier analyses of the same time series	82
A.3	Transformation of the time series	83
A.4	Spectral analysis	86
A.5	Predictability	89
A.5.1	Neural network	89
A.5.2	Testing for differences between the nonlinear and linear model	91

A.6	Methods for estimating Lyapunov exponents	92
A.6.1	Direct method by time-delay embedding	92
A.6.2	Jacobian method: a neural network food web model	95
A.7	Temperature fluctuations	98
B	Supplementary information to chapter 3	103
B.1	Introduction	103
B.2	A simple example	104
B.3	Theory of wavelet analysis	106
B.4	Cross-wavelet analysis	109
B.5	Wavelet Coherence	110
C	Supplementary information to chapter 4	115
C.1	Model attractors and Lyapunov exponents	115
C.1.1	The different attractors	115
C.1.2	Lyapunov exponent	115
C.2	Interpretation in terms of the Paradox of Enrichment	117
C.3	Parameter values	120
D	Supplementary information to chapter 5	133
D.1	Sources of the temperature data	133
D.2	Power spectral density of the temperature fluctuations	136
D.3	Power spectral density of red noise	136
D.4	Growth rates of zooplankton	137
	References	141
	Summary	159
	Samenvatting	161
	Sommario	163
	Acknowledgments	167

List of Figures

1.1	A trajectory in phase space for the Lotka-Volterra model	3
1.2	Types of attractor	4
1.3	Sensitive dependence on initial conditions of a chaotic system	6
1.4	Solutions of the single-population model of May (1976), for different values of the intrinsic growth rate r	8
2.1	Description of the plankton community in the mesocosm experiment	13
2.2	Predictability of the species decreases with increasing prediction time	20
2.3	Exponential divergence of the trajectories	21
3.1	Coupling of two predator-prey systems	25
3.2	Experimental data	28
3.3	Model predictions	31
3.4	Cross-wavelet spectra of the experimental data	35
4.1	Time series of marine phytoplankton species in the Marsdiep tidal inlet between the North Sea and Wadden Sea, the Netherlands	40
4.2	Community dynamics predicted by the model	45
4.3	Poincaré maps with annual snapshots of the model community collected over many years	47
4.4	Year-to-year variability in the population dynamics of two phytoplankton species and two zooplankton species	47
4.5	Relative frequency at which randomly generated model communities display chaos and box plots of the Lyapunov exponents both plotted as function of the amplitude of seasonal forcing	49
5.1	Representation of the main mechanisms driving fluctuations of natural plankton populations	56
5.2	Dynamical behavior of the phytoplankton-zooplankton model with or without white noise as a function of carrying capacity K	60
5.3	Amplification of red noise by phytoplankton and zooplankton as function of the characteristic time scale τ of red noise	63
5.4	Power spectral density of red noise	65

5.5	Noise amplification of the phytoplankton fluctuations as a function of the characteristic time scale of red noise and the period of the intrinsic phytoplankton-zooplankton oscillations	66
5.6	Time series analysis of daily surface temperature, illustrated by data of Lake Tarpon	68
5.7	Relationship between the maximum specific growth rates of different zooplankton species and the characteristic time scale, τ_{\max} , producing maximum amplification of red noise	69
6.1	Variability over time of phytoplankton and zooplankton abundances	76
A.1	Data treatment of the time series of bacteria	84
A.2	Stationary time series of the functional groups in the food web, after data treatment	85
A.3	Raw power spectra of the species	87
A.4	Welch periodogram of the species	88
A.5	Architecture of the neural network model	90
A.6	Exponential divergence of the trajectories of picophytoplankton as a function of time, calculated with different embedding dimensions	93
A.7	Space time separation plots of the functional groups	94
A.8	Time series of the temperature in the mesocosm experiment	99
B.1	A simple example illustrating the interpretation of wavelet power spectra	105
B.2	Morlet wavelet	106
B.3	Wavelet power spectra of the experimental data	108
B.4	Wavelet coherence spectra of the experimental data	112
C.1	Frequency of occurrence of the different dynamical behaviors as a function of seasonal forcing	116
C.2	Bifurcation diagram plotting the local maxima and minima of one of the zooplankton species in the model community as a function of productivity K	118
C.3	Phase-plane diagrams for a simple two-species version of our predator-prey model	119

List of Tables

2.1	Correlations between the species in the food web	18
3.1	Relative frequency distributions of the phase angles between the fluctuating species	33
4.1	Parameter ranges used in the model simulations	44
4.2	Occurrence of chaos in our simulated communities under different model assumptions	48
5.1	Surface water temperature records used to estimate the characteristic time scale of red noise, τ	67
A.1	Statistical evaluation of differences between the predictability of the nonlinear neural network model and the predictability of the best-fitting linear model	92
A.2	Correlations between species abundances and temperature	100
B.1	Relative frequency distributions of the phase angles between the fluctuating species, as determined by wavelet coherence analysis of the experimental data	111
D.1	Additional information on the time series of surface temperature analyzed in this paper	135
D.2	Maximum specific growth rates of the zooplankton species	139

Chapter 1

Introduction

1.1 The enigma of population oscillations

The first scientific study of population oscillations dates back to at least the 1920s with the work of the English zoologist Charles Elton. He was puzzled by multi-annual cycles in the population abundances of small mammals like lemmings, mice, voles and lynx. Based on data covering many years of study, he suggested that periodic fluctuations in the numbers of certain animals is likely to be due to climatic fluctuations as they have a similar frequency (Elton 1924).

Interestingly, shortly after Elton's empirical work, Alfred Lotka and Vito Volterra showed through simple mathematical models that population oscillations can be generated by predator-prey interactions (Lotka 1925; Volterra 1926). When Volterra's article appeared in *Nature* in 1926, Elton's certainties about externally driven population oscillations faded away. The idea that population cycles can be generated through interactions between species was an unexpected breakthrough.

1.2 The discovery of chaos: Lorenz's famous cup of coffee

In the 1960s another remarkable discovery was made that changed scientific thinking. Meteorologist Edward Lorenz had created a simple computer simulation model describing the weather. Having obtained some results from his numerical simulations, he decided to carry the calculations further. Instead of starting the simulations all over again (at that time the computers were really slow), he took a shortcut and started somewhere in the middle of the simulations. He entered new initial conditions at that midpoint by typing the numbers from his earlier printout. After going away for a cup of coffee, he came back to check the model's output and to his surprise the results were very different from the previous run. He soon understood the reason: the input data of the second run were rounded off and were slightly different from those of the first run (at the fourth decimal digit). Surprisingly, in the course

of a coffee break, that small difference in initial conditions had grown exponentially to provide a completely different result. Lorenz had accidentally discovered chaos (Lorenz 1963).

1.3 What is chaos?

1.3.1 Definition of chaos and the “butterfly effect”

Chaos is defined as *aperiodic long-term behavior* in a *deterministic* system that exhibits *sensitive dependence on initial conditions* (Strogatz 1994).

- “*Aperiodic long-term behavior*” means that the dynamics remain irregular ad infinitum, so the dynamics do not lead to a fixed point, periodic orbit, or quasi-periodic orbit.
- “*Deterministic*” means that the system has no random or noisy components. The irregular fluctuations arise from the system’s non-linearity and not from stochastic factors.
- “*Sensitive dependence on initial conditions*” means that small differences in the initial conditions grow exponentially in time. This means that minor deviations in the initial conditions cause large deviations in the long term, making long-term predictions of the state of the system impossible.

The last point is also known as the “butterfly effect” and has been made popular by Lorenz’s world famous talk entitled: “*Predictability: Does the flap of a butterfly’s wings in Brazil set off a tornado in Texas?*”. The flapping wing represents a small change in the initial conditions of the system, which causes a chain of events leading to large-scale alterations of events.

1.3.2 Strange attractors: patterns of chaos in phase space

In a dynamical system, phase space is defined as the collection of all possible states of the system. A specific evolution of the system’s state over time in this phase space is called a *trajectory* of the dynamical system. Consider for instance the Lotka-Volterra model describing the population dynamics of a predator and its prey:

$$\begin{aligned}\frac{dx}{dt} &= x(\alpha - \beta y) \\ \frac{dy}{dt} &= -y(\gamma - \delta x)\end{aligned}\tag{1.1}$$

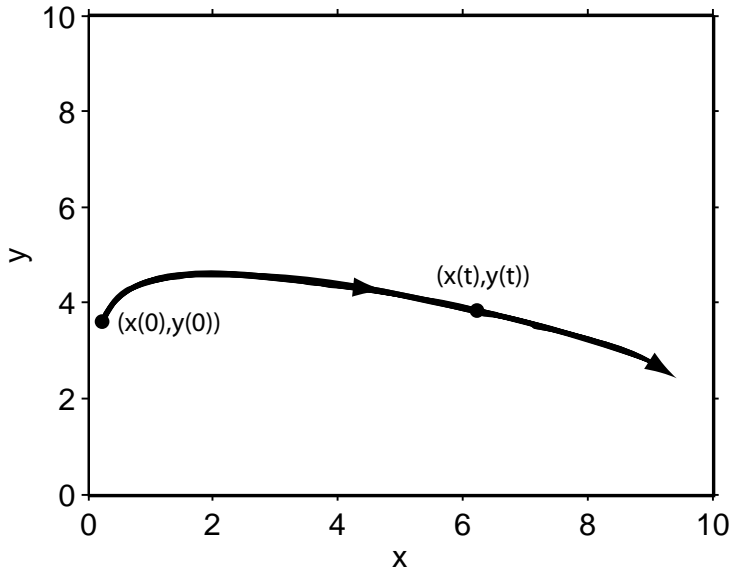


Figure 1.1: A trajectory in phase space for the Lotka-Volterra model.

where x is the abundance of the prey, y is the abundance of its predator, and α , β , γ and δ are parameters representing the interactions between the species. We can draw a trajectory in the phase space of this system by plotting the abundance of species x against the abundance of species y at each point in time, according to the solution $(x(t), y(t))$ of Eq. 1.1 (Figure 1.1).

An attractor is a set of points in phase space (for instance population abundances in the Lotka-Volterra model) that represents the states that the system reaches in the long run. An attractor has the following properties:

1. Any trajectory that starts on the attractor stays on the attractor for all time.
2. Any trajectory starting near enough to the attractor will always converge to the attractor.
3. The attractor is the minimum set of points that satisfies both 1 and 2.

Geometrically, an attractor can have different shapes depending on the solution of the system. The simplest attractor is the fixed point, where the trajectories approach a stable equilibrium (Figure 1.2a). A more complex attractor is the limit cycle, which is represented by a closed curve as the solutions oscillate periodically (Figure 1.2b). Another possibility is the quasi-periodic attractor which occurs if

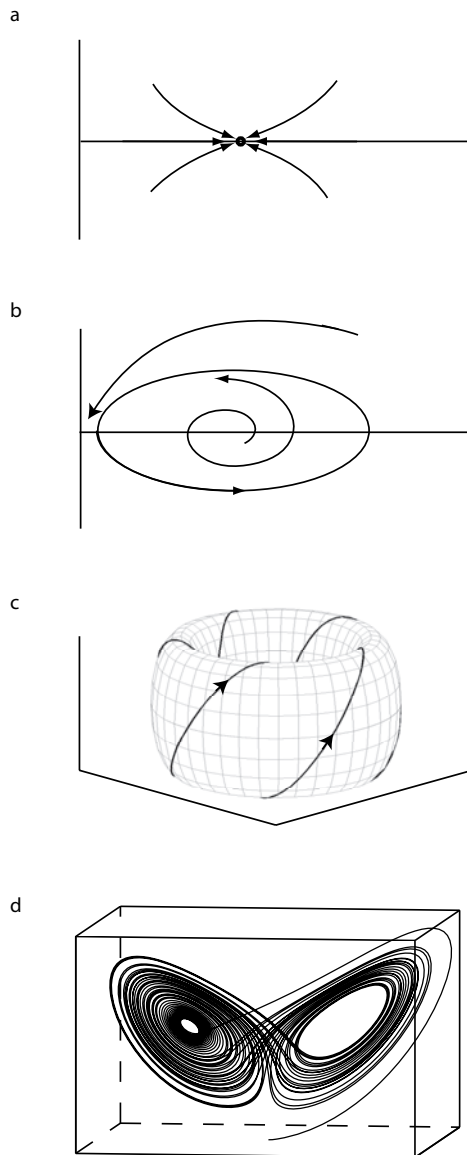


Figure 1.2: Depending on the solutions of the system different types of attractor may exist. **a**, The attractor is a fixed point if the solutions are equilibria. **b**, The attractor is a closed curve called a ‘limit cycle’ if the solutions oscillate periodically. **c**, The attractor is a torus if the solutions are quasi periodic with two or more incommensurate frequencies. **d**, The attractor is called a ‘*strange attractor*’ if the solutions are chaotic.

the oscillations consist of two or more incommensurate frequencies. The attractor then has the shape of a torus in phase space (Figure 1.2c). Every trajectory winds endlessly around the torus, yet never intersects with itself.

If the solutions are chaotic, the attractor is called a *strange attractor* (Figure 1.2d). Strange attractors have some important properties. The first property is that they are sensitively dependent on initial conditions, which means that two trajectories that are very close to each other will be arbitrarily far apart at later times. The only restriction is that the trajectories remain on the attractor. The second property is that strange attractors are never closed, which means that the motion of the system never repeats itself (aperiodic). The third property is that these attractors have a fractal structure, which means that their shape does not have an integer dimension (like a point, a line, a surface or a volume). A classical example of a strange attractor is the famous Lorenz attractor which has the typical shape of a butterfly (Figure 1.2d). Hence, the “butterfly effect” is indeed a very appropriate name!

1.3.3 A measure of chaos: the Lyapunov exponent

The sensitive dependence on initial conditions can be quantified by so-called Lyapunov exponents (often indicated by the Greek letter λ). To illustrate the basic idea of a Lyapunov exponent, we take a point s on the attractor and consider what happens to a small sphere of points close to s (Figure 1.3). This small sphere of nearby points can be interpreted as small perturbations of the initial conditions. If we follow the trajectory from the initial point s and trajectories starting from the small sphere of nearby initial conditions through time, we will see that the distances between the trajectory starting from s and its neighboring trajectories will either grow or shrink, causing the sphere to become distorted into an ellipsoid (Figure 1.3). The distances between the trajectory starting from s and the other trajectories in the ellipsoid can be followed in time. From the development of these distances we can determine the rates of exponential divergence (or convergence) of nearby trajectories. Each of these rates of change is a Lyapunov exponent. Thus, there is a set of n Lyapunov exponents $(\lambda_1, \dots, \lambda_n)$, with as many exponents as the n system’s variables in phase space. The attractor is chaotic if at least one of the Lyapunov exponents is positive, so that at least in one direction the trajectories are diverging. Since the Lyapunov exponent measures the rate at which nearby trajectories diverge, the magnitude of the Lyapunov exponent provides an indication of the predictability of the system. Fast divergence, and hence large Lyapunov exponents, implies low predictability.

It is common (and we also follow this approach in this thesis) to look only at the largest Lyapunov exponent (simply indicated as λ) to determine if a system is chaotic or not. The largest Lyapunov exponent determines to a large extent the rate of divergence of the entire system and thus provides information about the system’s predictability. In the example in Figure 1.3, we have a system of two variables in phase space. Hence, we will have two Lyapunov exponents, one (λ_1) in the direction

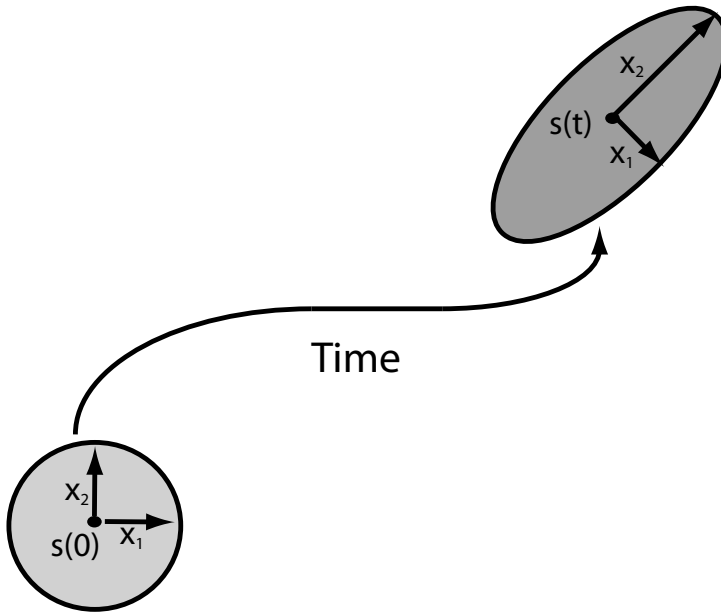


Figure 1.3: Sensitive dependence on initial conditions of a chaotic system. A small sphere of initial conditions close to reference point s evolves into an ellipsoid whose principal axes expand (or diverge) at rates given by the Lyapunov exponents. There are as many Lyapunov exponents as the number of variables in phase space (two in this case). Chaotic systems are characterized by at least one positive Lyapunov exponent, indicating that small initial differences expand along at least one of the axes.

of axis x_1 and the other (λ_2) in the direction of axis x_2 . In this example, the largest Lyapunov exponent is λ_2 , and the system will thus diverge most strongly in the direction x_2 (Figure 1.3).

1.3.4 Deterministic chaos versus stochasticity

Often chaos is misunderstood and wrongly associated with stochasticity. It is therefore important to underline that chaotic and stochastic dynamics are two very different phenomena. Chaotic systems follow deterministic rules and therefore have a high predictability in the short run. Because the divergence of trajectories takes times, chaotic systems have a low predictability when predictions are made over long time spans. In contrast, stochastic fluctuations are at least partly caused by chance. Therefore, stochastic systems never permit exact prediction, not even in the short run, but are predictable only in terms of probabilities.

In models of chaotic systems, if information is complete, predictions will be perfect. In other words, if we would start such a model twice with *exactly* the same initial conditions, we would obtain *exactly* the same result. The impossibility of making long-term predictions for chaotic systems derives from the lack of complete information about the initial conditions. As the tiniest difference in initial conditions grow exponentially in time, it is fundamentally impossible to predict the system dynamics in the long run.

1.4 Chaos in ecology

In the 1970s Sir Robert May showed that simple deterministic population models can generate chaos (May 1976). May worked with a simple discrete model (i.e., a difference equation) describing the logistic growth of a single population, when he observed that changing the intrinsic growth rate of the population led to a plethora of different model behaviors. At low growth rates, the population reached an equilibrium and stayed there (Figure 1.4a). As the intrinsic growth rate increased, the equilibrium population size increased gradually. However, at a certain level of the growth rate, the behavior of the model changed. Instead of settling down to a single population size, it jumped back and forth between two different values (Figure 1.4b). It had a higher value one year, and a lower value next year, and so on. Raising the growth rate a little more caused it to jump between four different values (Figure 1.4c). As the growth rate was increased further, the periodicity doubled again. These period doublings came faster and faster until chaos appeared. Thus, beyond a certain growth rate, it became impossible to predict the long-term dynamics of the population. From generation to generation, it jumped up and down in what looked like a random fashion (Figure 1.4d).

One might think that this result would have aroused immediate and huge interest from empirical ecologists, but it did not. One reason was the belief that such complex ecological dynamics arise only in models. This belief was at least partly fed by a follow-up study of May's single-population model, which showed that chaos in insect populations would require much higher intrinsic growth rates than observed in nature (Hassell et al. 1976). Consequently, and for the next ten years, the 'chaos revolution' proceeded mainly in the physical sciences, and much less in ecology.

In the 1990s a series of new model studies demonstrated that high intrinsic growth rates were not the only mechanism capable of generating chaos in population dynamics. It turned out that the phenomenon was not restricted to difference equations either. In particular, mathematical models showed that chaos can arise from many different ecological processes, including predator–prey interactions (Gilpin 1979; Scheffer 1991; Vandermeer 1993), food-chain dynamics (Hastings and Powell 1991), and multispecies competition for limiting resources (Huisman and Weissing 1999). However, despite the abundance of theoretical results, most ecologists remained skeptical and thought of chaos as something that may happen for a restricted range of pa-

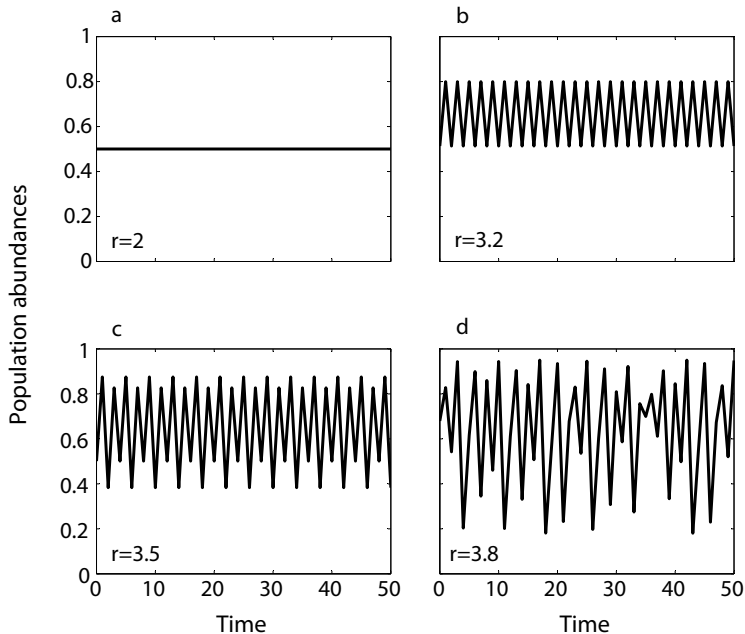


Figure 1.4: Solutions of the single-population model of May (1976), for different values of the intrinsic growth rate r . **a**, At growth rate $r=2$, the population reaches an equilibrium and stays there. **b**, At growth rate $r=3.2$, the population oscillates between two different values. **c**, At growth rate $r=3.5$, the population oscillates between four different values. **d**, At growth rate $r=3.8$, the population oscillates chaotically.

parameters in models, but is not really important for real ecosystems. In particular, some ecologists argued that chaotic fluctuations would be unlikely in nature, as the strong ups and downs would easily lead species to near-extinction (Philippi et al. 1987; Berryman and Millstein 1989). However, other studies counter argued that chaos could actually reduce the probability of species extinction (Allen et al. 1993), and that windows of opportunity created in nonequilibrium communities may enhance biodiversity (Huisman and Weissing 1999). However, the debate remained largely theoretical. One of the main reasons for the widespread belief that chaos would be rare in ecology was that it is really difficult to demonstrate chaos in real-world ecosystems. In the real world, the external conditions are never constant and the observed species fluctuations may be driven by these environmental fluctuations rather than by intrinsic dynamics. Moreover, the statistical techniques to demonstrate chaos in a rigorous manner require long and high-resolution time series, and such data are scarce in ecology.

To deal with this problem, ecologists have developed different methodologies to demonstrate chaos in natural populations. Pioneering work by Schaffer and colleagues, using techniques based on attractor reconstruction, indicated the likely chaotic character of various childhood epidemics (Schaffer and Kot 1986; Olsen et al. 1988; Olsen and Schaffer 1990; Schaffer et al. 1990). Almost at the same time Sugihara and May (1990) developed a non-linear forecasting method with which they pointed to the possibility of chaotic behavior in the dynamics of diatom populations along the Pacific coast of Southern California. Subsequently, various authors (Turchin and Taylor 1992; Hanski et al. 1993; Turchin 1993, 1995; Ellner and Turchin 1995) fitted nonlinear time-series models to long-term data, and their results suggest chaos in the population dynamics of several insects and small mammals.

Although these first results were exciting, it remains difficult to determine unequivocally whether intrinsic chaotic dynamics are the true explanation of species fluctuations observed in nature. Indeed, stronger evidence of chaos in ecology came from studies in the laboratory, where scientists could keep the environmental conditions constant. In 1997, biologist Robert Costantino and his colleagues reported chaos in flour beetles (Costantino et al. 1997). Costantino and co-workers raised flour beetles in flasks for over 20 years. The researchers built a mathematical model to represent the population dynamics of flour beetles. They showed that if adult mortality was high, the model became very sensitive to the rate of cannibalism, in some cases jumping to cycles and in other cases to chaos depending on the rate of cannibalism. To validate their model's results they tried to recreate this behavior in the lab. In their experiments, adult mortality rate was increased simply by regularly removing beetles which have reached maturity. Then they mimicked different cannibalism rates by taking away pupae from the flasks. The experiments confirmed the model predictions. Depending on the experimental settings, the beetle populations reached a stable equilibrium, oscillated regularly, or fluctuated chaotically.

About 10 years passed since the findings of Costantino and co-workers, when two other studies demonstrated chaos under controlled laboratory conditions. Becks et al. (2005) discovered chaotic dynamics in a simple three-species food web consisting of one protozoa and two bacterial species. A few years later, Graham et al. (2007) showed chaos in the dynamics of nitrifying bacteria in a wastewater bioreactor. So far, however, laboratory studies have not considered the natural complexity of real food webs and the time span of experiments has often been too short to detect chaos in a rigorous manner.

1.5 Thesis outline

In this thesis I provide the first experimental demonstration of chaos in a real complex food web. In **chapter 2** we analyze data from a marine planktonic food web isolated from the Baltic Sea and grown under constant laboratory conditions by Dr. Reinhard Heerkloss for nearly 8 years. The analysis demonstrates convincingly that

the species fluctuations in this food web show sensitive dependence on the initial conditions.

In **chapter 3** we use wavelet and cross wavelet analysis to investigate the chaotic fluctuations in our marine food web in more detail. The analysis reveals that the food web contains two interacting predator-prey cycles. The two cycles are coupled through competition for nutrients and light between the two prey species. The system shifts back and forth between the two predator-prey cycles in a chaotic fashion, which results in continued alternations in species dominance.

One may argue that external forcing by regular seasonal variation could prevent chaos in real ecosystems. In **chapter 4** we study a multispecies predator-prey model to investigate how seasonal forcing may affect chaos in plankton communities. Our results demonstrate that the chaotic dynamics may become entrained by the seasonal cycle in an intriguing way.

Another common argument is that real ecosystems also experience short-term stochastic variation, for instance by day-to-day variability in weather conditions. The effect of such environmental noise on plankton populations is investigated in **chapter 5**. Finally in **chapter 6** I summarize the results presented in this thesis and I give an outlook for future research.

Acknowledgements

I thank Marten Scheffer, Egbert van Nes and Jef Huisman for their helpful comments on this chapter.

Chapter 2

Chaos in a long-term experiment with a plankton community

Abstract

Mathematical models predict that species interactions such as competition and predation can generate chaos (May 1974, 1976; Gilpin 1979; Hastings and Powell 1991; Vandermeer 1993; Huisman and Weissing 1999; van Nes and Scheffer 2004; Huisman et al. 2006). However, experimental demonstrations of chaos in ecology are scarce, and have been limited to simple laboratory systems with a short duration and artificial species combinations (Ellner and Turchin 1995; Costantino et al. 1997; Becks et al. 2005; Graham et al. 2007). Here, we present the first experimental demonstration of chaos in a long-term experiment with a complex food web. Our food web was isolated from the Baltic Sea, and consisted of bacteria, several phytoplankton species, herbivorous and predatory zooplankton species, and detritivores. The food web was cultured in a laboratory mesocosm, and sampled twice a week for more than 2,300 days. Despite constant external conditions, the species abundances showed striking fluctuations over several orders of magnitude. These fluctuations displayed a variety of different periodicities, which could be attributed to different species interactions in the food web. The population dynamics were characterized by positive Lyapunov exponents of similar magnitude for each species. Predictability was limited to a time horizon of 15-30 days, only slightly longer than the local weather forecast. Hence, our results demonstrate that species interactions in food webs can generate chaos. This implies that stability is not required for the persistence of complex food webs, and that the long-term prediction of species abundances can be fundamentally impossible.

This chapter is based on the paper: Benincà, E., Huisman, J., Heerkloss, R., Jöhnk, K.D., Branco, P., van Nes, E.H., Scheffer, M. & Ellner, S.P. 2008. Chaos in a long-term experiment with a plankton community. *Nature* **451**, 822-825.

2.1 Introduction

The discovery by Sir Robert May in the 1970s that simple population models may generate complex chaotic dynamics (May 1974, 1976) triggered heated debate and caused a paradigm shift in ecology. Since May's pioneering findings, mathematical models have shown that chaos can be generated by a plethora of ecological mechanisms, including competition for limiting resources (Huisman and Weissing 1999; Huisman et al. 2006), predator-prey interactions (Gilpin 1979; Vandermeer 1993), and food-chain dynamics (Hastings and Powell 1991; van Nes and Scheffer 2004). In contrast to the overwhelming theoretical attention, convincing empirical evidence of chaos in real ecosystems is rare (Zimmer 1999). What could explain the paucity of empirical support? It might be that chaos is a rare phenomenon in natural ecosystems, for instance because food webs contain many weak links between species, which may stabilize food-web dynamics (McCann et al. 1998; Neutel et al. 2002). Alternatively, one might argue that there is a lack of suitable data to test for chaos in food webs. For instance, external variability (e.g., weather fluctuations) may obscure the role of intrinsic species interactions. In principle, laboratory experiments provide ideal conditions to obtain high-resolution data in a constant environment. Chaos has so far been demonstrated experimentally for a few single species (Ellner and Turchin 1995; Costantino et al. 1997), a simple three-species food web (Becks et al. 2005), and a wastewater bioreactor (Graham et al. 2007). Thus far, however, laboratory studies did not consider the natural complexity of real food webs, and the time span of experiments has often been too short to detect chaos in a rigorous manner.

2.2 The mesocosm experiment dataset

Here, we analyze a time series of a plankton community isolated from the Baltic Sea. The plankton community was cultured in a laboratory mesocosm under constant external conditions for more than 8 years (Heerkloss and Klinkenberg 1998). In total, two nutrients (N and P), one detritus pool, and ten different functional groups were distinguished (Figure 2.1a). The phytoplankton was divided into picophytoplankton, nanophytoplankton, and filamentous diatoms. The herbivorous zooplankton was classified into protozoa, rotifers, and calanoid copepods. The rotifers and protozoa were grazed by cyclopoid copepods. The microbial loop was represented by heterotrophic bacteria and two groups of detritivores: ostracods and harpacticoid copepods. The abundances of these functional groups were counted twice a week. Our analysis covers a period of 2,319 days, which yielded 690 data points per functional group. Since most species in this food web have generation times of only a few days, the time series spanned hundreds to thousands of generations per species. We performed several analyses to investigate the dynamics of this food web.

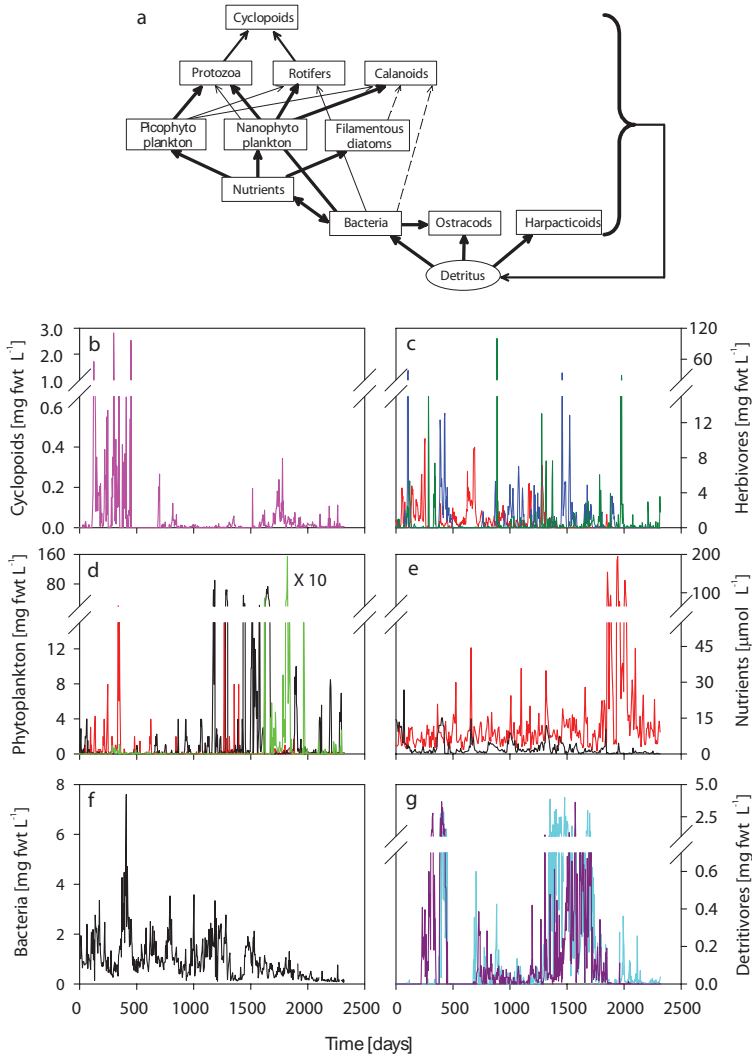


Figure 2.1: Description of the plankton community in the mesocosm experiment. **a**, Food web structure of the mesocosm experiment. The thickness of the arrows gives a first indication of the species preferences of the species, as derived from general knowledge of their biology. **b-g**, Time series of the functional groups in the food web (measured as freshweight biomass). **b**, Cyclopoid copepods; **c**, calanoid copepods (red), rotifers (blue), and protozoa (dark green); **d**, picophytoplankton (black), nanophytoplankton (red), and filamentous diatoms (green); note that the diatom biomass should be magnified by 10; **e**, dissolved inorganic nitrogen (red) and soluble reactive phosphorus (black); **f**, heterotrophic bacteria; **g**, harpacticoid copepods (violet) and ostracods (light blue).

2.3 Methods

2.3.1 Methods summary

The mesocosm consisted of a cylindrical plastic container (74 cm high, 45 cm diameter), which was filled with a 10 cm sediment layer and 90 liter of water from the Baltic Sea. This inoculum provided all species in the food web. The mesocosm was maintained in the laboratory at a temperature of $\approx 20^\circ\text{C}$, salinity of $\approx 9\text{‰}$, incident irradiation of $50 \mu\text{mol photons m}^{-2} \text{s}^{-1}$ (16/8 hours light-dark cycle), and constant aeration. Species abundances were measured twice a week, while nutrients were measured weekly.

We interpolated each time series to obtain data with equidistant time intervals of 3.35 days. The interpolated time series were subsequently transformed to stationary time series with mean zero and standard deviation of 1. Long sequences of zero values were removed from the analysis.

We calculated the predictabilities of the species by fitting a neural network model to the time series, following Nychka et al. (1992). For each species, the neural network predictions were based on the observed population abundances of the species itself and of those species with which it has a direct link in the food web (Figure 2.1a).

We used two different methods to calculate the Lyapunov exponent. The direct method was based on attractor reconstruction by time-delay embedding of each time series (Kantz and Schreiber 1997; Rosenstein et al. 1993). We chose an embedding dimension of 6 and a time delay of 1 time step (see Appendix A). This direct method yielded Lyapunov exponents for each species separately. The consistency of these Lyapunov exponents provides an additional check on the robustness of our conclusions. The indirect method was based on a neural network approach to estimate the deterministic skeleton of the dynamics (Ellner and Turchin 1995; Nychka et al. 1992). This deterministic skeleton was used to calculate one Lyapunov exponent characterizing the dynamics of the entire food web.

2.3.2 Experimental set-up

The experiment (Heerkloss and Klinkenberg 1998) started on 31 March 1989, when the mesocosm was filled with a 10 cm sediment layer and 90 liter of water from the Darss-Zingst estuary (southern Baltic Sea, $54^\circ 26' \text{N}$, $12^\circ 42' \text{E}$). Phytoplankton was divided in three functional groups: picophytoplankton consisting of 1-2 μm picocyanobacteria (mostly *Synechococcus* species), nanophytoplankton consisting of 3-5 μm eukaryotic flagellates (mainly *Rhodomonas lacustris* Pascher and Ruttner), and large filamentous diatoms (*Melosira moniliformis* (O.F.M.) C. Agardh). Herbivorous zooplankton was classified into three groups: protozoa (mainly large ciliates such as *Cyclidium* and *Strombidium* species), rotifers (mainly *Brachionus plicatilis* (O.F.M.)), and the calanoid copepod *Eurytemora affinis* (Poppe). Rotifers and protozoa were grazed by predators belonging to the cyclopoid copepods (unidentified

species of the *Eucyclops* genus). The microbial loop was represented by heterotrophic bacteria and two groups of detritivores: ostracods and the harpacticoid copepod *Halectinosoma curticorne* (Boeck). Sampling of the mesocosm is described in the Appendix A.

From 23 November 1990 to 5 March 1991, the length of the light period was temporarily reduced from 16 to 12 hrs per day. Accounting for a brief period of recovery, we therefore restricted our time series analysis to the period from June 16, 1991, onwards until the end of the experiment on 20 October 1997.

2.3.3 Data treatment

Several of our analyses required stationary time series, with equidistant data and homogeneous units of measurement. We therefore interpolated each time series using cubic hermite interpolation to obtain data with equidistant time intervals of 3.35 days. Nitrogen and phosphorus concentrations were transformed to equivalent units of ‘biomass’ assuming Redfield ratios (Redfield 1958). Some functional groups remained below the detection limit for a long time, yielding long sequences of zero values. We shortened these time series by removing these long sequences of zero values. Also, the time series showed sharp ups and downs in species abundances. Therefore, all time series were rescaled by a fourth-root power transformation. This power transformation homogenized the variances, and eliminated a possible bias in the ‘direct method’ calculation of the Lyapunov exponents (see Appendix A). Subsequently, we removed long-term trends from the data by utilizing a sliding window with a bandwidth of 300 days and a Gaussian kernel. Finally, the data were normalized by the transformation $\frac{x-\mu}{\sigma}$, where x is the original datapoint, μ is the mean of the time series, and σ is the standard deviation. Thus, we obtained stationary time series with mean zero and standard deviation of 1. The transformed time series are shown in the Appendix A.

2.3.4 Predictability

We developed a model to investigate the predictability of each species. Ideally, this model would be based on the biology of the species interactions. However, the exact mechanisms of species interaction in this food web are not known. For instance, we do not know the elemental stoichiometry of the different species, whether allelochemicals modified the species interactions, or whether zooplankton followed type-II or type-III functional responses. We may even lack information on some food-web components (e.g., viruses were not measured). Using a mechanistically incorrect parametric model can lead to spurious results in nonlinear time series analysis (Kendall 2001). Therefore, we used a semi-mechanistic approach in which the general model structure is based on biological knowledge about the food web, while nonparametric methods are used to fit aspects about which little is known.

In our case, we can exploit the food web structure to make predictions. For each species, we used the following nonlinear model:

$$N_{i,t+T} = f_{i,T}(N_{i,t}, N_{1,t}, N_{2,t}, \dots, N_{m,t}) \quad (2.1)$$

Here, $N_{i,t}$ is the population abundance (or nutrient concentration) of species i at time t , T is the prediction time (i.e., the number of days that we want to predict ahead), and $f_{i,T}$ is an unknown function describing the change in the population abundance of focal species i . The function $f_{i,T}$ uses the focal species i , and those species 1 to m that have a direct link in the food web to this focal species (Figure 2.1a). For instance, predictions for picophytoplankton are based on picophytoplankton abundance, the nutrients nitrogen and phosphorus, and its herbivores (rotifers, protozoa, and calanoid copepods) at the preceding time step. We estimated the unknown functions $f_{i,T}$ using the neural network algorithm of Nychka et al. (1992) (see Appendix A for details).

We tested whether the nonlinear neural network model yielded significantly better predictions than the corresponding linear model. For this purpose, each nonlinear function $f_{i,T}$ in Eq.2.1 was replaced by a linear function of the same population abundances. The coefficients of this linear model were estimated by multiple regression. The significance test comparing the predictions of the linear and nonlinear model is explained in the Appendix A.

2.3.5 Lyapunov exponents

We used direct methods and indirect methods (also called Jacobian methods) to estimate Lyapunov exponents. Direct methods search the data for nearby pairs of state vectors. In other words, the time series are searched for pairs of data points at which all species abundances in the food web are in a similar state. The rate of trajectory divergence at subsequent times, averaged over many such pairs, is an estimate of the dominant Lyapunov exponent (Kantz and Schreiber 1997; Rosenstein et al. 1993). Because state vectors that are close in time are often also close in state space, temporal correlation in the data may obscure the divergence of trajectories. Our time series was sufficiently long to solve this problem by a Theiler window (Theiler 1986), which is a moving window covering data before and after each data point (see Appendix A for details).

Jacobian methods are based on the development of a deterministic model of the underlying dynamics, called the deterministic skeleton. The Lyapunov exponent is here calculated from the sequence of Jacobian matrices of the deterministic skeleton, evaluated at the time series of observed or reconstructed state vectors (Ellner and Turchin 1995; Nychka et al. 1992). Thus, Jacobian methods require the preliminary step of estimating the deterministic skeleton. We estimated the deterministic skeleton using a similar neural network model as for the predictability (Eq. 2.1).

Both approaches have advantages and disadvantages. Direct methods cannot distinguish trajectory divergence caused by chaos from trajectory divergence due to

noise, and might therefore be less suitable for many ecological time series. Although our experimental system was maintained under controlled laboratory conditions, even small levels of environmental or demographic noise could bias direct methods towards positive estimates of the Lyapunov exponent. Jacobian methods are not biased by noise; their main problem is uncertainty in estimation of the deterministic skeleton. If the Lyapunov exponents obtained from both approaches are consistent, this adds further reliability to the results.

Further details on the calculation of Lyapunov exponents are provided in the Appendix A.

2.4 Data analysis

First, the time series showed remarkable fluctuations in species abundances over several orders of magnitude, despite constant external conditions (Figure 2.1). Spectral analysis revealed that the fluctuations covered a range of different periodicities (see Appendix A). In particular, picophytoplankton, rotifers and calanoid copepods seemed to fluctuate predominantly with a periodicity of ≈ 30 days, suggestive of coupled phytoplankton-zooplankton oscillations. Periodicities of ≈ 30 days are consistent with model predictions of phytoplankton-zooplankton oscillations (Scheffer and Rinaldi 2000), and have also been observed in earlier laboratory experiments with phytoplankton and zooplankton species (Fussmann et al. 2000).

Second, a closer look at the species fluctuations revealed several striking patterns (Table 2.1). Peaks of picophytoplankton, nanophytoplankton, and filamentous diatoms alternated with little or no overlap (Figure 2.1d), and picophytoplankton and nanophytoplankton concentrations were negatively correlated (Table 2.1), indicative of competition between the phytoplankton groups. Predator-prey interactions could also be discerned. We found negative correlations of picophytoplankton with protozoa, and of nanophytoplankton with both rotifers and calanoid copepods (Table 2.1). This indicates that protozoa fed mainly on picophytoplankton, while rotifers and calanoid copepods fed mainly on larger nanophytoplankton, consistent with the structure of the food web (Figure 2.1a). Conversely, the positive correlation of picophytoplankton with calanoid copepods may point at indirect mutualism between prey species and the predators of their competitors (that is, ‘the enemy of my enemy is my friend’). Other striking patterns included the negative correlation between bacteria and ostracods, and the positive correlation between bacteria and phosphorus. Although our interpretation of these correlation patterns is somewhat speculative, they correspond with the trophic links in the food web. This shows that the observed fluctuations in species abundances were largely driven by species interactions in the food web, not by external forcing.

Third, we investigated the long-term predictability of the food-web dynamics. The predictability of a deterministic non-chaotic system with uncorrelated noise (e.g., a limit cycle with sampling error) remains constant in time, while the pre-

	Bacteria	Harpacticoids	Ostracods	Nitrogen	Phosphorus	Picophytoplankton	Nanophytoplankton	Rotifers	Protozoa	Calanoids
Bacteria	1	0.03	-0.24***	0.05	0.19***	0.03	-0.17***	0.30***	-0.17	0.22***
Harpacticoids		1	0.17***	-0.12*	0.09	-0.04	-0.03	0.02	0.14	-0.04
Ostracods			1	-0.16***	-0.06	-0.04	0.01	-0.03	0.19*	-0.04
N				1	0.08	-0.00	-0.02	-0.04	0.02	0.04
P					1	-0.04	0.03	0.10*	-0.11	-0.09
Picophytoplankton						1	-0.17***	-0.03	-0.22***	0.26***
Nanophytoplankton							1	-0.19***	0.15	-0.14*
Rotifers								1	-0.02	-0.10
Protozoa									1	<i>n.a.</i>
Calanoids										1

Table 2.1: Correlations between the species in the food web. Table entries show the product-moment correlation coefficients, after transformation of the data to stationary time series (see Methods section). Significance tests were corrected for multiple hypothesis testing by calculation of adjusted p-values using the false discovery rate (Benjamini and Hochberg 1995). Significant correlations are indicated in bold: *** $p < 0.001$, ** $p < 0.01$, * $p < 0.05$. The correlation between calanoid copepods and protozoa could not be calculated, because their time series did not overlap. Filamentous diatoms and cyclopoid copepods were not included in the correlation analysis, because their time series contained too many zeros.

dictability of chaotic systems decreases in time (Sugihara and May 1990). We fitted the time series to a neural network model (Nychka et al. 1992) to generate predictions at different time intervals. For short-term forecasts of only a few days, most species had a high predictability of $R^2=0.70-0.90$ (Figure 2.2). However, the predictability of the species was much reduced when prediction times were extended to 15-30 days. This is a characteristic feature of chaos, where short-term predictability is high, while the predictability decreases when making forecasts further into the future. However, decreasing predictability can also occur in linear (and therefore non-chaotic) systems exposed to stochastic perturbations. We therefore tested (Sugihara and May 1990) whether the predictions of the nonlinear neural network model were significantly better than the predictions generated by the best-fitting linear model. Already after a few time steps, the nonlinear model yielded significantly higher predictabilities than the corresponding linear model for all species in the food web (Figure 2.2; see Appendix A for the statistics). These findings demonstrate that (i) the predictability of the species abundances in the food web decreased in time, and (ii) there was a strong nonlinear deterministic component in the food web dynamics.

Fourth, we calculated the Lyapunov exponent, the hallmark of chaos in nonlinear systems. The dominant Lyapunov exponent (λ) is a measure of the rate of convergence or divergence of nearby trajectories (Strogatz 1994). Negative Lyapunov exponents indicate that nearby trajectories converge, which is representative for stable equilibria and periodic cycles. Conversely, positive Lyapunov exponents indicate divergence of nearby trajectories, which is representative for chaos. We used two different methods to calculate the Lyapunov exponent: a direct method and an indirect method.

The direct method started with a reconstruction of the attractor by time-delay embedding of each time series (Strogatz 1994; Takens 1981; Kantz and Schreiber 1997). Exponential divergence (or convergence) of trajectories was calculated from nearby state vectors in the reconstructed state space (Rosenstein et al. 1993). The results show that the distance between initially nearby trajectories increased over time, and reached a plateau after about 20-30 days (Figure 2.3). This matches the time horizon of 15-30 days obtained from the predictability estimates (Figure 2.2). Lyapunov exponents were calculated from the initial slope of the exponential divergence, using linear regression. This yielded significantly positive Lyapunov exponents of strikingly similar value for all species (Figure 2.3; mean $\lambda \approx 0.057 \text{ day}^{-1}$, s.d.= 0.005 day^{-1} , $n=9$). This gives much confidence that the species in the food web were all fully connected, and that their population dynamics were governed by the same chaotic attractor.

Direct methods cannot distinguish trajectory divergence caused by chaos from trajectory divergence due to noise (Ellner and Turchin 1995; Nychka et al. 1992). Therefore, we also applied an indirect method, which calculates the Lyapunov exponent from a deterministic model. While indirect methods are not affected by noise, they rely on the assumption that the deterministic model provides an ade-

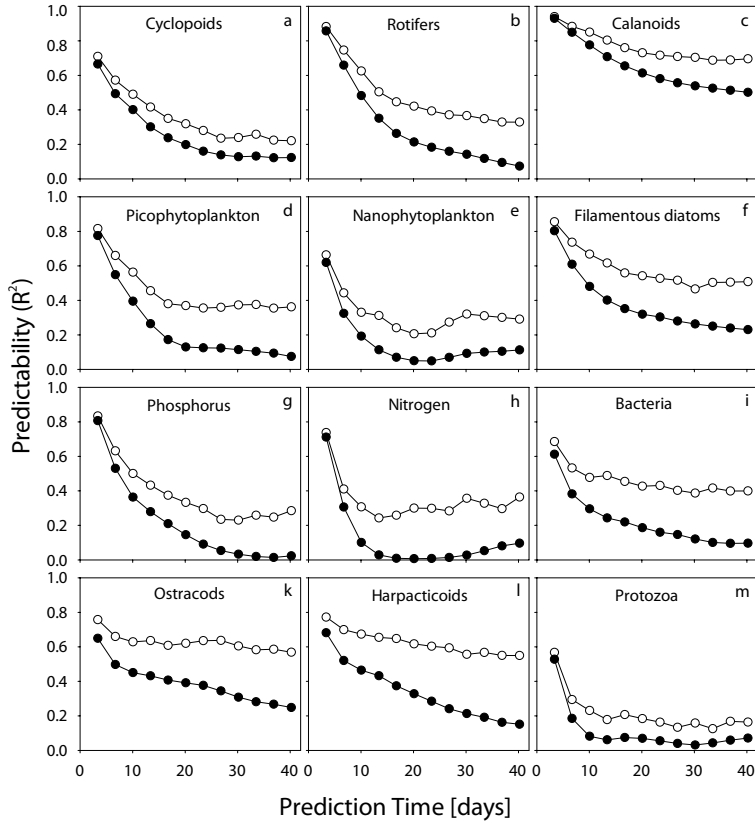


Figure 2.2: Predictability of the species decreases with increasing prediction time. The predictability is quantified as the coefficient of determination (R^2) between predicted and observed data. Already after a few time steps, predictions by the nonlinear neural network model (open circles) were significantly better than predictions by the best-fitting linear model (closed circles) (see Appendix A for further details). **a**, Cyclopoid copepods; **b**, rotifers; **c**, calanoid copepods; **d**, picophytoplankton; **e**, nanophytoplankton; **f**, filamentous diatoms; **g**, soluble reactive phosphorus; **h**, dissolved inorganic nitrogen; **i**, bacteria; **k**, ostracods; **l**, harpacticoid copepods; **m**, protozoa.

quate representation of the system's deterministic skeleton. In our case, the model structure again followed the trophic structure of the food web (Figure 2.1a). The model was used to calculate trajectory divergence at each time step by evaluation of the Jacobian matrix (see Appendix A for details). This indirect method yielded a global Lyapunov exponent of $\lambda=0.04 \text{ day}^{-1}$, characterizing the divergence of trajectories across the entire food web. We ran a bootstrap procedure based on 1000

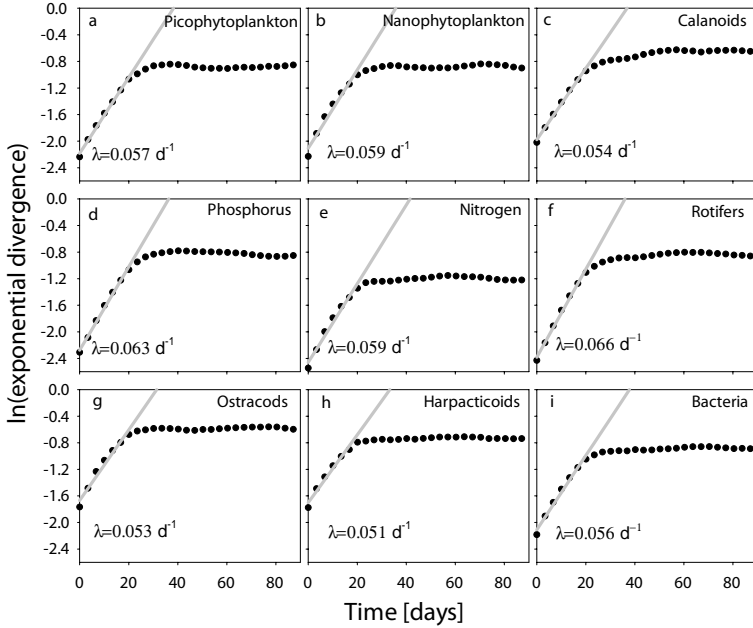


Figure 2.3: Exponential divergence of the trajectories. The Lyapunov exponent (λ) is calculated as the initial slope of the ln-transformed exponential divergence versus time, as estimated by linear regression (grey line). All Lyapunov exponents were significantly different from zero (linear regression: $P < 0.001$, $n=6$ or 7 depending on the species). **a**, Picophytoplankton; **b**, nanophytoplankton; **c**, calanoid copepods; **d**, soluble reactive phosphorus; **e**, dissolved inorganic nitrogen; **f**, rotifers; **g**, ostracods; **h**, harpacticoid copepods; **i**, bacteria. Exponential divergence could not be calculated for filamentous diatoms, protozoa, and cyclopoid copepods, because their time series contained too many zeros.

replicates to estimate the uncertainty of this value (see Appendix A). A one-sided confidence interval at the 95% confidence level yielded a lower bound of $\lambda = 0.03 \text{ day}^{-1}$. This confirmed that the Lyapunov exponent was significantly positive, and that this positive value was not due to noise.

2.5 Discussion

In total, our analysis revealed several signatures of chaos. Despite constant external conditions, the food web showed strong fluctuations in species abundances that could be attributed to different species interactions. We found high predictability on the short term, reduced predictability on the long term, and significantly positive

Lyapunov exponents. This shows that the population dynamics in the food web were characterized by exponential divergence of nearby trajectories, which provides the first experimental demonstration of chaos in a complex food web.

Compared with other systems, the time horizon for the predictability of our plankton community (15-30 days) is only slightly longer than the time horizon for the local weather forecast (≈ 2 weeks, Lorenz 1982). Lyapunov exponents were smaller in our plankton community ($\lambda=0.03-0.07 \text{ day}^{-1}$) than in recent experiments with microbial food webs (Becks et al. 2005; Graham et al. 2007) ($\lambda=0.08-0.20 \text{ day}^{-1}$). This might indicate that our plankton was ‘less chaotic’. Alternatively, these differences in Lyapunov exponents might be attributed to differences in generation times, because most phytoplankton and zooplankton species in our experiment have longer generation times than the bacteria and ciliates used in these microbial food webs. Since the time horizon is inversely proportional to the Lyapunov exponent (Strogatz 1994), this suggests that the time horizon for the predictability of chaotic food webs scales with the generation times of the organisms involved.

Our findings have important implications for ecology and ecosystem management. First, our data illustrate that food webs can sustain strong fluctuations in species abundances during hundreds of generations. Apparently, stability is not required for the persistence of complex food webs. Second, nonequilibrium dynamics in food webs affect biodiversity and ecosystem functioning. For instance, fluctuations on time scales of 15-30 days, as observed in our experiment, offer a suitable range of temporal variability to promote species coexistence in plankton communities (Gaedeke and Sommer 1986). Hence, chaotic fluctuations generated by species interactions may contribute to the unexpected biodiversity of the plankton, which provides a solution for one of the classic paradoxes in ecology known as the paradox of the plankton (Huisman and Weissing 1999). Third, chaos limits the predictability of species abundances. In our experimental food web, predictability was lost on a time scale of 15-30 days, which corresponds to 5-15 plankton generations depending on the species. Since many other food webs have a similar structure of plants, herbivores, carnivores and a microbial loop, it is tempting to suggest that the observed loss of predictability in 5-15 generations is likely to apply to many other food webs as well.

Acknowledgements

We thank W. Ebenhöf for fruitful suggestions on the experimental design, H. Albrecht, G. Hinrich, J. Rodhe, S. Stolle and B. Walter for help during the experiment, T. Huebener, I. Telesh, R. Schumann, M. Feike and G. Arlt for kind advice in taxonomic identification, and B.M. Bolker, V. Dakos and the anonymous referees for comments on the manuscript. The research of E.B., K.D.J. and J.H. was supported by the Earth and Life Sciences Foundation (ALW), which is subsidised by the Netherlands Organisation for Scientific Research (NWO). Research of S.P.E. was supported by a grant from the Andrew W. Mellon foundation.

Chapter 3

Coupled predator-prey oscillations in a chaotic food web

Abstract

Coupling of several predator-prey oscillations can generate intriguing patterns of synchronization and chaos. Theory predicts that prey species will fluctuate in phase if predator-prey cycles are coupled through generalist predators, whereas they will fluctuate in anti-phase if predator-prey cycles are coupled through competition between prey species. Here, we investigate predator-prey oscillations in a long-term experiment with a marine plankton community. Wavelet analysis of the species fluctuations reveals two predator-prey cycles that fluctuate largely in anti-phase. The phase angles point at strong competition between the phytoplankton species, but relatively little prey overlap among the zooplankton species. This food-web architecture is consistent with the size structure of the plankton community, and generates highly dynamic food webs. Continued alternations in species dominance enable coexistence of the prey species through a non-equilibrium ‘killing-the-winner’ mechanism, as the system shifts back and forth between the two predator-prey cycles in a chaotic fashion.

3.1 Introduction

In 1665, confined to his home by a minor illness, the Dutch physicist Christiaan Huygens discovered an ‘odd kind of sympathy’ between two pendulum clocks mounted next to each other on the same beam (Bennett et al. 2002). The two pendula oscillated with exactly the same frequency, but in opposite directions. When he disturbed one pendulum, the anti-phase oscillations were quickly restored. Apparently, the two pendula displayed coupled oscillations. Since Huygens’s discovery,

This chapter is based on the paper: Benincà, E., Jöhnk, K.D., Heerkloss, R. & Huisman, J. 2009. Coupled predator-prey oscillations in a chaotic food web. *Ecology Letters* **12**, 1367-1378.

coupled oscillations have been described in many biological, chemical and physical systems (Strogatz and Stewart 1993; Golubitsky et al. 1999; Rodriguez et al. 1999; Kiss et al. 2002). In food webs, resource-consumer interactions can generate oscillations, for instance in the form of predator-prey and host-parasitoid cycles. In a series of papers, Vandermeer (1993, 2004, 2006) showed that coupling of several predator-prey oscillations can lead to intriguing patterns of synchronization, as in Huygens's clockwork.

Vandermeer (2004) described two different ways in which several predator-prey oscillations can be coupled. If specialist predators each feed on only one prey species while these prey species compete with each other, we say that the predator-prey systems are 'coupled through competition' (Figure 3.1a). Conversely, if generalist predators feed on all prey species, we say that the predator-prey systems are 'coupled through predation' (Figure 3.1b). Interestingly, theory predicts that the mode of coupling affects the phase relationships between the species fluctuations. Prey species are predicted to oscillate all in phase with each other if predator-prey systems are coupled through generalist predation only. In contrast, prey species are predicted to oscillate in anti-phase if systems are coupled through competition only. Anti-phase oscillations are characterized by continued alternations in species dominance, such that the dominance of one prey species is followed by the dominance of another prey species, and so on. Likewise, predators are predicted to oscillate in phase if systems are coupled through predation, but in anti-phase if systems are coupled through competition (Vandermeer 2004).

In reality, of course, predator-prey systems will often be coupled through both competition and predation. In this mixed case, theory predicts that the population dynamics become chaotic for a relatively wide range of parameter values (Vandermeer 2004). Hence, species fluctuations will not display the strict regularity of Huygens's clockwork but will vary in frequency and amplitude, which makes it more difficult to identify patterns of synchrony. Still, some predator-prey systems may be coupled predominantly through competition, whereas others may be coupled mainly through predation, and the signatures of these different coupling modes may still be reflected in the phase relationships between the species (Vandermeer 2004).

With these intriguing model predictions in mind, the question is whether similar patterns of in-phase and anti-phase synchrony can be observed in real food webs. Recently, we demonstrated chaos in a long-term experiment with a plankton community (Benincà et al. 2008). The plankton community was isolated from the Baltic Sea, and consisted of phytoplankton species, herbivorous and predatory zooplankton species, and a microbial loop. It was maintained in a laboratory mesocosm for more than 8 years. Despite constant laboratory conditions, the species abundances fluctuated over several orders of magnitude. We showed that the predictability of these species fluctuations was limited to a time horizon of only 15-30 days (Benincà et al. 2008). However, we were unable to pinpoint the underlying mechanisms causing these chaotic fluctuations. Mathematical models suggest several possible mechanisms that can generate chaos in plankton communities, including multispecies

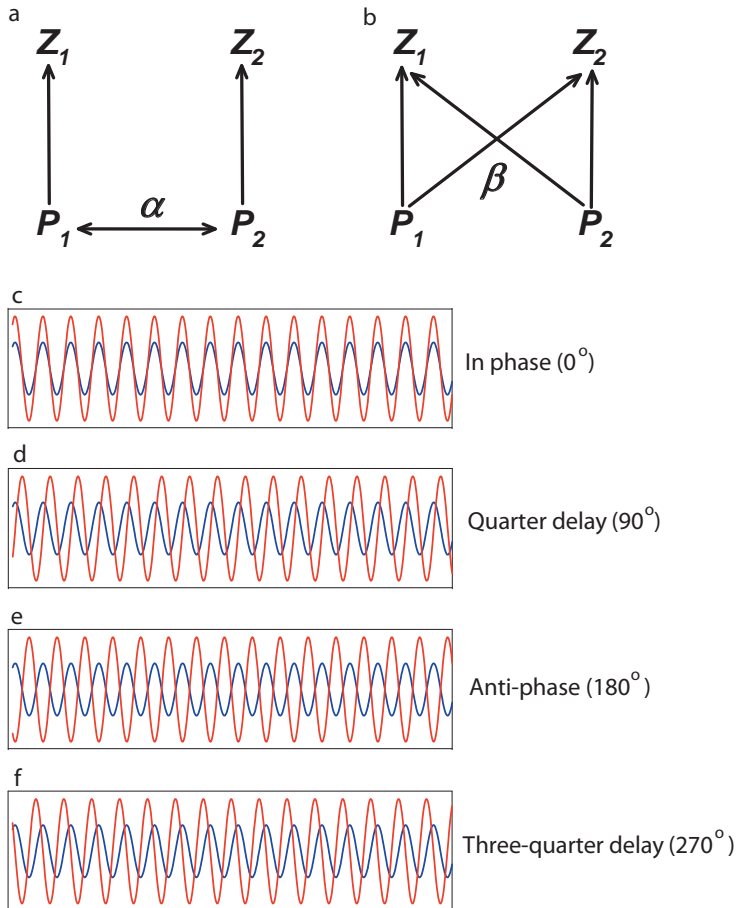


Figure 3.1: Coupling of two predator-prey systems. **a**, Coupling through competition: two specialist predators each feed on only one prey species, while the prey species (P_1 and P_2) interact through competition. The magnitude of the competition coefficient α is a measure of the strength of coupling. **b**, Coupling through predation: two generalist predators (Z_1 and Z_2) feed on both prey species. The magnitude of the selectivity coefficient β is a measure of the strength of coupling (note that high β implies low selectivity). **c-f**, Coupled oscillations may lead to different phase angles between the species fluctuations: **c**, in-phase oscillations (0°); **d**, quarter-delay oscillations (90°); **e**, anti-phase oscillations (180°); **f**, three-quarter-delay oscillations (270°).

competition (Huisman and Weissing 1999, 2001), tritrophic interactions (Hastings and Powell 1991), coupled predator-prey oscillations (Vandermeer 2004; Dakos et al.

2009), intraguild predation (Tanabe and Namba 2005), and the interplay between mixing and sinking of plankton populations (Huisman et al. 2006).

In this study, we compare the results of this long-term experiment with predictions of the coupled predator-prey model of Vandermeer (2004). For this purpose, we use a simple statistical test to establish whether the experimental time series is characterized by alternations in species dominance. In addition, we apply an advanced statistical technique, known as cross-wavelet analysis (Torrence and Compo 1998; Grinsted et al. 2004), to investigate the phase relationships between the dominant phytoplankton and zooplankton species. The analyses show that the chaotic ups and downs of the species are essentially driven by two coupled predator-prey cycles fluctuating largely in anti-phase. This presents the first experimental demonstration of two coupled oscillations in a chaotic food web.

3.2 Theory

Consider a simple food-web model consisting of two coupled predator-prey systems. Let P_1 and P_2 denote the two prey species, and Z_1 and Z_2 the two predator species. We assume that the prey species interact through Lotka-Volterra competition, and are consumed by the predators according to a saturating functional response. The model can then be written as (Rosenzweig and MacArthur 1963; Vandermeer 2004; Dakos et al. 2009):

$$\frac{dP_i}{dt} = r_i P_i \left(1 - \frac{\sum_j \alpha_{ij} P_j}{K_i} \right) - \sum_k \frac{g_k \beta_{ik} P_i}{H_k + \sum_j \beta_{jk} P_j} Z_k \quad i = 1, 2 \quad (3.1)$$

$$\frac{dZ_k}{dt} = \frac{g_k \sum_j \beta_{jk} P_j}{H_k + \sum_j \beta_{jk} P_j} Z_k - m_k Z_k \quad k = 1, 2 \quad (3.2)$$

Here, r_i is the specific growth rate of prey species i and K_i is its carrying capacity, the competition coefficients α_{ij} describe competition between the two prey species, g_k is the maximum specific grazing rate of predator species k and H_k is its half-saturation constant, β_{ik} is the selectivity coefficient of predator species k for prey species i (where $0 \leq \beta_{ik} \leq 1$), and m_k is the specific mortality rate of the predator species. Without loss of generality, we scale the model equations such that intraspecific competition equals unity ($\alpha_{11} = \alpha_{22} = 1$) and that predators have maximum selectivity for their preferred prey species ($\beta_{11} = \beta_{22} = 1$). For the purpose of illustration, we simplify the model by assuming symmetric competition between the prey species ($\alpha_{12} = \alpha_{21} = \alpha$) and symmetric selectivity of predators for their less-preferred prey species ($\beta_{12} = \beta_{21} = \beta$).

The coupling between the two predator-prey systems is now captured by two coefficients, α and β (Vandermeer 2004). If $\alpha = \beta = 0$, the prey species do not com-

pete and the predator species consume only their preferred prey species. The two predator-prey systems are thus independent of each other. If $\alpha > 0$, the prey species compete and we say that the two predator-prey systems are coupled through competition (Figure 3.1a). Conversely, if $\beta > 0$, both predators feed on both prey species. In this case, we say that the predator-prey systems are coupled through predation (Figure 3.1b).

3.3 Material and methods

3.3.1 Long-term experiment

We investigated coupled oscillations between predators and prey species in a long-term experiment with a plankton community isolated from the Baltic Sea (Heerkloss and Klinkenberg 1998; Benincà et al. 2008). Figure 3.2 shows the food-web structure of this plankton community. Phytoplankton was divided in three functional groups: picophytoplankton consisting of 1–2 μm picocyanobacteria (mostly *Synechococcus* species), nanophytoplankton consisting of 3–5 μm eukaryotic flagellates (mainly *Rhodomonas lacustris* Pascher and Ruttner), and large filamentous diatoms (*Melosira moniliformis* (O.F.M.) C. Agardh). Herbivorous zooplankton was also classified into three groups: protozoa (mainly large ciliates such as *Cyclidium* and *Strombidium* species), rotifers (mainly *Brachionus plicatilis* (O.F.M.)), and the calanoid copepod *Eurytemora affinis* (Poppe). Feeding relationships of the species are indicated by arrows in Figure 3.2. Previously, we assumed that rotifers fed mainly on nanoflagellates, and to a lesser extent on picocyanobacteria, based on the correlations between their species abundances (Benincà et al. 2008). However, the phase relationships reported in this paper (see Results) suggest that rotifers fed mainly on picocyanobacteria, and to a lesser extent on nanoflagellates. Rotifers and protozoa were eaten by cyclopid copepods. The microbial loop was represented by heterotrophic bacteria and two groups of detritivores (ostracods and harpacticoid copepods).

The experiment started on 31 March 1989, when the mesocosm was filled with a 10 cm sediment layer and 90 L of water from the Darss-Zingst estuary (southern Baltic Sea; 54° 26' N, 12° 42' E). This inoculum provided the plankton community for the entire experiment, which was maintained at a temperature of $\approx 20^\circ\text{C}$, salinity of $\approx 9\text{‰}$, incident irradiation of 50 $\mu\text{mol photons m}^{-2} \text{ s}^{-1}$ with a 16 hr : 8 hr light-dark cycle, and constant aeration for more than 8 years (Heerkloss and Klinkenberg 1998; Benincà et al. 2008). The population abundances of the species were counted twice a week, from 12 July 1990 until the experiment was terminated on 20 October 1997. From 23 November 1990 to 5 March 1991, however, the length of the light period was temporarily reduced from 16 to 12 hr per day (Heerkloss and Klinkenberg 1998). Wavelet analysis does not require stationary time series. Therefore, we decided to make use of the entire time series, including these few months with a reduced light period. This resulted in a time series of 2,657 days, which is 338 days

longer than the time series analyzed previously (Benincà et al. 2008). Further details of the mesocosm experiment are provided in Appendix A.1.

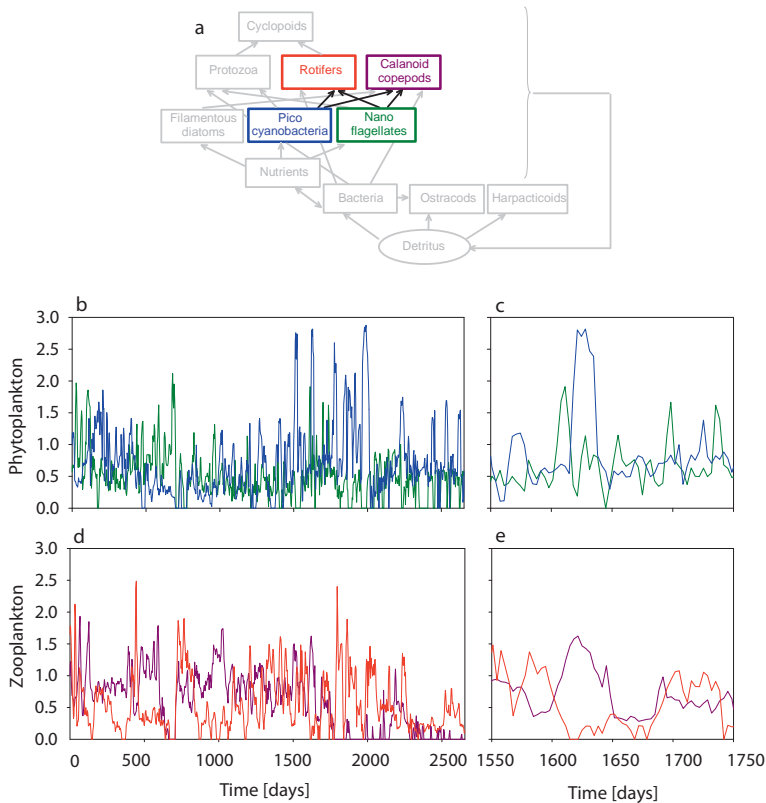


Figure 3.2: Experimental data. **a**, Food web structure of the mesocosm experiment. Our analysis focuses on coupled oscillations between picocyanobacteria (mainly *Synechococcus* spp.), nanoflagellates (mainly *Rhodomonas lacustris*), rotifers (mainly *Brachionus plicatilis*), and calanoid copepods (*Eurytemora affinis*). **b**, Time series of picocyanobacteria (blue) and nanoflagellates (green). **c**, Close-up of the species fluctuations shown in panel b. **d**, Time series of rotifers (red) and calanoid copepods (purple). **e**, Close-up of the species fluctuations shown in panel d. The time series were transformed by a fourth-root power transformation to suppress sharp peaks, and hence phytoplankton and zooplankton abundances are expressed as $(\text{mg fwt L}^{-1})^{1/4}$.

In this study, we are particularly interested in the phytoplankton and herbivorous zooplankton, because their ups and downs resembled typical predator-prey

oscillations (Benincà et al. 2008). Of these species, picocyanobacteria, nanoflagellates, rotifers and calanoid copepods were present in large numbers during the entire experiment, whereas the time series of filamentous diatoms and protozoa contained long sequences of zero values. This does not imply that filamentous diatoms and protozoa were completely absent from the food web, but at least their concentrations remained below the detection limit during most of the experimental period. We therefore focus specifically on picocyanobacteria, nanoflagellates, rotifers and calanoid copepods (Figure 3.2). We applied nearly the same data transformation as in Benincà et al. (2008). First, we interpolated each time series using cubic hermite interpolation, to obtain data with equidistant time intervals of 3.35 days. As a result, the time series contains 794 data points for each species. Next, the time series were rescaled by a fourth-root power transformation to suppress sharp peaks that may obscure less conspicuous periodicities. Contrary to Benincà et al. (2008) however, we did not detrend the time series, because wavelet analysis can handle non-stationary data.

3.3.2 Alternations in species dominance

We tested for alternations in species dominance simply by counting the number of times that a peak of one phytoplankton species was followed by a peak of the other phytoplankton species. Therefore, we searched all local maxima in the transformed time series of a species, and identified these local maxima as ‘peaks’ if they were at least 0.2 units higher than nearby local minima and at least 12 days spread apart. Our null hypothesis is that the species identity of peaks is randomly distributed. Hence, since both phytoplankton species had approximately the same number of peaks in the time series, the probability that two consecutive phytoplankton peaks are dominated by the same species would be 0.5. This can be tested against the alternative hypothesis that two consecutive peaks are more likely to be dominated by different species using the binomial distribution $B(n; 0.5)$, where n is the total number of phytoplankton peaks in the time series. The same test was applied to the two zooplankton species.

3.3.3 Wavelet analysis

We investigated the species fluctuations in further detail using wavelet analysis, a powerful statistical technique for the analysis of periodic signals in non-stationary time series (Torrence and Compo 1998; Cazelles et al. 2008). Traditionally, periodic signals in time series are analyzed by spectral analysis. However, classic spectral analysis requires stationary time series. This limits the applicability of spectral analysis, because many ecological time series are not stationary but display temporal changes in their trends and fluctuations. This limitation is overcome by wavelet analysis, which is specifically tailored for the analysis of non-stationary time series. Wavelet analysis decomposes local fluctuations observed during a small stretch of

time into a series of different frequencies (periods). This decomposition is based on a local wave function, known as the wavelet function, which captures the local fluctuations in terms of both their time and frequency (period). Thus, wavelet analysis allows investigation of changes in the frequency distribution of species fluctuations during time. Given its applicability to non-stationary data, wavelet analysis is rapidly becoming a popular tool for the analysis of ecological time series (Grenfell et al. 2001; Keitt and Fisher 2006; Ménard et al. 2007; Keitt 2008). Appendix B presents a simple example illustrating the basic idea of wavelet analysis.

Cross-wavelet analysis is an extension of wavelet analysis. It compares the wavelet power spectra of two time series (Grinsted et al. 2004). This enables detection of similarities in the local fluctuations of the two time series, and allows estimation of the phase angles between these fluctuations. This makes cross-wavelet analysis a very useful technique for the study of predator-prey oscillations. To identify significant results, we investigated whether the cross-wavelet spectra of two time series were significantly different (at the 0.05 level) from the cross-wavelet spectra of two independent red-noise processes with the same first-order autoregression coefficients as the time series (Appendix B; see also Grinsted et al. 2004). We used comparison against red noise, because the time series in our study showed a high degree of temporal autocorrelation (Gilman et al. 1963; Grinsted et al. 2004)

To investigate the robustness of our findings, we also applied a related method called wavelet coherence (Grinsted et al. 2004; Maraun and Kurths 2004). Wavelet coherence measures the coherence of the fluctuations in two time series by normalizing their cross-wavelet spectra by the product of the two single wavelet spectra. Thus, cross-wavelet analysis and wavelet coherence provide different perspectives on coupled fluctuations of two time series. While cross-wavelet analysis emphasizes the common power spectrum of two time series (i.e., the magnitude of the fluctuations), wavelet coherence emphasizes the correlations between the fluctuations of two time series (i.e., the coherence of the fluctuations). For more details on cross-wavelet analysis and wavelet coherence the interested reader is referred to Appendix B.

3.4 Results

3.4.1 Theoretical predictions

The model predicts that, if two predator-prey systems are coupled through predation only, the two prey species will fluctuate in phase (Figure 3.3a). In this specific case, with $\alpha=0$ and $\beta=0.0015$, the two prey species fluctuated at a periodicity of ≈ 40 days. Cross-wavelet analysis successfully captured these patterns (Figure 3.3b). Colour coding in the contour plots indicates the local power of the cross-wavelet spectra. Black contour lines enclose regions of greater than 95% confidence that the observed local cross-wavelet power exceeds the cross-wavelet power that would have been generated by two independent red-noise processes. Shaded areas on both sides of the contour plots represent the cone of influence, where edge effects might distort

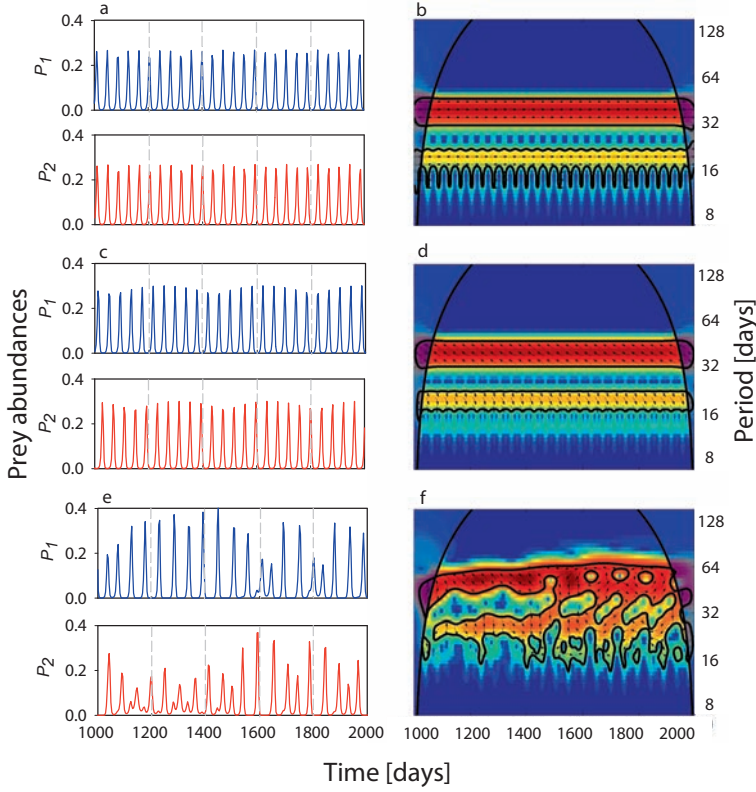


Figure 3.3: Model predictions. Time plots (left panels) and cross-wavelet spectra (right panels) of the two prey species, predicted by the model for various modes of coupling. **a-b**, In case of coupling through predation only ($\alpha=0, \beta=0.0015$), the two prey species oscillate in phase (phase angle of 0°). **c-d**, In case of coupling through competition only ($\alpha=0.075, \beta=0$), the two prey species oscillate almost in anti-phase (phase angle of 135°). **e-f**, Coupling through both competition and predation ($\alpha=1.5, \beta=0.1$) may lead to chaotic population dynamics with a range of different phase angles between the two prey species. The cross-wavelet power spectra are presented as contour plots, where the y-axis plots the common periodicities in the fluctuations of the two prey species, and the x-axis plots how these common periodicities change over time. Colour coding indicates the cross-wavelet power (ranging from low power in blue to high power in red), which is a measure of the relatedness between the fluctuations of the two prey species. Black contour lines enclose significant regions in the cross-wavelet power spectra (i.e., regions of greater than 95% confidence that the cross-wavelet power of the two prey species exceeds red noise). Arrows indicate the phase angles between the fluctuations of the two prey species, where arrows pointing to the right represent in-phase oscillations (0°) while arrows pointing to the left represent anti-phase oscillations (180°). Shaded areas on both sides of the contour plots represent the cone of influence, where edge effects might distort the signal. For more details on cross-wavelet analysis, see Appendix B. Parameter values used in the simulations: $r_1=r_2=1, K_1=K_2=1, m_1=m_2=0.1, g_1=g_2=1.5, H_1=H_2=0.8$. Initial conditions: $P_1=0.28, P_2=0.50, Z_1=0.14, Z_2=0.18$.

the signal. Therefore, we restrict our interpretation of the cross-wavelet spectrum to the non-shaded areas. According to the cross-wavelet spectrum, the two prey species fluctuated with high common power at a significant periodicity of 32-64 days (red band in Figure 3.3b). In addition, cross-wavelet analysis also points at a slightly less significant periodicity of 16-32 days (yellow band in Figure 3.3b), which is half the period of the actual fluctuations. Such harmonics are commonly observed in spectral analysis and wavelet analysis, if the waveform of the fluctuations is not perfectly sinusoidal. The arrows in the significant common power area all point to the right, which accurately reflect a phase angle of 0° between the fluctuations of the two prey species (Figure 3.3b). We also applied cross-wavelet analysis to all other species combinations in this food-web model. The results are summarized in Table 3.1. This shows that, analogous to the prey species, the two predator species also fluctuated in phase (i.e., at a phase angle of 0°), and that the prey species were tracked by fluctuations of the predators with a quarter delay (phase angle of 90°). A quarter delay between the fluctuations of predator and prey species is typical for many predator-prey models (e.g., Begon et al. 2006).

Coupling through competition only ($\alpha=0.075$, $\beta=0$) revealed a different pattern. In this case, the model predicts that the two prey species fluctuate almost in anti-phase (Figure 3.3c). Cross-wavelet analysis reveals that the two prey species fluctuate again at a significant periodicity of 32-64 days, but the arrows now indicate a phase angle of $\approx 135^\circ$ (Figure 3.3d, Table 3.1). Thus, interestingly, the oscillations produced by coupling through competition are not in perfect anti-phase (180°), but cover $3/8^{\text{th}}$ (i.e., 135°) of the full circle. The phase angle distribution of the two prey species also points at a less significant periodicity of 16-32 days with a phase angle centered around 290° (Figure 3.3d, Table 3.1), which is again explained by the non-sinusoidal waveform of the signal.

Models that include coupling through both competition and predation often display chaotic dynamics (Vandermeer 2004). In this case, the dynamics are still dominated by fluctuations with a periodicity of 32-64 days, but with clear variations in the phase relationships between the species (Figure 3.3e). This is confirmed by cross-wavelet analysis, which detects the dominant periodicity of the species fluctuations, and shows that the phase angles vary in all directions (Figure 3.3f). Still, some pattern in the distribution of the phase angles can be discerned. In this model example, coupling through competition was stronger than coupling through predation ($\alpha=1.5$, $\beta=0.1$), and therefore the chaotic fluctuations of the two prey species were quite often in anti-phase with a main phase angle at $\approx 135^\circ$ (Figure 3.3f; Table 3.1).

3.4.2 Experimental analysis

The mesocosm experiment showed strong fluctuations of the phytoplankton and zooplankton species (Figure 3.2). A close look at the phytoplankton fluctuations suggests alternating dominance of picocyanobacteria and nanoflagellates (Figure 3.2b,c). To quantify this observation, we identified the species composition of all local phyto-

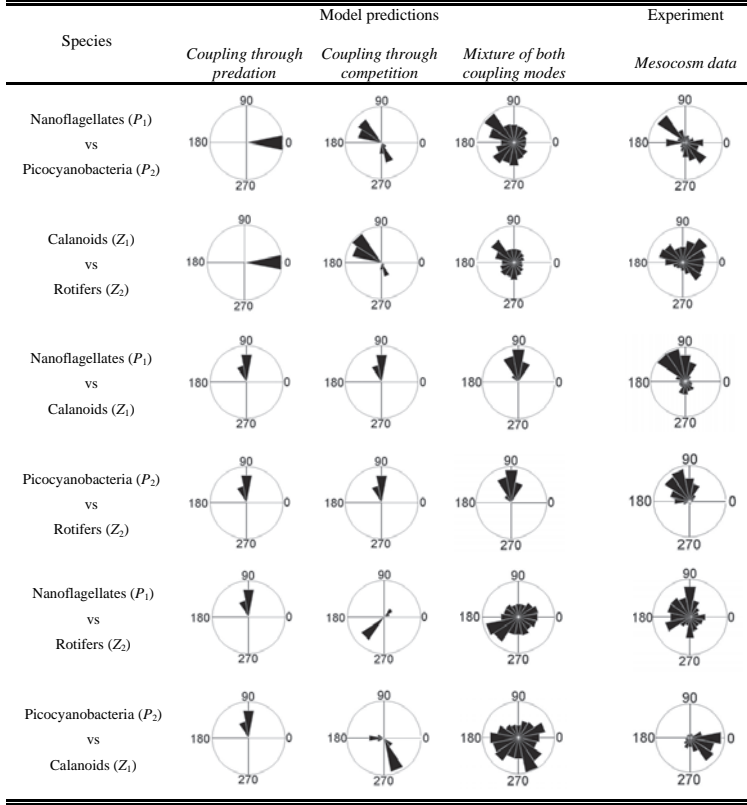


Table 3.1: Relative frequency distributions of the phase angles between the fluctuating species. The relative frequency distributions are obtained from cross-wavelet spectra of the model predictions (Figure 3.3) and experimental data (Figure 3.4). We selected all phase angles located within significant regions of the cross-wavelet spectra but outside the cone of influence. The second, third, and fourth column show the phase angles predicted by the model, assuming coupling through predation ($\alpha=0$; $\beta=0.0015$), coupling through competition ($\alpha=0.075$; $\beta=0$), and the combination of both modes of coupling that gave the best fit between model predictions and experimental data ($\alpha=1.5$; $\beta=0.1$), respectively. The fifth column shows the phase angles detected in the experimental data.

plankton peaks in the time series. This yielded 118 cases in which the phytoplankton species composition of consecutive peaks alternated between picocyanobacteria and nanoflagellates, and only 34 cases in which the phytoplankton species composition of consecutive peaks remained the same. These alternations in species composition deviate significantly from the null hypothesis that the peaks of picocyanobacteria and nanoflagellates are randomly distributed (i.e., the probability of drawing 118 or

more cases from the binomial distribution $B(152; 0.5)$ is $p < 0.001$). We found similar patterns in the zooplankton community (Figure 3.2d,e), with 69 cases in which the zooplankton species composition of consecutive peaks alternated between rotifers and calanoid copepods, but only 33 cases in which the zooplankton species composition of consecutive peaks remained the same. Again, this pattern of alternating species composition deviates significantly from the null hypothesis that the peaks of rotifers and calanoid copepods are randomly distributed (the probability of drawing 69 or more cases from $B(102; 0.5)$ is $p < 0.001$).

As a next step, we investigated the species fluctuations using cross-wavelet analysis. The cross-wavelet spectrum shows that nanoflagellates and picocyanobacteria displayed coupled fluctuations with a significant periodicity of 32-64 days during the time periods from 1300 to 1700 days and from 1900 to 2100 days (Figure 3.4a). Arrows in significant regions of the cross-wavelet spectrum point at anti-phase fluctuations of nanoflagellates and picocyanobacteria, characterized by a main phase angle at $\approx 135^\circ$ and an additional phase angle at $\approx 315^\circ$. Both phase angles were also predicted by the model if the predator-prey systems would be coupled through competition (Table 3.1). Calanoid copepods and rotifers displayed coupled oscillations with a significant periodicity of 16-64 days from day 500 to day 1700 (Figure 3.4b). Significant regions in their cross-wavelet spectrum reveal a wide distribution of different phase angles, with dominant phase angles at $\approx 45^\circ$ and at 135° - 157° . The latter angle is close to the phase angle predicted for predator-prey systems coupled through competition (Table 3.1).

Phase angles of picocyanobacteria versus rotifers and of nanoflagellates versus calanoid copepods pointed at 90° - 135° (Figure 3.4c,d; Table 3.1). Thus, we observed roughly a quarter delay between fluctuations of predators and their preferred prey species, consistent with the phase angle of 90° predicted by the model irrespective of the mode of coupling. Rotifers and their less-preferred prey (nanoflagellates) also showed coupled oscillations; their phase angles point to a range of different directions, but phase angles at $\approx 90^\circ$ and $\approx 202^\circ$ seem dominant (Figure 3.4e; Table 3.1). Interestingly, the phase angle of $\approx 90^\circ$ is consistent with coupling through predation, while the phase angle of 202° is consistent with coupling through competition. The phase angles of calanoid copepods and their less-preferred prey (picocyanobacteria) are far from the phase angle of 90° predicted by coupling through predation, but close to the phase angle of 293° predicted by coupling through competition (Figure 3.4f; Table 3.1).

Time series analysis by wavelet coherence demonstrated significant coherence in the species fluctuations during at least part of the time series (Figure B.4 in Appendix B), meaning that the ups and downs of the different species in the plankton community were indeed related with each other. Moreover, wavelet coherence detected similar phase angles between the species fluctuations as cross-wavelet analysis (Table B.1). This confirms the consistency of our results.

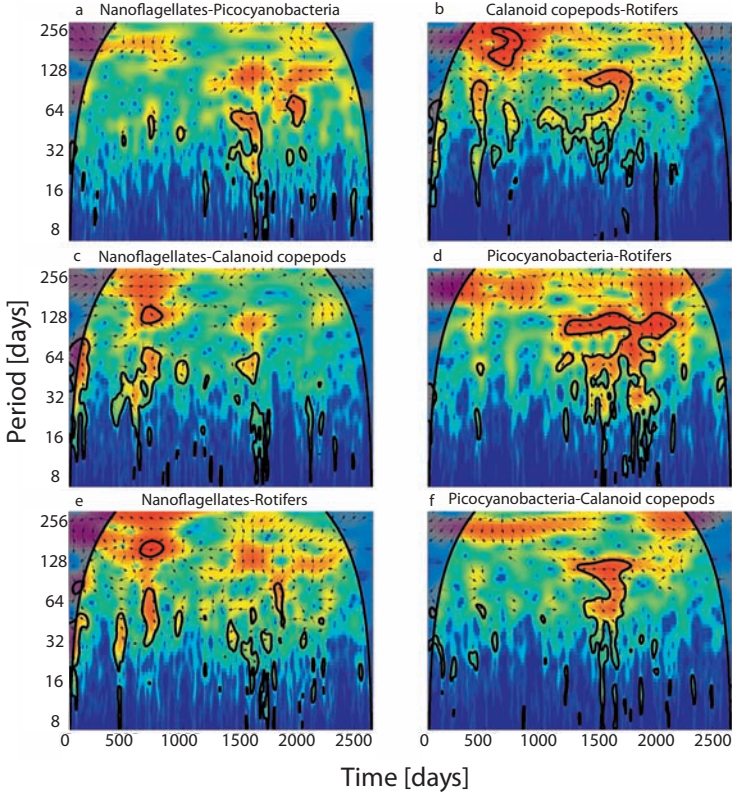


Figure 3.4: Cross-wavelet spectra of the experimental data. **a**, Nanoflagellates versus picocyanobacteria (P_1 vs P_2); **b**, Calanoid copepods versus rotifers (Z_1 vs Z_2); **c**, Nanoflagellates versus calanoid copepods (P_1 vs Z_1); **d**, Picocyanobacteria versus rotifers (P_2 vs Z_2); **e**, Nanoflagellates versus rotifers (P_1 vs Z_2); **f**, Picocyanobacteria versus calanoid copepods (P_2 vs Z_1). Colour coding indicates the cross-wavelet power, while arrows indicate the phase angles between the fluctuations of the two time series (as in Figure 3.3). Black contour lines enclose significant regions in the cross-wavelet power spectra. Shaded areas on both sides of the contour plots represent the cone of influence, where edge effects might distort the signal (see Appendix B).

3.4.3 Comparison between theoretical predictions and experimental data

To investigate these patterns in further detail, we ran many model simulations using different strengths of coupling (i.e., different combinations of α and β). More specifically, we screened the entire parameter space that allowed coexistence of all four

species in the model ($0 \leq \alpha \leq 1.5$ and $0 \leq \beta \leq 0.7$; see Figure 6 in Vandermeer (2004), with a resolution of 0.05 for both α and β , and calculated the relative frequency distribution of the phase angles predicted by the model for each point in parameter space. We then minimised the total Euclidean distance between the phase angles predicted by the model and the phase angles derived from the experimental data to find the parameter values that gave the best fit. The best fit of the model to the experimental data was obtained for $\alpha=1.5$ and $\beta=0.1$ (compare columns 4 and 5 in Table 3.1). Interestingly, for these parameter values, the model simulations show considerable variation in the phase angles between the fluctuating species, even though the main phase angles still point at coupling through competition (Table 3.1). More specifically, the model predicts chaos for this parameter combination of strong coupling through competition (high α) but weak coupling through predation (low β), consistent with the chaotic dynamics observed in the experiment.

3.5 Discussion

It is well known from classic ecological theory that predator-prey interactions can generate oscillations (Lotka 1925; Volterra 1926; Rosenzweig and MacArthur 1963). The existence of predator-prey oscillations predicted by theory has been confirmed by many laboratory experiments and field observations. Textbook examples of predator-prey oscillations include the famous hare-lynx cycles in northern Canada (Elton and Nicholson 1942; Stenseth et al. 1997), Huffaker's (1958) experiments with herbivorous and predatory mite species, and several laboratory experiments with microbial predator and prey species (Gause 1934; Luckinbill 1973; Fussmann et al. 2000; Yoshida et al. 2003; Becks et al. 2005). Food webs typically contain multiple predator and prey species. Thus, food webs provide many opportunities for coupled oscillations driven by the interplay between several predator-prey cycles. Yet, coupled oscillations of multiple predator and prey species have thus far received surprisingly little attention in experimental studies.

Theory predicts that coupled predator-prey oscillations can generate complex dynamics, including chaos (Vandermeer 1993, 2004; Dakos et al. 2009). Yet, coupled predator-prey oscillations do not provide the only source of chaos in population dynamics. Models predict that chaos can also be generated by a plethora of other mechanisms, including multispecies competition (Huisman and Weissing 1999, 2001), tritrophic food chains consisting of a prey, predator and top-predator (Hastings and Powell 1991), intraguild predation (Tanabe and Namba 2005), and the interplay between mixing and sinking of plankton populations (Huisman et al. 2006). Which of these mechanisms are most relevant for the generation of chaos in natural communities is an important but, as yet, unanswered question. In our experimental system, however, the focus on two coupled predator-prey oscillations arises quite naturally, because the phytoplankton and herbivorous zooplankton were each dominated by two species (picocyanobacteria and nanoflagellates in the phytoplankton, rotifers

and calanoid copepods in the herbivorous zooplankton), and their ups and downs resembled typical phytoplankton-zooplankton oscillations (Benincà et al. 2008).

Although our study presents the first experimental analysis of two coupled predator-prey oscillations, it has several limitations. First, the population dynamics of the phytoplankton and herbivorous zooplankton species investigated in this paper were embedded in a larger food web, including a top-predator (cyclopoid copepods of the *Eucyclops* genus) and a microbial loop (Benincà et al. 2008). We do not know to what extent the coupled oscillations between our focal species may have been influenced by interactions with these other food-web components. Second, the phytoplankton and zooplankton species in our study will probably have shown considerable intraspecific variation, since the organisms were not obtained from well-defined laboratory clones but were simply scooped up from sea. In addition, calanoid copepods have stage-structured life cycles consisting of naupliar, copepodid and adult stages, and may feed on different prey at different life stages. It is well-known that genetic variation or phenotypic plasticity within prey species (Abrams and Matsuda 1997; Yoshida et al. 2003; Vos et al. 2004) and stage-structured variation within predator species (De Roos et al. 2003; McCauley et al. 2008) can affect the stability of predator-prey interactions, and may modify the phase relationships between predator and prey species.

Despite these limitations, statistical analysis revealed that the time series showed persistent alternations in species dominance. The phytoplankton species composition switched between picocyanobacteria and nanoflagellates, while the zooplankton species composition shifted back and forth between rotifers and calanoid copepods. Moreover, cross-wavelet analysis and wavelet coherence were able to detect significant phase relationships between the ups and downs of the phytoplankton and zooplankton species (Figure 3.4, Figure B.4). The time periods with a significant signal covered only a limited part of the time series. However, since the total time series spanned more than 2,600 days, the significant signal still covered several hundred days, which is longer than the entire duration of many earlier experimental studies of predator-prey oscillations. During these significant periods, we observed a quarter delay between fluctuations of the predators and their preferred prey species (Table 3.1). Moreover, the two phytoplankton groups fluctuated in anti-phase (at $\approx 135^\circ$; Table 3.1), confirming the alternations in species dominance of the phytoplankton. The two zooplankton groups also seemed to fluctuate largely in anti-phase, although for them the pattern was less clear. Comparison between theory and experiment shows that these phase relationships are representative of two coupled predator-prey cycles, with strong coupling through competition but weak coupling through predation (Table 3.1).

This food-web structure is consistent with the size structure of our experimental plankton community. Irrespective of their size, all phytoplankton species compete for the same resources, viz. nutrients and light. Hence, resource competition among phytoplankton species promotes strong coupling through competition. However, small phytoplankton (picocyanobacteria, in our study) are mainly eaten by small

zooplankton (rotifers), whereas larger phytoplankton (nanoflagellates) are eaten by larger zooplankton (calanoid copepods). These size differences restrict overlap in the diet of the zooplankton species, which results in weak coupling through predation. Interestingly, comparison of the observed and predicted phase relationships showed that the model parameters yielding the best fit to the experimental data actually predict chaos. This is in agreement with previous analysis, which demonstrated chaos in this food web using a completely independent approach (Benincà et al. 2008). The general picture thus emerging from these findings is that the size structure of the plankton in our experimental food web has resulted in two parallel food chains, one of them consisting of small zooplankton specialized on small phytoplankton and the other of larger zooplankton specialized on larger phytoplankton. The two parallel food chains are weakly coupled through predation, but strongly coupled through phytoplankton competition. Coupling of the predator-prey oscillations in these two parallel food chains has, in turn, contributed to the chaotic nature of the species fluctuations.

Intuitively, it is straightforward to understand why this food-web structure, with two predator species specialized on different prey species, leads to continued alternations in species dominance. In essence, coexistence of prey species is achieved through a non-equilibrium version of the ‘killing-the-winner’ mechanism (Thingstad and Lignell 1997; Thingstad 2000). Every time one of the prey species tends to dominance, its key predator shows up, suppresses further population development, and thereby swings the competitive balance to the other prey species. For instance, if picocyanobacteria are abundant, the rotifer population will increase and will suppress the picocyanobacteria. Hence, nanoflagellates can gain a competitive advantage, and will displace the picocyanobacteria. This will benefit the calanoid copepods, which rise in abundance, and subsequently suppress the nanoflagellates. This, in turn, gives new opportunities for picocyanobacteria to seize the available resources. In this way, the system rocks back and forth between the two predator-prey cycles. These non-equilibrium dynamics prevent competitive exclusion, and could therefore play an important role in the maintenance of biodiversity (Huisman and Weissing 1999; Vandermeer 2006; Brose 2008). It would be intriguing to learn whether similar patterns of alternating species dominance can also be observed in other food webs.

Acknowledgements

We thank Gilbert Compo, Christopher Torrence and Aslak Grinsted for helpful feedback on the wavelet analysis, Tom van Engeland, Marten Scheffer, Egbert van Nes and Mercedes Pascual for useful discussions, and the anonymous reviewers for their helpful comments on the manuscript. The investigations of E.B., K.D.J. and J.H. were supported by the Earth and Life Sciences Foundation (ALW), which is subsidized by the Netherlands Organization for Scientific Research (NWO).

Chapter 4

Interannual variability in species composition explained as seasonally entrained chaos

Abstract

The species composition of plankton, insect and annual plant communities may vary markedly from year to year. Such interannual variability is usually thought to be driven by year-to-year variation in weather conditions. Here we examine an alternative explanation. We studied the effects of regular seasonal forcing on a multispecies predator-prey model consisting of phytoplankton and zooplankton species. The model predicts that interannual variability in species composition can easily arise without interannual variability in external conditions. Seasonal forcing increased the probability of chaos in our model communities, but squeezed these irregular species dynamics within the seasonal cycle. As a result, the population dynamics had a peculiar character. Consistent with long-term time series of natural plankton communities, seasonal variation led to a distinct seasonal succession of species, yet the species composition varied from year to year in an irregular fashion. Our results suggest that interannual variability in species composition is an intrinsic property of multispecies communities in seasonal environments.

4.1 Introduction

Aquatic and terrestrial communities are often characterized by a complex wax and wane of species driven by the seasonal cycle. Plankton communities show some regularity in the form of an annually recurring spring bloom. Yet, the height, timing, and

This chapter is based on the paper: Dakos, V., Benincà, E., van Nes, E.H., Philippart, C.J.M., Scheffer, M. and Huisman, J. 2009. Interannual variability in species composition explained as seasonally entrained chaos. *Proceedings of the Royal Society of London B.* **276**, 2871-2880.

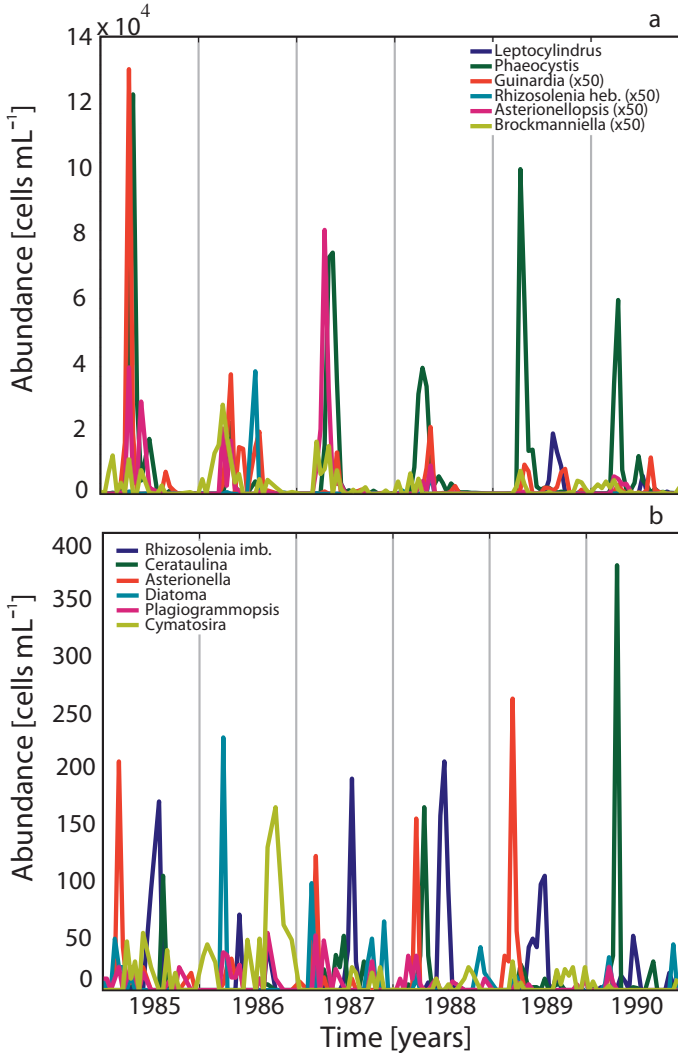


Figure 4.1: Time series (bi-weekly averages) of marine phytoplankton species in the Marsdiep tidal inlet between the North Sea and Wadden Sea, the Netherlands, from January 1985 to December 1990. Different species are depicted by different colors, viz. *Leptocylindrus minimus*, *Phaeocystis globosa*, *Guinardia delicatula*, *Rhizosolenia hebetata*, *Asterionellopsis glacialis*, *Brockmanniella brockmannii* in top graph, and *Rhizosolenia imbricata*, *Cerataulina pelagica*, *Asterionella kariana*, *Diatoma elongatum*, *Plagiogrammopsis vanheurckii* and *Cymatosira belgica* in bottom graph. Details of sampling and counting are described in Philippart et al. (2000).

species composition of the spring bloom often vary strongly from year to year (Figure 4.1; see also Talling 1993; Harris and Baxter 1996; Smayda 1998; Philippart et al. 2000). Similar year-to-year variability in species composition has been observed in multispecies communities of insects (Wolda 1988; Raimondo et al. 2004), soil fauna (Giller and Doube 1994; Berg et al. 1998) and annual plants (Guo et al. 2002). Often, this interannual variability in species composition is attributed to year-to-year variation in weather conditions (i.e., exceptionally cold winters, wet springs, or hot summers). However, mathematical models (Hastings and Powell 1991; Vandermeer 1993; Huisman and Weissing 1999; Brose 2008) and laboratory experiments (Becks et al. 2005; Graham et al. 2007; Benincà et al. 2008) have shown that interactions between species may generate striking chaotic fluctuations in species abundances even without external forcing. One might therefore hypothesize that interannual variability in species composition may not require year-to-year variation in weather conditions. Interannual variability could be an intrinsic property of multispecies communities in seasonal environments. To investigate this hypothesis, it is interesting to assess to what extent complex dynamics in multispecies communities are modified by the seasonal cycle.

The effects of regular seasonal variation on population models of two or three interacting species have been studied extensively (Kot and Schaffer 1984; Doveri et al. 1993; Rinaldi et al. 1993; Steffen et al. 1997; Huppert et al. 2005). These studies have shown that periodically forced populations can display a rich repertoire of dynamical behaviours, including simple and complex periodic cycles, quasi-periodicity, and chaos (Rinaldi et al. 1993; King and Schaffer 1999; Vandermeer et al. 2001). However, the parameter space in which chaotic behaviour occurs is usually small. Typically, the population dynamics show repeatable patterns. Slow-growing species may fluctuate on seasonal or multi-annual time scales, as exemplified by the famous cycles of voles and lemmings at northern latitudes (Stenseth 1999; Turchin 2003). Fast-growing species, such as bacteria or plankton, may display multiple ups and downs per year. The frequency of the population fluctuations can be remarkably persistent as a result of frequency-locking (e.g., Scheffer et al. 1997; Vandermeer et al. 2001). Seasonal forcing tends to ‘lock’ the frequency of population oscillations, such that populations oscillate at the same frequency as the seasonal cycle or integer multiples of it.

While many theoretical studies have examined effects of seasonality on model systems of only a few species, seasonal forcing of multispecies communities has received surprisingly little theoretical attention (but see Ebenhöh 1992). Yet, bacterial, plankton, and insect communities may contain tens, hundreds, and sometimes even thousands of species (Hutchinson 1961; Erwin 1982; Irigoien et al. 2004; Venter et al. 2004). Generally speaking, multispecies models display more complex dynamics than models with two or three species only (May 1973; Ellner and Turchin 1995; Huisman and Weissing 2001). From a conceptual perspective, multispecies food webs can be interpreted as systems with several interacting oscillations (e.g., several predator-prey cycles). Coupled oscillations are known to generate complex dynam-

ics, including chaos (Hastings and Powell 1991; Vandermeer 1993, 2004; Huisman and Weissing 2001; Benincà et al. 2008). The prevalence of complex dynamics is of interest, because these non-equilibrium dynamics may help to sustain the biodiversity of natural communities (Armstrong and McGehee 1980; Huisman and Weissing 1999; Brose 2008), and also because complex dynamics can induce regime shifts in ecosystems with important implications for their management (Scheffer et al. 2001; Hsieh et al. 2005; Ives et al. 2008).

Here, we study the effect of seasonal forcing on the dynamics of a multispecies predator-prey model, using phytoplankton and zooplankton as our model organisms. We use this model to assess to what extent a regular seasonal cycle will modify chaos in multispecies communities. Our results show that regular seasonal forcing can promote year-to-year variability in species composition. In addition, our results suggest that this interannual variability in species composition is affected by ecosystem productivity in a manner analogous to Rosenzweig's (1971) classical paradox of enrichment.

4.2 Methods

4.2.1 Model description

We study a minimal model that is sufficiently complex to investigate the impact of seasonal forcing on multispecies communities, yet sufficiently simple to produce generic insights. The model is based on a straightforward multispecies version of the classical Rosenzweig-MacArthur predator-prey model (Rosenzweig and MacArthur 1963; Vandermeer 1993; van Nes and Scheffer 2004), extended with seasonal forcing (Rinaldi et al. 1993; Scheffer et al. 1997). In our interpretation, the model represents a plankton community, although our findings can probably be generalized to other multispecies communities in which organisms have fast growth rates and short generation times compared to the length of the growing season (e.g., microbial food webs, soil fauna, tropical insects). Let P_i and Z_k denote the population abundances of phytoplankton species i and zooplankton species k , respectively. Then, the model reads:

$$\frac{dP_i}{dt} = \sigma(t)r_iP_i \left(1 - \frac{\sum_j (\alpha_{ij}P_j)}{\sigma(t)K_i} \right) - \sum_k \left(\sigma(t)g_kZ_k \frac{S_{ik}P_i}{\sum_j (S_{jk}P_j) + H_k} \right) + u \quad (4.1)$$

$$\frac{dZ_k}{dt} = \sigma(t)e_kg_kZ_k \left(\frac{\sum_j (S_{jk}P_j)}{\sum_j (S_{jk}P_j) + H_k} \right) - \sigma(t)m_kZ_k + u \quad (4.2)$$

$$\sigma(t) = 1 - a \cos \frac{2\pi t}{365} \quad (4.3)$$

The phytoplankton species (Eq. 4.1) grow logistically with maximum specific growth rates r_i , carrying capacities K_i , and competition coefficients α_{ij} to describe competition between species. The phytoplankton species are consumed by zooplankton species, as described by a multispecies functional response (of Holling type II) with a fixed half-saturation constant H_k and maximum grazing rate g_k . Selective predation (Chesson 1978) is introduced through the selectivity coefficient S_{ik} of zooplankton species k for phytoplankton species i and it can take values between 0 and 1, indicating the preference of the predator for its prey (van Nes and Scheffer 2004). The factor u accounts for small levels of immigration and it is introduced to reduce the probability of heteroclinic cycles. Heteroclinic cycles are considered mostly biologically unrealistic, since species reach extremely low population abundances during these cycles without going extinct (May and Leonard 1975). The zooplankton species (Eq. 4.2) grow on the consumed phytoplankton with an assimilation efficiency e_k , suffer a mortality rate m_k , and immigrate at a small rate u similar to the phytoplankton.

Many biological parameters are sensitive to seasonal forcing. One might thus argue that seasonal forcing should be applied to all model parameters, perhaps with different parameters affected by seasonality in different ways depending on the species. However, this would yield a rather complex model, while we aim at a simple model that captures the essence of multispecies dynamics in a seasonal environment. Accordingly, we choose a simple way to incorporate seasonal forcing following earlier contributions (Doveri et al. 1993; Scheffer et al. 1997). In particular, seasonal variation in temperature and light conditions has a major impact on the growth rates and mortality rates of plankton species (Raven and Geider 1988; Litchman and Klausmeier 2001), and on the seasonal development of total plankton biomass (Sommer et al. 1986; Longhurst 2006). We therefore assume that seasonal fluctuations in the species' growth rates, mortality rates, and carrying capacity (r_i , K_i , g_k , m_k) can be described by a sinusoidal forcing function $\sigma(t)$ (Eq. 4.3), which can be interpreted as the environmental forcing imposed by seasonal variation in temperature or light. Factor a determines the amplitude of the seasonal forcing (Rinaldi et al. 1993) and takes values between 0 and 1. The cosine function is chosen to produce maximum rates in summer and minimum rates in winter ($t=0$ is January 1st), and the period is set to 365 days (Scheffer et al. 1997).

4.2.2 Parameterization

We parameterized the model for 10 competing phytoplankton species ($i=1, \dots, 10$) grazed by 6 zooplankton species ($k=1, \dots, 6$). The parameter values assigned to the different species were selected from the ranges indicated in table 1, which are representative for plankton communities (Scheffer et al. 1997; Reynolds 2006). Phytoplankton intraspecific competition was set to unity ($\alpha_{ii}=1$ for all i), while the interspecific competition coefficients (α_{ij}) were drawn randomly from the interval (0.5, 1.5). Differences in grazing rate were introduced through the selectivity

Symbol	Interpretation	Range	Units
r_i	Maximum specific growth rate of phytoplankton	0.2–2	d ⁻¹
α_{ij}	Competition coefficient among phytoplankton species i and j	0.5–1.5	–
g_k	Maximum grazing rate of zooplankton	0.4	d ⁻¹
S_{ik}	Selectivity coefficient of zooplankton	0–1	–
H_k	Half-saturation constant of zooplankton	0.9–1.5	mg L ⁻¹
e_k	Assimilation efficiency of consumed phytoplankton	0.6–0.9	–
m_k	Mortality rate of zooplankton	0.1–0.2	d ⁻¹
u	Immigration rate	10 ⁻⁷	mg L ⁻¹ d ⁻¹
K	Carrying capacity of phytoplankton	2–10	mg L ⁻¹
a	Amplitude of seasonal forcing	0–1	–

Table 4.1: Parameter ranges used in the model simulations. (Note: The exact parameter values of each individual simulation presented in the figures are given in the Appendix C).

coefficients S_{ik} , which were drawn randomly from the interval (0, 1) to create a food web of generalists where predators utilize prey species with average selectivity $S_{avg,k} = \sum_i \frac{S_{ik}}{10} = 0.5$. We assumed that the carrying capacities of all phytoplankton species are the same (i.e., $K_i=K$ for all species i) following the rationale that K is an environmental parameter reflecting the local nutrient and light conditions.

We analyzed the model without seasonal forcing ($a=0$) and with seasonal forcing ($0 < a < 1$); the time-averaged parameter values in the model simulations with seasonal forcing were equal to the fixed parameter values used in the model simulations without seasonal forcing. We investigated the model communities at different levels of productivity ($K=2, 5, 10, 20, 50$ mg L⁻¹), to compare the species dynamics in oligotrophic and eutrophic conditions.

4.2.3 Assessment of complex dynamics

We assessed how frequent the model communities displayed chaos and we calculated the corresponding values of the Lyapunov exponent by assembling 100 randomly generated model communities for every model scenario that we investigated. For this purpose, the parameter values of the 6 predator and 10 prey species in each model community were drawn randomly from uniform distributions covering the ranges indicated in Table 4.1, and the initial biomasses of the species were drawn randomly from the interval (0, 10 mg L⁻¹). The model communities were first simulated for 1,000 years to ensure that the population dynamics had reached an attractor. Thereafter, we continued the model simulation for another 40 years, we calculated the Lyapunov exponent, and determined the nature of the attractors as

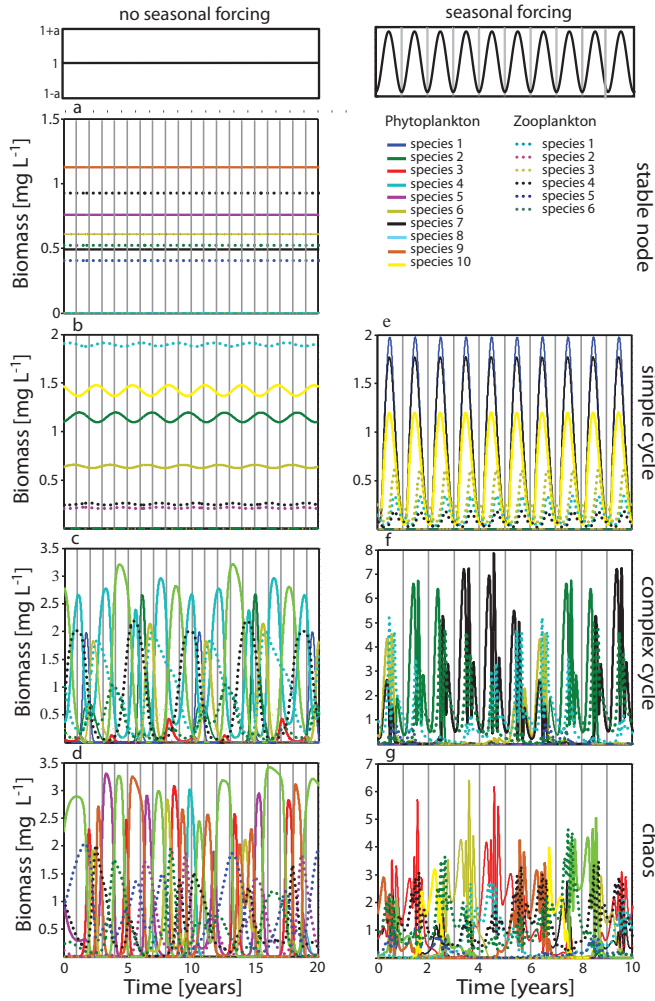


Figure 4.2: Community dynamics predicted by the model. The two top panels indicate the nature of the environmental forcing. Without seasonal forcing, the model produces **a**, stationary equilibria, **b**, simple cycles, **c**, complex periodic cycles, or **d**, chaotic dynamics. With seasonal forcing, the model produces a similar repertoire of attractors: **e**, simple cycles, **f**, complex periodic cycles (in this example a periodicity of 6 years), or **g**, chaotic dynamics, all entrained by seasonal forcing. Parameter values are given in Appendix C.

stable, simple periodic (period-one limit cycles), complex periodic (multiple-period cycles), quasiperiodic, and chaotic. The Lyapunov exponent quantifies the rate

of exponential divergence (or convergence) of nearby trajectories (Strogatz 1994; Sprott 2003). A positive Lyapunov exponent indicates chaos, and its magnitude is a measure of the system's sensitivity to initial conditions. Our calculation of the Lyapunov exponent is explained in the Appendix C. We used visual inspection and Poincaré maps as additional methods to verify the computed nature of the attractors or to check for undetermined cases. All simulations were carried out in MATLAB using our software package GRIND (freely available at <http://www.dow.wau.nl/aew/grind>).

4.3 Results

Without seasonal forcing, the model predicts various kinds of asymptotic regimes, including stable equilibria (Figure 4.2a), simple limit cycles (Figure 4.2b), complex periodic cycles (Figure 4.2c), and chaos (Figure 4.2d). At first sight, seasonal forcing seems to have little influence on the dynamical repertoire of the model. With seasonal forcing, the model also displays simple limit cycles (Figure 4.2e), complex periodic cycles (Figure 4.2f), and chaos (Figure 4.2g). However, a closer look reveals differences between the model behavior with and without seasonal forcing. With seasonal forcing, the periodic solutions are 'locked' within the seasonal cycle, i.e. the same pattern repeats each year (Figure 4.2e) or after some years (Figure 4.2f). In addition, the model can also produce quasi-periodic cycles, where solutions are entrained within the seasonal cycle yet never repeat themselves as they slightly shift phase every year. Chaotic communities seem to experience similar seasonal patterns. However, the fluctuations of phytoplankton and zooplankton species in chaotic communities remain irregular even when entrained in a regular seasonal environment (Figure 4.2g).

These dynamics can be illustrated by Poincaré maps sampling the model communities once per year for many consecutive years. Model communities with a periodicity of one year return to exactly the same species composition year after year, which appears as a single point on the Poincaré map. Communities with a periodicity of N years produce N points on the Poincaré map, quasi-periodicity produces a closed curve (Figure 4.3a), while chaos produces a complex fractal structure (Figure 4.3b).

Many of the model communities exposed to seasonal forcing displayed chaos with remarkable synchronization patterns at the species level (Figure 4.4). The species fluctuations are irregular, yet these irregular fluctuations are squeezed within the seasonal cycle. As a consequence, each fall species enter the winter season in different proportions, and this affects the species composition of the next spring bloom. For instance, Figure 4.4a shows a typical phytoplankton spring species. It reaches peak abundance in March, although its peak abundance varies from year to year, and some years it does not peak in spring at all. Figure 4.4b shows another phytoplankton species from the same plankton community. This species could be called a typical

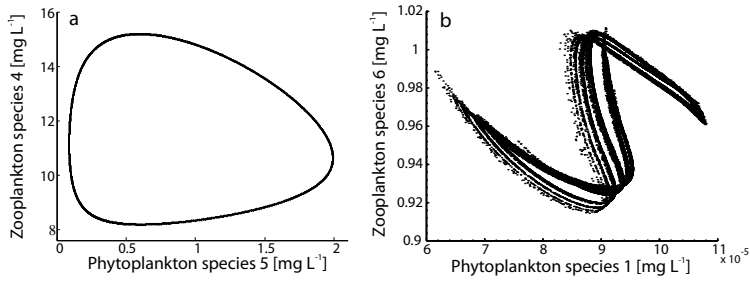


Figure 4.3: Poincaré maps with annual snapshots of the model community collected over many years. More specifically, the maps plot the biomasses of two plankton species sampled from the model community at the 1st of January of each year for 100,000 years. **a**, Poincaré map of a quasi-periodic model community. **b**, Poincaré map of a chaotic model community. Parameter values for both panels are given in the Appendix C.

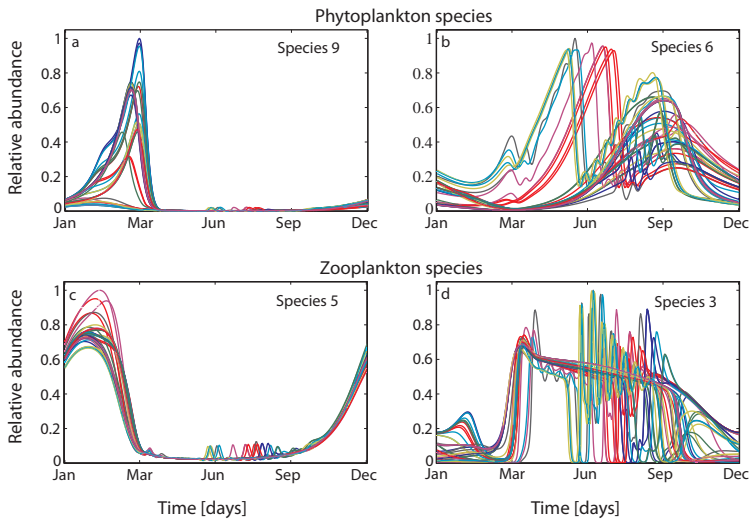


Figure 4.4: Year-to-year variability in the population dynamics of **a**, **b**, two phytoplankton species and **c**, **d**, two zooplankton species. All four species are from the same model community, simulated for a total period of 40 years. Each colored line corresponds to a different year. The abundances of the species are scaled relative to their maximum abundance observed during the entire simulation period. Parameter values are given in Appendix C.

Model assumptions	Occurrence of chaotic dynamics (%)	
	No seasonality ($a=0$)	Seasonality ($a=0.7$)
Reference model (competition and predation, $K=10$)	54	56
Competition		
interspecific > intraspecific ($\alpha_{ij} > 1; \alpha_{ii} = 1$)	41	46
interspecific < intraspecific ($\alpha_{ij} < 1; \alpha_{ii} = 1$)	41	55
Predation		
no zooplankton predation ^a	0	4
inefficient zooplankton predation ^b	4	28
specialist zooplankton predation ^c	11	38
Productivity, K (mg L ⁻¹)		
2	3	14
5	23	59
10 (=reference model)	54	56
20	36	48
50	15	27
Seasonal forcing		
forcing on phytoplankton only	n.a.	52
forcing on zooplankton only	n.a.	66

Table 4.2: Occurrence of chaos in our simulated communities under different model assumptions. The first row shows the percentage of chaotic communities predicted by the reference model used in our study, both without seasonal forcing ($a=0$) and with seasonal forcing ($a=0.7$).

^a Zooplankton absent ($Z_k = 0$).

^b Half-saturation constants H_k drawn from the range 3.5–4.5.

^c Each zooplankton species is specialized on a phytoplankton species ($S_{kk}=1$), while it feeds on the other phytoplankton species with lower preference ($0 < S_{ik} < 1$).

summer species. It is present every summer. However, some years it peaks twice, with a first peak in May-June and a second smaller peak in September. In other years, it peaks in September only. The zooplankton species show similar seasonal patterning. For instance, some zooplankton species are mainly present in winter (Figure 4.4c) while others dominate during the summer period (Figure 4.4d). The example in Figure 4.4d is particularly interesting. In some years, this zooplankton species shows little variability from March to September, while in other years it fluctuates wildly during the same period. Accordingly, the species composition in our model communities shows distinct patterns of seasonal organization, but with strong year-to-year variability.

Which species traits and environmental conditions are responsible for the widespread chaotic dynamics in our model communities? A complete answer to this question is beyond the scope of this paper. However, some insight can be obtained by modifying the model assumptions systematically. This shows that more than 50% of the model simulations produced chaos when using our default parameter settings (Table 4.2, first row). The occurrence of chaos was not very sensitive to the relative magnitude of intraspecific versus interspecific phytoplankton competition (Table 4.2). In contrast, modifying zooplankton predation had a striking effect on the occurrence of chaos. When zooplankton was removed from the model, very few

simulations showed chaotic dynamics and only under seasonal forcing (Table 4.2). Similarly, inefficient zooplankton grazing and specialist zooplankton reduced the occurrence of chaos. This shows that predator-prey oscillations, and the nature of predation, played a key role in the generation of complex dynamics in our model communities.

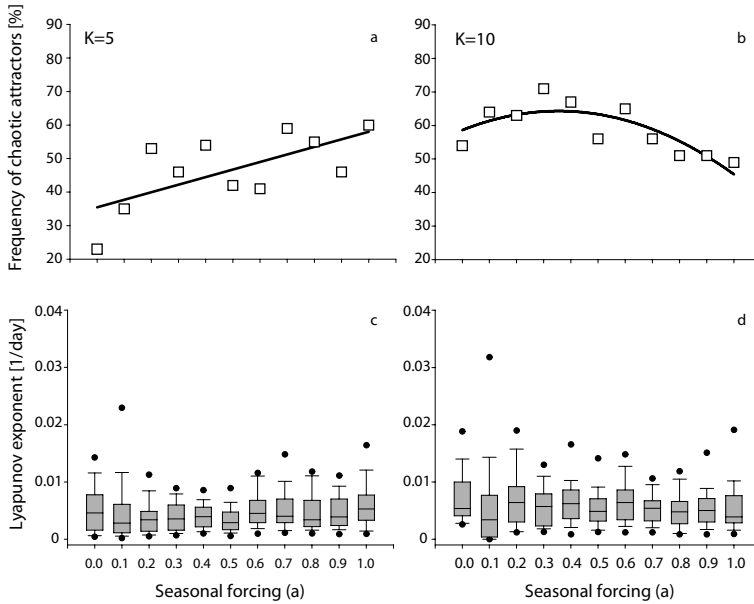


Figure 4.5: **a, b**, Relative frequency at which randomly generated model communities display chaos, plotted as function of the amplitude of seasonal forcing. Results are shown for model communities grown at two productivities: **a**, $K=5$ mg L^{-1} , and **b**, $K=10$ mg L^{-1} . A linear regression line is fitted to the data in **a**, and a quadratic regression to the data in **b**. **c, d**, Boxplots of the Lyapunov exponents of the chaotic communities, plotted as function of the amplitude of seasonal forcing. Results are again shown for **c** $K=5$ mg L^{-1} , and **d**, $K=10$ mg L^{-1} . Black dots represent the 5 and 95 percentiles. The results are based on 100 simulations for each level of seasonal forcing.

Productivity also had a clear effect on the occurrence of chaotic dynamics. At low productivity ($K=2$), stationary dynamics prevailed in constant environments, simple periodic dynamics prevailed in seasonal environments, and chaos occurred only in a few model communities with strong seasonal forcing (Table 4.2; see also Appendix C). Chaos was widespread at intermediate productivity ($K=5$ and $K=10$). At high productivity ($K=20$ and $K=50$), the occurrence of chaos declined slightly and the population dynamics often shifted to periodic cycles in both constant and seasonal environments.

In all cases summarized in Table 4.2, seasonal forcing increased the occurrence of chaos. To investigate this aspect in further detail, we estimated whether the amplitude of seasonal forcing affected the occurrence of chaos in our model communities (Figure 4.5). We focused on the intermediate productivities ($K=5$ and $K=10$). At $K=5$ mg L⁻¹, the amplitude of seasonal forcing increased the occurrence of chaos (Figure 4.5a; linear regression: $R^2=0.45$, $N=11$, $p=0.024$). At $K=10$ mg L⁻¹, mild forcing ($0.1 < a < 0.4$) caused a slight increase in the probability of chaos, but when the amplitude of seasonal forcing was further increased ($a > 0.6$), the probability of chaos declined (Figure 4.5b; quadratic regression: $R^2=0.66$, $N=11$, $p=0.013$). We further explored the predictability of these communities by calculating their Lyapunov exponents. A positive Lyapunov exponent indicates chaos. The inverse value of the Lyapunov exponent is often used as a simple metric of the predictability of chaotic systems (Strogatz 1994). In those simulations that displayed chaotic dynamics, the magnitude of the Lyapunov exponent was not affected by the amplitude of seasonal forcing (Figure 4.5c,d). This indicates that the predictability of the chaotic plankton communities was neither enhanced nor reduced by a stronger seasonality. However, the median values of the Lyapunov exponents were significantly higher at $K=10$ mg L⁻¹ than at $K=5$ mg L⁻¹ (Figure 4.5c,d; t -test: $t=-3.77$, d.f.=20; $p>0.002$), which indicates that the predictability of the model communities was affected by productivity.

4.4 Discussion

4.4.1 Interannual variability as an intrinsic property

Our model results show that interannual variability in species composition is an intrinsic property of multispecies communities in a seasonal environment. It does not require year-to-year variability in weather conditions. In many simulations the timing and abundances of different plankton species varied strongly, both within years and among years. Some species peaked only once per year, while others peaked two or three times; some species were present every year, while other species popped up only occasionally (Figure 4.4). An often invoked and seemingly straightforward intuitive explanation for this interannual variability in species composition is that winter ‘resets’ population densities, whereas stochastic variation in weather conditions during spring and summer determines interannual differences in community composition. However, this idea of winter resetting is obviously an oversimplification. Each fall, species enter the winter season in different proportions. Thus, the species composition from the previous fall affects the species composition of the next spring bloom. Our model results show that this mechanism of seasonally entrained chaos can easily create interannual variability in species composition without invoking year-to-year differences in external environmental conditions.

Interannual variability in species composition does not imply that the species composition varies at random. The model predicts temporal organization of the

species, even if their population dynamics are chaotic, in the form of a seasonal succession. Some species occur mainly in spring, while others dominate in summer (Figure 4.4). Which mechanisms are responsible for this seasonal pattern? For instance, what makes a species a typical spring species? The model assumes similar thermal physiologies for all species (i.e., they are all forced by the same function $\sigma(t)$). Therefore, interspecific differences in thermal physiology or other species-specific seasonal cues cannot explain the seasonal succession predicted by the model. Instead, the spring species in Figure 4.4a peaks in March, because its main predators (e.g., zooplankton species 5) have just declined while its key competitors (phytoplankton species 6) are still low in abundance. Apparently, seasonal forcing locks the species interactions, such that the only window of opportunity for this species is restricted to the spring time. This illustrates that seasonal succession can be an emergent property of the underlying community dynamics, in which species are sorted according to their positions in the complex network of species interactions.

4.4.2 Comparison with empirical data

The classical predator-prey model of Rosenzweig and MacArthur (1963), which provided the point of departure in our study, is clearly a major simplification of reality. For instance, the model does not specify the underlying mechanisms of phytoplankton competition for nutrients and light (Tilman 1977; Huisman et al. 1999), ignores induced defenses and other forms of phenotypic plasticity (Vos et al. 2004; Stomp et al. 2008), does not detail the population structure and life history of plankton species (De Roos et al. 1992; Nelson et al. 2005), neglects the potentially stabilizing effect of planktivorous fish on zooplankton dynamics (Scheffer et al. 1997; Gliwicz and Wrzosek 2008), does not take into account species-specific adaptations to the seasonal cycle such as resting stages (Marcus and Boero 1998), and ignores many other factors that may play a role in the population dynamics of natural plankton communities. However, the model does describe the essence of multispecies predator-prey interactions. As such, it provides the core of more complex plankton models widely used in aquatic ecology and oceanography (e.g., Fasham et al. 1990; Franks 2002; Lima et al. 2002). It is therefore interesting to assess to what extent the key qualitative predictions of the model, most notably the interannual variability in species composition, are consistent with empirical data.

The predicted patterns of seasonal organization with interannual variability at the species level are well in line with observations from real plankton communities. A closer look at the time series of the Dutch coastal zone, in Figure 4.1, reveals typical spring species like the diatom *Asterionella kariana* (Figure 4.1b). If present, this species blooms in March, although its peak abundance varies from year to year, and some years it does not peak in spring at all. The prymnesiophyte *Phaeocystis globosa*, a nuisance species that can leave large layers of foam on the beach, reaches its maximum in late spring or early summer, and in some years with a smaller

second peak in late summer (Figure 4.1a). The diatoms *Rhizosolenia imbricata* and *Guinardia delicatula* bloom mainly in the period between June and August, and can thus be called summer species. Whereas *Rhizosolenia imbricata* typically blooms only once per year, *Guinardia delicatula* can display several peaks per year. All species in this time series show striking year-to-year variability in timing and/or peak abundance.

Similar examples of interannual variability have been documented in many studies. Maberly et al. (1994) report considerable year-to-year variation in the timing and peak abundance of the diatom *Asterionella formosa* in a 45-year time series in Lake Windermere, UK. Smayda (1998) recognized different patterns of species variability in a 37-year time series of the plankton in Narragansett Bay, USA. For instance, the diatom *Asterionellopsis glacialis* displayed episodic irregular blooms, while the diatom *Thalassiosira nordenskiöldii* peaked at 5-year intervals. Interannual variation in species composition can have dramatic consequences. The spring bloom in the Kattegat between Denmark and Sweden is usually dominated by diatom species. In the late spring of 1988, however, the prymnesiophyte *Chrysochromulina polylepis* produced a major bloom with severe toxic effects on higher organisms, including fish, molluscs, ascidians and cnidarians (Nielsen et al. 1990; Lekve et al. 2006). Since the 1988 event, large-scale blooms of *Chrysochromulina* have not returned in the area. Numerous other studies have described similar patterns of interannual variability in plankton community composition (Talling 1993; Harris and Baxter 1996; Reynolds and Bellinger 1992; Arhonditsis et al. 2004; Huisman et al. 2006; Valdés et al. 2007; Smetacek and Cloern 2008). In many of these case studies, the underlying causes for the observed interannual variability were not apparent.

Not all model simulations produced interannual variability. For the same environmental setting (i.e., same values of a and K), some simulations generated chaos whereas other simulations with different species combinations generated simple periodic solutions (Figure 4.2). This seems in line with real plankton communities, where some time series display less interannual variability than other time series (Smetacek and Cloern 2008). For example, phytoplankton in Lake Kinneret showed little interannual variability during 20 years, with dinoflagellate species dominant in late winter-spring and small chlorophytes in summer-fall (Berman et al. 1992). In a brackish lagoon along the Baltic Sea, a copepod and polychaete species showed very stable seasonal succession during 22 years, while rotifers displayed high interannual variability (Feike and Heerkloss 2008). Thus, it would be interesting to investigate to what extent interannual variability of plankton communities depends on community composition. For instance, would plankton communities dominated by buoyant cyanobacteria be more regular than communities dominated by diatom species?

4.4.3 The role of seasonality and productivity

One might think that seasonality would enhance the predictability of multispecies communities. Indeed, our results show that seasonal forcing enables temporal or-

ganization of the species. Species are entrained within the seasonal cycle, and become dominant during specific periods in the year that match their highest growth potential (Figure 4.4). In this sense, seasonality generates recurrent patterns in species composition. Yet, the seasonal cycle also interferes with intrinsic species interactions, which can have both stabilizing and destabilizing effects (e.g., Rinaldi et al. 1993; King and Schaffer 1999). In particular, mild seasonal forcing increases the likelihood of chaotic dynamics (Figure 4.5a,b), whereas strong seasonal forcing may lead to synchronization of the species dynamics (Figure 4.5b). Strikingly, for chaotic communities, the magnitude of the Lyapunov exponent was not affected by the strength of seasonal forcing (Figure 4.5c,d). Thus, the rate of divergence of species trajectories was independent of the strength of seasonal forcing, which suggests that seasonality per se does not necessarily affect the time horizon for accurate prediction of changes in plankton community structure.

Our model predicts that the productivity of ecosystems will affect the nature of the species fluctuations. This result can be explained by Rosenzweig's (1971) 'Paradox of Enrichment' (see Appendix C, for a complete discussion). In short, this classic work showed that stable predator-prey systems start to display oscillations when productivity is increased beyond a certain threshold value. In our multi-species communities, with 10 phytoplankton and 6 zooplankton species, there are 60 predator-prey pairs. With increasing productivity, many of these predator-prey pairs will start to oscillate, each with its own characteristic frequency. It is well-known that such systems of coupled nonlinear oscillators have a strong tendency to generate chaos (Vandermeer 1993, 2004; Huisman and Weissing 2001; Benincà et al. 2008), which explains the widespread occurrence of chaos in model communities at intermediate productivity (Table 4.2). Interestingly, we found that many of these chaotic predator-prey fluctuations coalesced to periodic cycles at high productivity (i.e., in hypertrophic environments). These model predictions, if correct, suggest that changes in productivity, for instance through human-induced eutrophication, are likely to alter patterns of interannual variability in multispecies communities.

Acknowledgements

We thank G. Sugihara, K.D. Jöhnk, T. Fukami and the anonymous reviewers for their constructive comments on earlier versions of the manuscript, and C. Sprott for his valuable advice. C.G. Cadée and J.M. van Iperen are acknowledged for the plankton counts of the Marsdiep. V.D. was supported by a Bodossakis Foundation Fellowship. E.B. and J.H. were supported by the Earth and Life Sciences Foundation (ALW), which is subsidized by the Netherlands Organization for Scientific Research (NWO).

Chapter 5

Resonance of plankton communities to temperature fluctuations

Abstract

Fluctuations in species abundances are often driven by the interplay between environmental variation and the intrinsic dynamics of species interactions. Yet, little is known about the way in which this interplay should be expected to affect natural populations. Here, we show that temperature fluctuations in lakes and oceans can be described as a red noise process, and use a simple phytoplankton-zooplankton model to explore the expected sensitivity of plankton communities to such natural fluctuations. The effect of red noise on our predator-prey model is particularly large if the intrinsic population dynamics are on the edge of stability, close to the transition to predator-prey oscillations. In this situation even mild temperature fluctuations can be amplified to large fluctuations in population abundances. However, the magnitude of this resonance effect depends critically on the characteristic time scale of the temperature fluctuations. Communities that have an intrinsic tendency to oscillate with a period of T are particularly sensitive to environmental noise characterized by a time scale of $\tau = \frac{T}{2\pi}$. The intrinsic periodicity of plankton oscillations depends largely on the growth rates of the organisms involved, which are inversely correlated to body size. We predict the resonance peak for natural plankton to vary from a characteristic time scale of 1-2 days for small nano-flagellates and ciliates, about 5-15 days for cladocerans and copepods, to 80 days for large krill species. In measured time series, we found characteristic time scales of temperature fluctuations ranging from 7 to 50 days. Thus, the characteristic time scales of temperature fluctuations in lakes and oceans fall largely within the range to which plankton communities are most sensitive.

This chapter is based on the manuscript: Benincà, E., Dakos, V., van Nes, E.H., Huisman, J. & Scheffer, M. Resonance of plankton communities to temperature fluctuations. (Submitted).

5.1 Introduction

It is long known that interactions between species may cause oscillations in species abundances (Lotka 1925; Volterra 1926). Famous examples include the predator-prey oscillations of hares and lynx in northern Canada (Elton and Nicholson 1942; Stenseth et al. 1997), Huffaker's (1958) experiments with herbivorous and predatory mite species, and a wide variety of laboratory studies with bacterial and plankton communities (Gause 1934; Luckinbill 1973; Fussmann et al. 2000; Yoshida et al. 2003). The basic mechanism is that a predator depletes the prey population, leading to a lack of food and thus a decrease in the predator population. This releases the predation pressure allowing the prey to recover, implying the start of a new cycle. If multiple predator and prey species are involved, such predator-prey cycles can interact to produce chaotic dynamics (Gilpin 1979; Vandermeer 1993; Becks et al. 2005; Benincà et al. 2009). In addition, other ecological interactions may also lead to oscillations and chaos in species abundances, for instance due to multispecies competition (Huisman and Weissing 1999, 2001) or host-parasite relationships (May and Hassell 1981; Hochberg et al. 1990).

While there is good evidence that intrinsic oscillations occur in biological communities, most ecologists will probably sustain that fluctuations in species abundances are often driven by external factors such as variation in weather conditions (Figure 5.1).

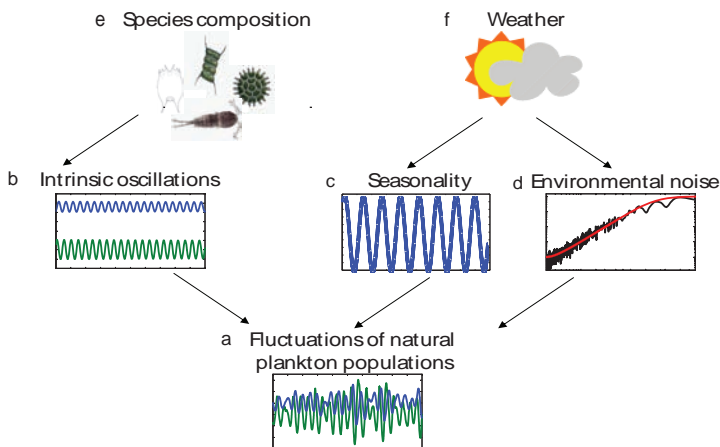


Figure 5.1: Representation of the main mechanisms driving fluctuations of natural plankton populations, illustrating the interplay between intrinsic population dynamics and external forcing by seasonal variation and environmental noise.

Indeed, many species do not have an intrinsic tendency to cycle (Kendall et al. 1998), and even notoriously oscillating organisms such as waterfleas (*Daphnia*) can be relatively stable in some situations (McCauley and Murdoch 1987; Murdoch et al. 1998). Various mechanisms might explain why intrinsic oscillations occur in some situations but not in others. For instance, models predict that predator-prey interactions may lead to stable communities in nutrient-poor environments, but to predator-prey oscillations in nutrient-rich ecosystems. This phenomenon, known as the ‘paradox of enrichment’ (Rosenzweig 1971), has also been documented in laboratory experiments (Luckinbill 1973; Bohannan and Lenski 1997; Fussmann et al. 2000). Also, spatial heterogeneity may commonly cause oscillating systems to become stable or almost stable (Scheffer and de Boer 1995). Here, we investigate how environmental fluctuations might affect the transition from stable to unstable community dynamics.

Several studies have shown that communities that are at the edge of stability might be pushed into an oscillatory mode by environmental fluctuations (e.g. Nisbet and Gurney 1976; Kaitala et al. 1996; Greenman and Benton 2003; Mankin et al. 2006). Indeed, it is well known that strong oscillations can be induced in some systems by slight periodic forcing, provided that the intrinsic frequency of the cycle is equal (or has a simple ratio) to the frequency of the forcing. For instance, a child on a swing can reach large amplitudes even if it receives only small periodic pushes at the right frequency. Similarly, a bridge may start to vibrate dangerously under the periodic forcing of a marching group of soldiers. These are examples of the general phenomenon known as ‘resonance’: oscillations of large amplitude produced by a relatively small input signal near the same frequency as the natural frequency of the resonating system. Resonance can also happen if a system is exposed to stochastic forcing. As an example consider a flute. The noise invoked by blowing across an edge causes a perturbation that is resonated in the instrument with a frequency depending among other things on e.g. its length. In the essence, the question we address in this paper, is whether noise in environmental conditions such as random fluctuations temperature could ‘blow’ natural communities into resonance.

In the theoretical literature, environmental fluctuations are often referred to as environmental noise. The effect of environmental noise on community dynamics may vary widely depending on characteristics of the system (May 1973; Kendall 2001; Billings and Schwartz 2002; Mankin et al. 2006; Scheffer et al. 2009). Moreover, many studies have revealed that the ‘color’ of noise can make a large difference (Steele and Henderson 1994; Ripa and Ives 2003; Greenman and Benton 2003). Noise is called white if there is no correlation between its subsequent values. In colored noise the subsequent values are correlated. In practice, environmental fluctuations often resemble red noise, with positive correlations between subsequent values (Mandelbrot and Wallis 1969; Steele 1985; Pelletier 2002; Király et al. 2006; Roe 2009). For instance, the temperature of a lake today will be positively correlated to that of yesterday, since heating or cooling of a lake simply takes time. An important parameter in this context is the characteristic time scale of red noise, which essentially

describes the time it takes before perturbations in temperature are smoothed out again.

In this paper, we use a simple predator-prey model to investigate whether environmental fluctuations can ‘blow’ natural communities into resonance. Our work is motivated by earlier studies on the interplay between intrinsic population fluctuations and external noise (Nisbet and Gurney 1976; Greenman and Benton 2003; Bjørnstad and Grenfell 2001; Coulson et al. 2004; Ruokolainen et al. 2009), but with a specific application to the plankton of freshwater and marine ecosystems. Plankton communities can display striking intrinsic population fluctuations (Scheffer 1991; Huisman and Weissing 1999; Fussmann et al. 2000; Benincà et al. 2008), and are strongly affected by variations in environmental conditions (Grover 1991; Sommer 1995; Descamps-Julien and Gonzalez 2005). We will analyze the sensitivity of the model to different characteristic time scales of red noise. The model results are then compared against red noise spectra derived from temperature measurements in lakes and oceans. Our findings show that the characteristic time scale of temperature fluctuations in aquatic ecosystems matches the intrinsic frequency of phytoplankton-zooplankton oscillations, such that small temperature fluctuations can be amplified to large-amplitude oscillations in species abundances.

5.2 Predator-prey model

We consider a simple model consisting of a phytoplankton and a zooplankton species, both exposed to the same environmental noise. The model is based on the classical Rosenzweig-MacArthur predator-prey model (Rosenzweig and MacArthur 1963, see also, e.g., Vandermeer 1993; Scheffer et al. 1997). More specifically, let P denote the phytoplankton abundance and Z the zooplankton abundance. Then our model reads:

$$\frac{dP}{dt} = (1 + n_t) r P \left(1 - \frac{P}{(1 + n_t)K} \right) - (1 + n_t) \left(\frac{gP}{P + H} \right) Z \quad (5.1)$$

$$\frac{dZ}{dt} = (1 + n_t) \left(\frac{egP}{P + H} \right) Z - (1 + n_t) m Z \quad (5.2)$$

Phytoplankton growth is described by the logistic equation, where r is the maximum specific growth rate (d^{-1}) and K is the carrying capacity (mg DW L^{-1}) of the phytoplankton. Grazing by zooplankton is formulated as a Holling type II functional response with half-saturation constant H (mg DW L^{-1}) and a maximum specific grazing rate g (d^{-1}). Zooplankton growth depends on the grazing rate, the food assimilation efficiency e and a zooplankton mortality rate m (d^{-1}). Environmental fluctuations are incorporated by the noise term n_t , which is assumed to affect the growth rates, grazing rates, mortality rates and carrying capacity.

Parameter values were chosen to represent the interaction between *Daphnia* and edible phytoplankton in lakes (Rose et al. 1988; Scheffer et al. 1997; Reynolds 2006). The phytoplankton growth rate r was set to 0.5 d^{-1} . We varied carrying capacity K from near zero to 4 mg DW L^{-1} . The maximum grazing rate g was set to 0.4 d^{-1} , assimilation efficiency e to 0.6, the half-saturation constant H to 0.6 mg DW L^{-1} , and the zooplankton mortality rate m to 0.15 d^{-1} . Initial values of phytoplankton and zooplankton were both set to 3 mg DW L^{-1} . All simulations were carried out in MATLAB using our software package GRIND (freely available at <http://www.dow.wau.nl/aew/grind>).

5.3 The paradox of enrichment

Without noise (i.e., $n_t = 0$), the population dynamics of this standard predator-prey model is well understood. For $K < 1$, the model has a stable boundary equilibrium where only phytoplankton is present (Figure 5.2b). The carrying capacity is too low to support a zooplankton population. For $1 < K < 1.5$, the boundary equilibrium becomes unstable; there is sufficient phytoplankton food available for the zooplankton population to invade. The phytoplankton and zooplankton coexist at a stable internal equilibrium. The equilibrium point is a stable node. For $1.5 < K < 2.6$, phytoplankton and zooplankton still coexist at a stable internal equilibrium, but now this equilibrium is a stable spiral. That is, the predator and prey population approach equilibrium through damped oscillations (Figure 5.2c). When the carrying capacity is increased further, the system passes through a Hopf bifurcation. For $K > 2.6$, the internal equilibrium is no longer stable and the system displays predator-prey oscillations in the form of a stable limit cycle (Figure 5.2d).

Hence, with increasing carrying capacity, the dynamics change from a stable node to a stable spiral and then to sustained predator-prey oscillations. This destabilization of the predator and prey populations has been confirmed by laboratory experiments with phytoplankton and zooplankton species (Luckinbill 1973; Fussmann et al. 2000), and is known as the ‘paradox of enrichment’ (Rosenzweig 1971). The period of the predator-prey oscillations depends on the generation times of the organisms involved. For instance, the phytoplankton and zooplankton in our model oscillate with a period of about 50 days, which is consistent with the time scale of plankton fluctuations typically observed in laboratory experiments (Luckinbill 1973; Fussmann et al. 2000; Benincà et al. 2008), but much faster than the predator-prey oscillations of larger organisms such as the ten-year cycle of hare and lynx in northern Canada (Elton and Nicholson 1942; Stenseth et al. 1997).

5.4 Adding noise

What happens if we add small environmental fluctuations to our phytoplankton-zooplankton model? To address this question, we introduce a measure of noise

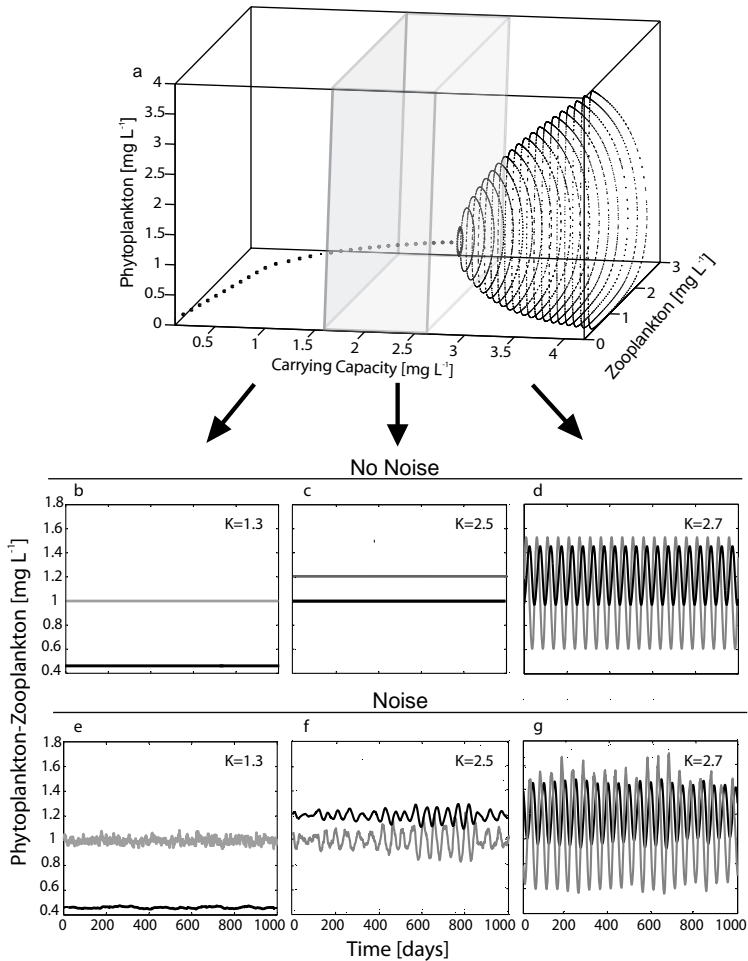


Figure 5.2: Dynamical behavior of the phytoplankton-zooplankton model with or without white noise as a function of carrying capacity K . **a**, Asymptotic regimes (attractors) as a function of carrying capacity K . Bifurcations occur at three different values of K . At $K=1$, zooplankton can invade the system (transcritical bifurcation). At $K=1.57$, the internal equilibrium changes from a stable node to a stable spiral (spiral-node bifurcation). At $K=2.6$, the internal equilibrium becomes unstable as the solutions change from a stable spiral to a limit cycle (Hopf bifurcation). The lower panels illustrate the population fluctuations of phytoplankton (gray) and zooplankton (black), **b-d**, without white noise ($\sigma_\epsilon=0$), and, **e-g**, with white noise ($\sigma_\epsilon=0.05$). Parameter settings for carrying capacity are indicated in panels **b-g**.

amplification. We use a similar definition as Greenman and Benton (2003), but with a correction for intrinsic population fluctuations. That is, we quantify noise amplification as the difference between the coefficient of variation of a population in the presence of noise (CV_{noise}) and the coefficient of variation of that population in the absence of noise ($CV_{intrinsic}$) divided by the standard deviation of environmental noise (σ_ϵ):

$$A = \frac{CV_{noise} - CV_{intrinsic}}{\sigma_\epsilon} \quad (5.3)$$

We estimated noise amplification of phytoplankton and zooplankton dynamics from simulated dynamics over 5,000 days after discarding the first 1,000 days to avoid transients. To obtain accurate estimates, the simulations were repeated 100 times and the average noise amplification is reported.

5.4.1 White Noise

We first consider random environmental fluctuations in the form of white noise. In our application, white noise is drawn from a Gaussian distribution with zero mean and standard deviation σ_ϵ , at a time step of one day. For low carrying capacities ($K < 1.5$), white noise produces only minor stochastic variation in the population abundances (Figure 5.2e). The environmental fluctuations are damped by the stabilizing dynamics of the stable node. At high carrying capacity ($K > 2.6$), where the undisturbed system displays a limit cycle, white noise just makes the predator-prey oscillations somewhat irregular (Figure 5.2g). However, white noise has a pronounced effect in the intermediate parameter region, especially close to the bifurcation point (approximately $2.3 < K < 2.6$) where the phytoplankton and zooplankton populations displayed damped oscillations towards a stable spiral in the absence of noise. Here, even minor white noise generates a striking pattern of oscillations (Figure 5.2f), with similar frequency as the predator-prey oscillations observed for $K > 2.6$ (compare Figure 5.2f and Figure 5.2g). Hence, adding noise has the effect that the system shows predator-prey fluctuations over a wider range of carrying capacities.

5.4.2 Red noise

In many cases, environmental fluctuations do not mimic the random scatter of white noise. Instead, fluctuations often show some memory or persistence in time. Temperature fluctuations in aquatic ecosystems present a clear example. When a lake has warmed up during an exceptionally hot summer day, its excess heat content will be slowly released such that the lake will return to average temperatures only after several days. Such persistent variation can be described by red noise.

Red noise, n_t , can be generated by a simple autoregressive model (Box and Jenkins 1970):

$$n_{t+1} = \alpha n_t + \sigma_\epsilon \sqrt{(1 - \alpha^2)} \epsilon \quad (5.4)$$

Again we consider a time step of one day. At each time step, the stochastic term ϵ_t is randomly drawn from a Gaussian distribution with zero mean and unit standard deviation. The term σ_ϵ determines the magnitude of environmental noise and the autocorrelation coefficient α describes its color (where $-1 < \alpha < 1$). When environmental variation is uncorrelated in time ($\alpha=0$), it is called white noise. When environmental variation is positively autocorrelated ($\alpha > 0$), it is called red noise. The term σ_ϵ is multiplied by $\sqrt{(1 - \alpha^2)}$ to ensure that the asymptotic variance of n_t is independent of the autocorrelation coefficient α (Roughgarden 1975; Petchey et al. 1997; Ives and Jansen 1998).

The autocorrelation function for red noise, $r(t)$, is given by:

$$r(t) = e^{(-\frac{t}{\tau})} \quad (5.5)$$

This equation implies that environmental variation generated by red noise decays exponentially with time. The rate at which the variation decays is described by the *characteristic time scale* of red noise, τ (also called e-folding time; e.g. (von Storch and Zwiers 2003), which is related to the autocorrelation coefficient α :

$$\tau = -\frac{1}{\ln \alpha} \quad (5.6)$$

Thus, systems in which environmental fluctuations decay very slowly have a long characteristic time scale (and a high autocorrelation coefficient).

As a starting point we studied the effect of red noise on plankton populations assuming a carrying capacity close to the Hopf bifurcation point ($K=2.5$). Red noise yields strong population fluctuations, with higher noise amplification than white noise (Figure 5.3). Interestingly, noise amplification depends on the characteristic time scale of red noise. At the default parameter settings, mimicking phytoplankton-zooplankton interactions, the strongest noise amplification occurred for red noise with a characteristic time scale τ of 8-10 days (Figure 5.3).

5.5 Resonance and the power spectrum of red noise

The observation that noise amplification peaks at a particular characteristic time scale of red noise can be interpreted as the result of resonance of the intrinsic predator-prey oscillations in response to the power spectrum of red noise. The power spectrum of red noise summarizes the extent to which different frequencies (periods) contribute to the total red noise signal. Thus, the interesting question is which characteristic time scale of red noise generates the highest power at the frequency to which the plankton community is most sensitive? In other words, which characteristic time scale generates the highest power at the intrinsic frequency of the phytoplankton-zooplankton oscillations?

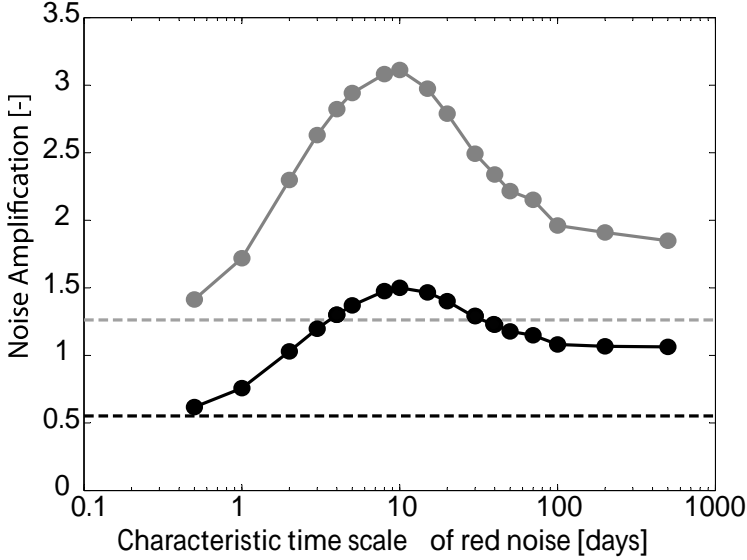


Figure 5.3: Amplification of red noise by phytoplankton (gray) and zooplankton (black) as function of the characteristic time scale τ of red noise. Maximum amplification of red noise occurs at a characteristic time scale τ_{\max} of about 8-10 days. For comparison, the horizontal dashed lines indicate noise amplification generated by white noise. Each data point is based on 100 simulations of the phytoplankton-zooplankton model, with a carrying capacity of $K = 2.5$.

According to the Wiener-Khinchin theorem, the power spectral density of a red noise process, $P(f, \tau)$, is the Fourier transform of the autocorrelation function $r(t)$. In view of Eq. 5.5 this can be written as:

$$P(f, \tau) = \int_{-\infty}^{+\infty} e^{-\frac{t}{\tau}} e^{-i2\pi ft} dt \quad (5.7)$$

where f is frequency, and τ is the characteristic time scale of red noise as defined in Eq. 5.6. Contour integration yields:

$$P(f, \tau) = \frac{2\tau}{1 + (2\pi f\tau)^2} \quad (5.8)$$

or in terms of periods T rather than frequencies:

$$P(T, \tau) = \frac{2\tau}{1 + \left(\frac{2\pi\tau}{T}\right)^2} \quad (5.9)$$

This equation shows that the power spectral density of red noise is an increasing function of the period T (Figure 5.4a), and a unimodal function of the characteristic time scale of red noise τ (Figure 5.4b). The characteristic time scale of red noise that yields maximum power can be derived by evaluating $\frac{dP}{d\tau} = 0$ and solving for τ . In view of Eq. 5.9, this yields:

$$\tau_{max} = \frac{T}{2\pi} \quad (5.10)$$

This simple expression is one of the key equations in our paper. It shows that the characteristic time scale of red noise that generates maximum power at a given period T is given by $\frac{T}{2\pi}$. For instance, the predator-prey oscillations in our model have a period of about 50 days. According to Eq. 5.10, red noise generates maximum power at a period of $T=50$ days if $\tau \approx 8$ days. This explains why our model predicts the strongest noise amplification for plankton populations exposed to red noise with a characteristic time scale of about 8 days (compare Figure 5.3 and Figure 5.4b).

Changing the period of the phytoplankton-zooplankton oscillations will shift the characteristic time scale τ of red noise with which the plankton dynamics will resonate. This is illustrated in Figure 5.5. The growth rates and mortality rates of the zooplankton species were rescaled to produce oscillations with different periods. For instance, when the period of intrinsic predator-prey oscillations is halved to 25 days, maximum amplification of the plankton is obtained for red noise with a characteristic time scale τ of 4 days. Conversely, when the period of intrinsic predator-prey oscillations is doubled to 100 days, maximum amplification is obtained for red noise with a characteristic time scale τ of 16 days (Figure 5.5). This illustrates that the interplay between the period of the plankton oscillations and the characteristic time scale of red noise determines when the plankton dynamics will be amplified the most.

5.6 Time scales of plankton populations and temperature fluctuations

What are the characteristic time scales of red noise in aquatic ecosystems? Many factors in aquatic ecosystems may show considerable variation (e.g., temperature, pH, light, nutrients), and the answer to this question will probably depend on the variable concerned. Here, we focus on temperature fluctuations, since temperature is a key variable that affects almost all aquatic organisms and many physical and chemical processes as well (e.g., stratification, dissolution of gases and salts). We analyzed time series of daily surface water temperature for a range of water bodies in Europe and the USA (Table 5.1). First, we removed the seasonal component of the temperature fluctuations (Figure 5.6a). This was done by calculating the mean temperature for each particular day of the year (i.e., averaged over all years in the time series), and subsequently subtracting this seasonal pattern from the time series. Then, we used the seasonally detrended time series to calculate the autocorrelation

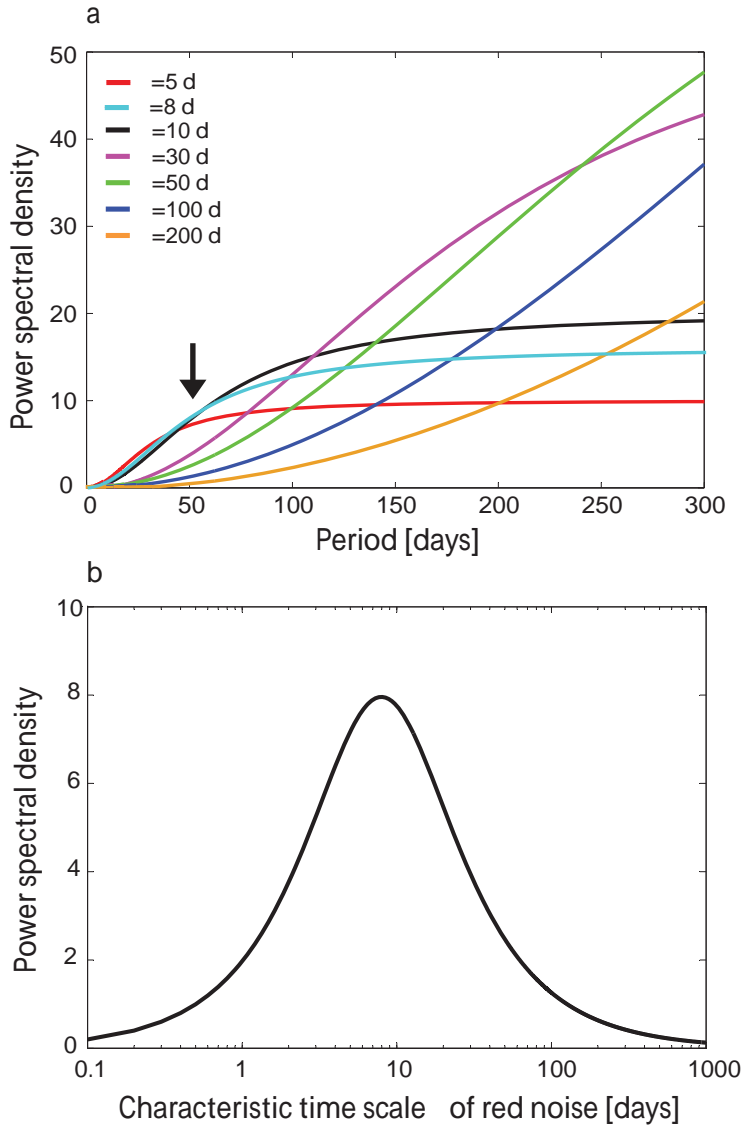


Figure 5.4: Power spectral density of red noise. **a**, Power spectral density as function of periodicity, for different characteristic time scales τ . The arrow indicates a period of 50 days. **b**, Power spectral density at a period of 50 days as function of the characteristic time scale τ of red noise. The power spectral density is described by Eq. 5.9.

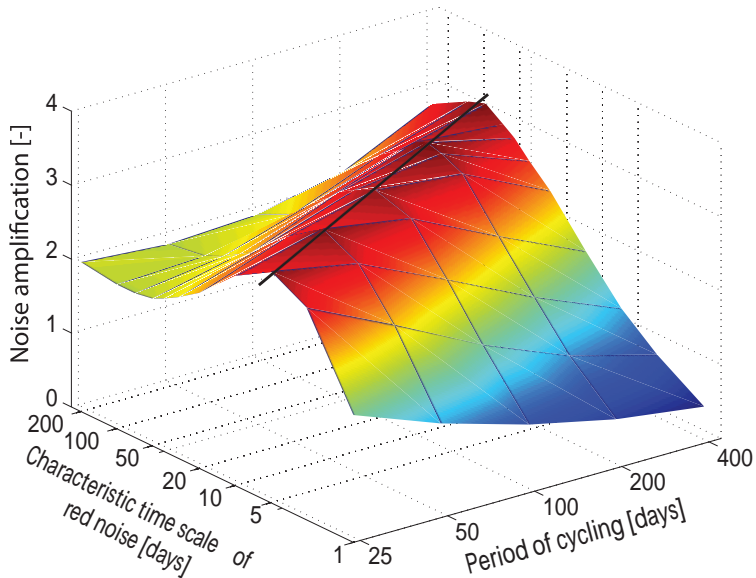


Figure 5.5: Noise amplification of the phytoplankton fluctuations as a function of the characteristic time scale of red noise and the period of the intrinsic phytoplankton-zooplankton oscillations. The black line indicates the characteristic time scale of red noise that yields the highest noise amplification. Slower-growing plankton species will display predator-prey oscillations with a longer period, which will increase the characteristic time scale of red noise for which the plankton will be most sensitive.

coefficient α from the product-moment correlation between the temperature at day t and at day $t+1$ (Figure 5.6b). Subsequently, we visually compared the power spectral density of the time series against the power spectral density of red noise generated with the autocorrelation coefficient α (see Appendix D for methodological details). This illustrated that the power spectra of the temperature fluctuations could indeed be characterized as a red noise process (Figure 5.6c). Finally, we computed the characteristic time scale τ of red noise from the corresponding autocorrelation coefficient α using Eq. 5.6.

The results show that the characteristic time scale of temperature fluctuations ranged from 7 days in Lake Champlain to almost 50 days in the Atlantic Ocean (Table 5.1). One might hypothesize that the temperature fluctuations will be faster in small shallow lakes than in large deep ocean basins. However, according to our analysis, it is not that simple. For instance, Lake IJsselmeer is a shallow lake with an average depth of only 2-3 m, yet its temperature fluctuations show a relatively long characteristic time scale compared to other aquatic ecosystems. Conversely, we also found a station in the Atlantic Ocean with a short characteristic time scale of 8

Water body	Description	Sampling period	Characteristic time scale of red noise (days) [95% confidence interval]
Atlantic Ocean (Mid Atlantic)	Open tropical ocean	2005-2007	48 [42-54]
IJsselmeer (The Netherlands)	Large shallow lake	1972-1993	43 [41-45]
Crater Lake (Oregon, USA)	Deep lake	1998-2003	28 [25-31]
Pacific Ocean (Southwest of Hilo, Hawaii, USA)	Open tropical ocean	2006-2009	27 [24-30]
Cedar Lake (Wisconsin, USA)	Small shallow lake	1974-1976	25 [22-28]
Bee Lake (Mississippi, USA)	Small shallow lake	2005-2008	22 [20-24]
Gulf of Mexico (South of Freeport, Texas, USA)	Coastal subtropical ocean	2000-2006	19 [18-21]
Gulf of Alaska (Shumagin Islands, Alaska, USA)	Coastal subpolar ocean	2005-2009	19 [17-21]
Caillon Lake (Louisiana, USA)	Small shallow lake	1997-2002	11 [10-12]
Tarpon Lake (Florida, USA)	Medium-sized shallow lake	1964-1968	8 [7-9]
Atlantic Ocean (Southeast of Nantucket, Massachusetts, USA)	Coastal temperate ocean	2005-2008	8 [7-9]
Lake Meredith (Colorado, USA)	Medium-sized shallow lake	2004-2009	8 [7-9]
Lake Champlain (New York, USA)	Large deep lake	2005-2010	7 [7-8]

Table 5.1: Surface water temperature records used to estimate the characteristic time scale of red noise, τ . Additional information on these time series is presented in the Appendix D.

days only. Most likely, the characteristic time scale of the temperature fluctuations will strongly depend on the local climatic and hydrodynamic conditions.

Which aquatic organisms would be most sensitive to the temperature fluctuations observed in aquatic ecosystems? The generic rule is that maximum amplification of red noise occurs when the intrinsic species oscillations would have a period of about $2\pi\tau$. The period of intrinsic predator-prey oscillations depends on the generation times of the organisms involved. For instance, the phytoplankton and zooplankton populations in our model oscillate with a period of about 50 days. Thus, they would be very sensitive to temperature fluctuations with a characteristic time scale of 8-10 days, as in Lake Meredith, Lake Champlain, and the above-mentioned station in the North Atlantic Ocean. We also calculated the periodicity of predator-prey oscillations in case our model *Daphnia* would be replaced by zooplankton species with

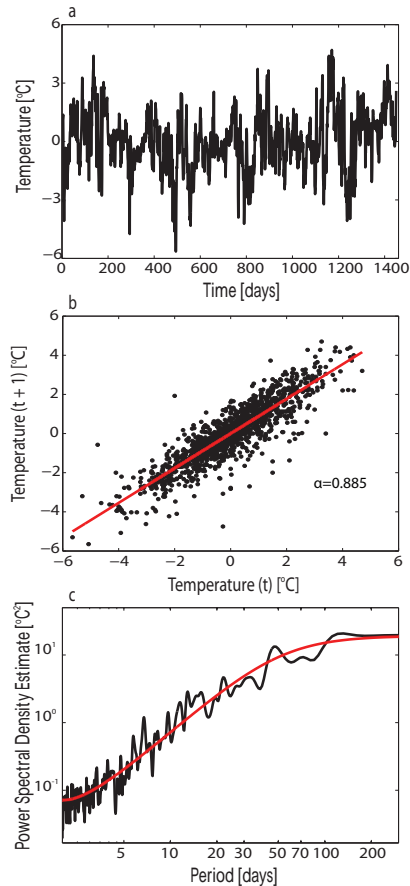


Figure 5.6: Time series analysis of daily surface temperature, illustrated by data of Lake Tarpon. **a**, Detrended time series of daily surface temperature after the seasonal trend was removed from the original data. **b**, Plotting the seasonally detrended temperature on day $t+1$ against the temperature on the previous day t yields the autocorrelation coefficient α . **c**, The power spectral density of the seasonally detrended temperature data (black line) corresponds well with the power spectral density of red noise with the autocorrelation coefficient α estimated from panel b (red line). (See Appendix D for details on the spectral analysis).

other generation times (Figure 5.7). For instance, for fast-growing zooplankton like phagotrophic nanoflagellates and ciliates the strongest noise amplification would be expected for temperature fluctuations with a short characteristic time scale τ of 1.5 to 5 days (Figure 5.7). Large zooplankton like krill (euphasiids) have a much longer

generation time, and they would respond more strongly to temperature fluctuations with a characteristic time scale of 80 to 90 days (Figure 5.7).

Comparing the estimates in Figure 5.7 and Table 5.1, it seems that particularly the population dynamics of cladocerans and copepods will be very sensitive to the temperature fluctuations observed in many aquatic ecosystems.

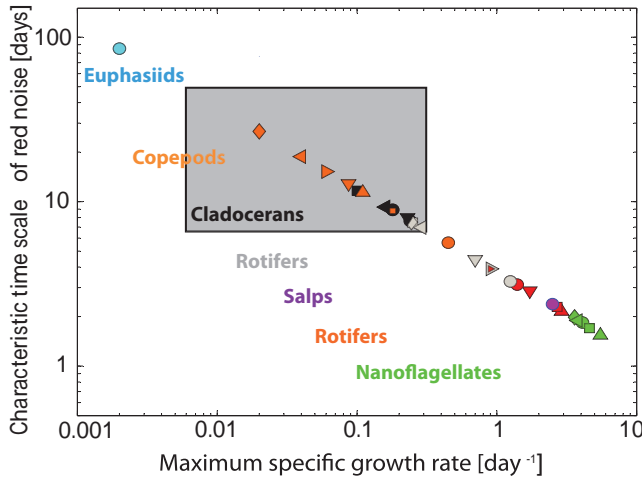


Figure 5.7: Relationship between the maximum specific growth rates of different zooplankton species and the characteristic time scale, τ_{\max} , producing maximum amplification of red noise. The species include heterotrophic flagellates (green), ciliates (red), rotifers (gray), salps (violet), cladocerans (black), copepods (orange) and euphasiids (light blue). Maximum specific growth rates of the species were obtained from the literature (see Table D.2 in Appendix D). To calculate τ_{\max} from the model, we assumed that the maximum growth rate of the zooplankton equaled the product eg and that the mortality rate m was proportional to the maximum specific growth rate (with a constant of proportionality of 0.62 as in our parameter setting for *Daphnia*).

5.7 Discussion

Our results illustrate that small stochastic fluctuations in the environment can invoke large oscillations in natural communities that would otherwise be stable. Specifically this can happen if the community contains ‘damped oscillators’. Such systems do not oscillate autonomously, but upon perturbation they return to a stable state through damped oscillations. The observation that environmental noise can sustain the fluctuations of damped oscillators is well known in physics, and several studies hint at its potential relevance to ecological systems (Nisbet and Gurney 1976; Kaitala

et al. 1996; Greenman and Benton 2003, 2005). Not surprisingly, this resonance effect depends on the intrinsic rates of the system relative to the characteristic time scale of the environmental fluctuations (Greenman and Benton 2003, 2005). It is commonly believed that resonance requires a very precise match between the intrinsic periodicity of a system and the frequency of external forcing. In case of noisy forcing, however, the power of the external fluctuations is spread out over a range of frequencies. Hence, the time scale of the intrinsic dynamics and the time scale of external forcing do not have to match exactly. In Figure 5.3, for instance, the noise amplification peak is quite wide, and there is substantial noise amplification for red noise with characteristic time scales ranging from 3 to 30 days.

Our analysis illustrates that there is a straightforward relationship between the intrinsic periodicity of the system and the time scale of red noise that provokes the strongest oscillations. Since the intrinsic periodicity of predator-prey oscillations depends on the growth rates of the predator and prey species, one can thus indicate which (range of) characteristic time scales of environmental fluctuations should provoke resonance in a given predator-prey system. Interestingly, the characteristic time scales of natural temperature variations in aquatic ecosystems ranges from 7 to 50 days (Table 5.1). This happens to match surprisingly well with the range to which plankton communities should resonate most strongly, especially when dominated by cladocerans and copepods (Figure 5.7). Plankton communities are notorious for their striking fluctuations in species abundances. Our results suggest that a substantial part of such fluctuations might result from resonance of the intrinsic community dynamics to temperature fluctuations.

Of course, natural systems are far more complicated than the minimal model we used to highlight the resonance phenomenon. For instance, in addition to temperature, many other environmental factors of relevance for plankton communities fluctuate as well (e.g., nutrients, light, pH). Some of these factors might fluctuate more or less in synchrony with temperature, while others may have different characteristic time scales. Also, natural plankton communities consist of many different species, each with their own typical characteristics. This may give rise to interactions between different oscillatory components within the community (Vandermeer 2004; Benincà et al. 2009) and to a plethora of different population dynamics ranging from stable states to chaos (Scheffer 1991; Huisman and Weissing 1999, 2001; Benincà et al. 2008; Dakos et al. 2009). It would be interesting to explore how resonance to external fluctuations cascades through such multispecies communities depending on the color of the forcing noise in relation to constituent intrinsic frequencies. This is a complex issue, as the web of interactions that link the different species implies indirect responses that may in many ways alter the way communities react to environmental noise (Ives and Jansen 1998; Xu and Li 2002, 2003; Greenman and Benton 2005; Brassil 2006; Vasseur 2007; Vasseur and Fox 2007).

Clearly, we have only scratched the surface of the intriguing question what the role of resonance in natural communities might be, and there are many ways in which this idea may be developed further. In addition to more sophisticated model-

ing exercises, experimental analysis of the effects of different types of environmental fluctuations on plankton communities would help probing the hypothesis of resonance further. Meanwhile, it is tempting to speculate about the implications of resonance for ecological theory.

In view of the relatively few possibilities for niche differentiation in aquatic ecosystems, the biodiversity of plankton communities has puzzled ecologists for decades (Hutchinson 1961). It is well known that environmental fluctuations may help to prevent competitive exclusion (Connell 1978; Reynolds et al. 1993; Chesson 2000; Descamps-Julien and Gonzalez 2005), which may offer a plausible solution for Hutchinson's paradox of the plankton. Other studies have shown that intrinsic nonequilibrium dynamics can play an important role in the maintenance of biodiversity as well (Huisman and Weissing 1999; Scheffer et al. 2003; Benincà et al. 2008, 2009). The phenomenon of resonance connects these two lines of thinking, by providing a link between intrinsic population dynamics and external fluctuations. In particular, the remarkable correspondence between the intrinsic periodicity in plankton communities and the characteristic time scales of temperature fluctuations suggests that resonance could be an important mechanism to generate the permanent turmoil that helps numerous plankton species to coexist in nature. Interestingly, experiments indicate that environmental fluctuations with a period of 6-10 days yield the highest biodiversity in plankton communities (Gaedeke and Sommer 1986; Sommer 1995; Flöder and Sommer 1999). This corresponds quite well to the time scales that we estimated to invoke oscillations most easily in a range of plankton types.

Another obvious question to ask is how climate change could affect temperature fluctuations, and thus the resonance of plankton communities to these fluctuations. Global warming is predicted to increase climatic variability (Solomon et al. 2007), and may also alter the characteristic time scales of environmental fluctuations (Wigley et al. 1998; Easterling et al. 2000). In addition to model studies, experiments and long-term observations of temperature fluctuations and associated community dynamics in different climatic regions might help to explore these ideas further.

In the introduction we asked whether environmental fluctuations could blow natural communities into resonance, much as the breath of a musician may cause a flute to resonate. Our study shows that in plankton communities resonance to temperature fluctuations might play an important role. Perhaps more importantly, our findings suggest a way to predict from the characteristic time scales of intrinsic dynamics versus external fluctuations when resonance phenomena are most likely to occur in natural communities.

Acknowledgements The authors thank Klaus Jöhnk for useful discussion on the data analysis. The research of E.B., V.D. and M.S. was supported by the Earth and Life Sciences Foundation (ALW), which is subsidized by the Netherlands Organization for Scientific Research (NWO).

Chapter 6

Afterthoughts

6.1 Is there chaos out there?

The title of my thesis refers to one of the big questions in ecology today. While I have elaborated on this issue from different angles for plankton communities in the different chapters, I will reflect on the broader question of the role of chaos in ecosystems here.

Our analysis of the extraordinary time series from an experimentally isolated community from the Baltic Sea (**Chapter 2**) implies a firm demonstration of intrinsic chaos in this case. The results convincingly show that a realistic complex food web can generate chaotic dynamics and imply that a stable equilibrium is not required for the persistence of complex food webs. The cross-wavelet analysis of phase angles strongly indicates that coupled oscillating predator-prey systems are at the root of the chaotic dynamics (**Chapter 3**). In plankton communities numerous potentially oscillatory predator-prey links exist. Therefore, our results suggest that chaos may well be an important driver of plankton dynamics in nature. Nonetheless, the step from simple models and experimental data from an isolated community under constant conditions to the real dynamics in lakes and oceans is of course still large.

One important aspect of natural situations is the permanent variation in external conditions such as temperature and light. Should such variation in conditions be expected to mask or even suppress intrinsically generated oscillations or might it work in synergy, catalyzing the occurrence of chaos and cycles? We have looked at potential effects of seasonality and of stochastic fluctuations in the environment as two (of the many) components of environmental change.

Seasonality may in principle lock chaotic systems into a simple seasonal pattern. However, seasonal variation in conditions may also invoke chaos in otherwise stable communities (Rinaldi et al. 1993) or perhaps more commonly, lead to a subtle interplay that creates a particular kind of chaos, that looks regular when it comes to overall patterns, but allows different species to dominate in different years (**Chapter 4**). Such interannual variation in species composition is commonly ob-

served in nature (Berg et al. 1998; Smayda 1998; Philippart et al. 2000; Raimondo et al. 2004), and often leads biologists to speculate whether interannual differences in species dominance might be explained by particularly warm springs (Straile 2000), ice-cover in winter (Adrian et al. 1999; Weyhenmeyer et al. 1999) or other variations in climatic conditions (Reynolds and Bellinger 1992; Harris and Baxter 1996). Our results suggest that ‘perhaps there is no explanation’ for interannual variation in species composition, just intrinsic sensitivity to initial conditions resulting in highly unpredictable chaos, or more plausibly that there is an interplay between intrinsic and extrinsic factors that makes it difficult to explain much of the ecological dynamics.

Another aspect of temporal variation we examined is stochastic variation in temperature (**Chapter 5**). This analysis highlighted the possibility that ‘noise’ in the external conditions may sometimes invoke intrinsically generated oscillations in species abundances. This can happen when the system behaves as a damped oscillator. Upon a single perturbation such systems would return to a stable state through damped oscillations, but under continued external perturbations the oscillations can be sustained (Nisbet and Gurney 1976; Kaitala et al. 1996; Greenman and Benton 2003, 2005). As we argue such noise-induced oscillations could be relevant for many predator-prey systems in nature. We also show that the characteristic time scales of the environmental fluctuations matter, and that one can predict from the growth rates of species which characteristic time scales would most easily invoke oscillations. Surprisingly, the characteristic time scales of temperature fluctuations typically found in aquatic ecosystems fall in the range to which important plankton groups such as copepods and cladocerans are predicted to be most sensitive. This leads us to conclude that environmental fluctuations may often catalyze rather than mask intrinsic oscillations in plankton. More importantly, it suggests ways to probe other biological communities for the potential of resonance to fluctuations in their environment. Interestingly, climate change may modify the characteristic time scales of environmental fluctuations (Wigley et al. 1998; Easterling et al. 2000). While this component of climate change received little attention so far, our results suggest that it may affect the dynamics of biological communities in surprising ways.

Clearly the question ‘is there chaos out there?’ remains far from resolved when it comes to ecosystems in general. While my thesis has carried the topic a few steps further, many issues remain to be addressed that separate the simple models and controlled communities from natural communities. Nonetheless, the presence of chaotic dynamics has been observed in many other instances: in lab experiments with microbial communities (Becks et al. 2005; Graham et al. 2007), in the time series of epidemics (Schaffer and Kot 1986; Olsen et al. 1988; Olsen and Schaffer 1990; Schaffer et al. 1990) and in the time series of populations of insects and small mammals (Turchin and Taylor 1992; Hanski et al. 1993; Turchin 1993, 1995; Ellner and Turchin 1995). Another reason to think that chaotic dynamic could be important is that some of the underlying mechanisms, such as multi-species competition and predation, that are assumed to generate the chaotic behavior, are widespread in nature. This all

suggests that yes, most likely, there will be chaos out there.

6.2 Limits to prediction

While discussions on chaos may sometimes appear rather academic, the existence of intrinsic chaos implies a formidably different view of explanations of trends in nature. Much of ecology evolves around the search for explanations of trends in population densities. The idea that there may be no particular explanations for some of these trends other than intrinsically chaotic alternations in dominance challenges the traditional way in which the majority of ecologists view ecosystems. The core of this traditional view is that nature is either at equilibrium or is returning to equilibrium after a disturbance. The work in this thesis suggests that in the absence of external disturbances, *intrinsic* processes will still cause population densities to rise and fall forever in a chaotic way.

One of the fundamental implications of such chaos is that unless the abundances of species and all external influences are known at infinite precision, predictions of population development in the long term are impossible. The limited prediction horizon in chaotic systems is due to the phenomenon of sensitivity to initial conditions. For our enclosed plankton system we estimated a prediction horizon in the order of a few weeks; surprisingly close in fact to that of the weather. However, prediction horizons arising from intrinsic chaos in communities are scaled to generation times, implying large differences if one moves from microbes to communities of fish, corals, large terrestrial herbivores or trees.

Although the verdict ‘unpredictable in the long term’ may sound harsh, it is important to become slightly more specific if we want to understand what this means in practice. A first point to clarify is, what it is we would like to predict. For instance, in the case of plankton, are we interested in the biomass of a single species, of functional groups, or of the total biomass of an entire community? We might also be interested in predicting the timing of a bloom rather than its magnitude. Different targets can have different predictabilities. Consider for instance the results from our model exercise (**Chapter 4**) shown in Figure 6.1. The species fluctuations are irregular, yet these irregular fluctuations are locked within the seasonal cycle. As a consequence, each year species enter the winter season in different proportions, and this affects the species composition of the next spring bloom (Figure 6.1a). The interannual variability of plankton species is thus very high: the timing and height of each species peak may vary strongly between years (Figure 6.1a). However, when we lump all phytoplankton species and all zooplankton species together much less variability is observed (Figure 6.1b). The phytoplankton and zooplankton blooms start each year essentially at the same time, although some variability in maximum biomass during the bloom is observed between years (Figure 6.1b). Thus, it may be quite feasible in this system to predict the timing and magnitude of algal blooms, even though the ups and downs of the individual species are quite unpredictable.

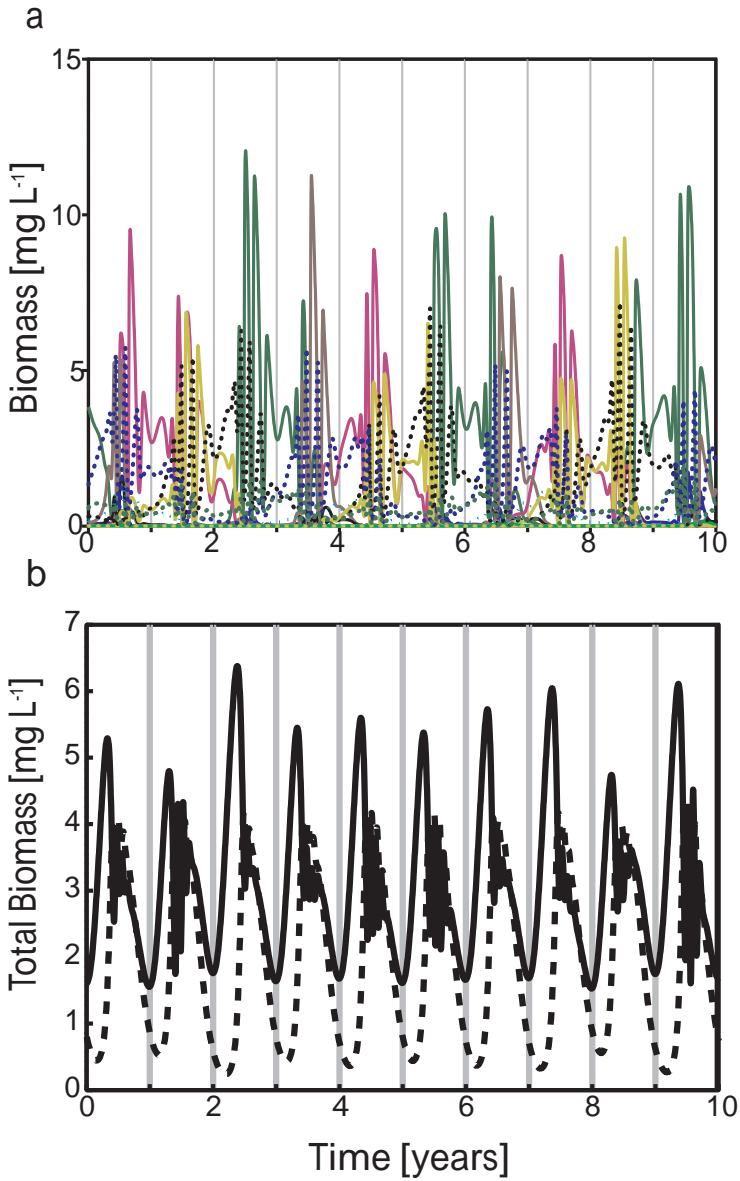


Figure 6.1: **a**, The biomass of individual phytoplankton and zooplankton species over time. **b**, Total phytoplankton biomass (solid line) and total zooplankton biomass (dashed line) over time. The graphs are based on simulations with the model of (Dakos et al. 2009) (**Chapter 4** of the thesis).

6.3 Methodological considerations

Although it is tempting to philosophize about possibilities for smart prediction of chaotic systems, we should recognize that even demonstrating that a system is driven by intrinsically chaotic processes remains remarkably hard in ecology. Obviously, the plankton time series of Dr. Reinhard Heerkloss was a gold-mine when it comes to detecting chaos. The food web was kept under constant conditions, and sampled with high frequency for thousands of generation times. For the detection of chaos in natural communities, the interplay of intrinsic population dynamics with external disturbances implies an extra challenge. In addition, a critical issue for the analysis of chaotic dynamics is the length of the time series in relation to the generation times of the organisms. This is one of the reasons why it may not be easy to repeat the power of our plankton analyses for other ecosystems like forests and savannas. Indeed, when corrected for generation times, a single summer for the plankton may compare to an entire interglacial period for a community of trees.

Certainly, closing in on the big question which systems may be governed to a large extent by intrinsic chaos will require a combination of approaches, ranging from models and experiments to smart data analysis. In the last 20 years many techniques have been developed for detecting chaos in ecosystems. Unfortunately, none of these methods is a silver bullet approach.

For instance, one option (used in **Chapter 2**) is a model-free approach, where the largest Lyapunov exponent is calculated directly from the time series (e.g., Rosenstein et al. 1993). Such approaches are called ‘direct methods’. Some authors have applied direct methods to very short time series. However, to obtain reliable estimates of Lyapunov exponents, temporally correlated data points should be removed by a so-called Theiler window (Kantz and Schreiber 1997). Therefore, direct methods require stationary time series of considerable length. In addition, direct methods assume that noise is negligible in comparison to the deterministic signal of the system. This assumption may be realistic for experiments performed under highly controlled laboratory conditions, but will be unrealistic for many natural ecosystems.

Alternatively, one may use time series data to fit statistical models (e.g., Ellner and Turchin 1995). The detection of chaos is then based on these statistical models, which can be used to calculate the largest Lyapunov exponent and to estimate the predictability of the system. Such approaches are called ‘indirect methods’, and were also applied in **Chapter 2** of the thesis. Fitting statistical models does not necessarily require long time series: in some cases, 50 points might even be sufficient (Hastings et al. 1993). Moreover, indirect methods can accommodate environmental noise, which makes this approach highly suitable for ecological data (Ellner and Turchin 1995).

Finally, instead of statistical models, one may develop a plausible mechanistic model to explain the population dynamics and estimate the model parameters from observations or experiments (e.g., Costantino et al. 1997). If the dynamic behavior of the parameterized population model is chaotic this suggests that the real population

could also be chaotic. This method has the advantage that lengthy time series are not needed, but has the disadvantage that the results will depend critically on the a priori choice of the population model. One way to deal with this limitation is to study a broad range of feasible models and parameter settings. The statistical analysis of the resulting behavior can then yield some estimate of the probability of chaos. Our analysis in **Chapter 4** of the thesis works along these lines.

Since each of these approaches has different strengths and weaknesses, the best way to analyze whether a system is chaotic, is to combine the different types of analyses.

6.4 The challenge ahead

The emerging view of chaotically driven communities suggests that for such systems, ecologists may have to shift away from the idea of forecasting the precise numbers of each individual species at any given time. Instead, ecologists could shift towards the equivalent of climate forecasting, where meteorologists cannot say whether it will rain on a given day in three months but can make predictions about whether a summer will be particularly dry, or a winter particularly cold. The monitoring and modelling methodology developed by meteorologists may provide a good example for improved prediction of ecosystems. Looking into this field further, we may also want to invest more in monitoring efforts for some important ecosystems, and use these monitoring results to continuously update model predictions, as is common practice in weather forecasts.

In addition, new approaches to investigate species fluctuations, such as the cross-wavelet analysis used in this thesis (**Chapter 3**), will be needed to make most out of the limited possibilities we have to unravel the dynamics of the hugely complex natural systems on which humanity depends. While our insight is deepening at a tantalizing slow pace, understanding the role of chaos is worth the effort. It fundamentally delineates what are relevant ambitions for ecologists when it comes to understanding and predicting changes in the abundances of species in nature.

Acknowledgements

I thank Marten Scheffer, Egbert van Nes and Jef Huisman for their helpful comments on this chapter.

Appendices

Appendix A

Supplementary information to chapter 2

A.1 Materials and methods of the mesocosm experiment

In spring 1989, the mesocosm was filled with a 10 cm sediment layer from the Darss-Zingst estuary (southern Baltic Sea, 54° 26' N, 12° 42' E). After preincubation for one week to stabilize the sediment, the mesocosm was filled with 90 litres of water from the same location, which had been filtered through a 200 μm gauze. This inoculum provided all species in the food web. During the first weeks, several plankton species were lost, as they were not able to survive the laboratory conditions. The sediment layer served as a source and refuge for resting stages and buffered the nutrient cycles.

The mesocosm was placed in a 15°C climate room, and heated by an aquarium thermostat (Rena Cal Excel aquarium heater, 100 Watt, Aquarium Pharmaceuticals, Chalfont, PA, USA) to maintain the mesocosm temperature at 20°C. The mesocosm was illuminated from above, by neon fluorescent lamps providing an incident irradiation of 50 $\mu\text{mol photons m}^{-2} \text{ s}^{-1}$ (16 hours/8 hours light-dark cycle). The mesocosm walls were not transparent. Salinity was maintained at 9‰, reflecting the salinity of the Darss-Zingst estuary. The mesocosm was constantly aerated by bubbling with compressed air.

Nutrients were measured weekly after filtration of 20-mL samples through glass fiber filters (Whatman GF/F, 0.7 μm). Concentrations of soluble reactive phosphorous and dissolved inorganic nitrogen (nitrate, nitrite and ammonium) were analyzed according to standard methods (Rohde and Nehring 1979; Grasshoff et al. 1983) using a flow-injection autoanalyzer (Alpkem RFA-300, Alpkem, Wilsonville, OR, USA).

Species abundances were measured twice a week. Picophytoplankton, nanophytoplankton, and protozoa were counted alive, immediately after sampling, in a Kolkwitz plankton chamber under fluorescence light using an interference contrast microscope (Olympus research microscope BH-2). Bacteria were counted using fluores-

cence microscopy, in samples fixed with 2% glutaraldehyde and stained with DAPI (Porter and Feig 1980). Zooplankton, detritivores, and filamentous diatoms were sampled by scooping 10 litres from the mesocosm using a 2-litre beaker. The water was sieved through a 50 μ m net to retain the plankton, and the filtrate was returned to the mesocosm. The sieved material was washed off into 20 ml aged biotope water and fixed with neutralized formaldehyde to a final concentration of 4%. For the abundant species, 200 individuals were counted. For less abundant species (i.e., with less than 200 individuals per sample), the total number of individuals per sample were counted. It was difficult to take a representative sample of the cyclopid copepods. The adults and later copepodite stages moved very fast, and escaped the scooping procedure by the beaker. Therefore, only the nauplii of the cyclopid copepods were counted. The abundances of the species were converted into biomass using geometric equivalents of the body volumes. A list of the geometric conversion factors of the different species is provided in Heerkloss et al. (1991).

Attached algae were brushed from the walls of the mesocosm once a month. During the entire experiment, small quantities of biotope water filtered (0.4 μ m pore size) from the Darss-Zingst estuary were added to compensate for water losses due to sampling. In addition, small quantities of distilled water were added to compensate for water loss due to evaporation.

A.2 Earlier analyses of the same time series

Part of the same time series has been presented in earlier publications (Heerkloss and Klinkenberg 1993, 1998; Dippner et al. 2002). The papers of Heerkloss and Klinkenberg (1993, 1998) present graphs of the time series, and suggest from visual inspection of the irregular ups and downs of the species that this food web might display chaotic dynamics. However, a nonlinear analysis of the data is not presented in their papers.

In contrast, Dippner et al. (2002) present a nonlinear analysis of the mesocosm data. However, they could not detect chaos in these time series. Why did Dippner et al. (2002) reach a conclusion that is completely different from our findings?

There were several differences between the approach of Dippner et al. (2002) and our approach.

First, Dippner et al. (2002) analyzed a shorter time series. They used the mesocosm data obtained until May 11, 1995 (day 1425 in our time series).

Second, Dippner et al. (2002) did not transform the time series to obtain stationary data with homogenized variances. As a consequence, their time series showed sharp spikes which may have hampered the interpretation of their results.

Third, Dippner et al. (2002) applied a different analysis. They used a graphical method known as recurrence quantification analysis (RQA). RQA is based on the analysis of recurrence plots, which were introduced by Eckmann et al. (1987). A recent review of recurrence plots is provided by Marwan et al. (2007). In essence, re-

currence plots visualize the times at which a trajectory visits roughly the same area in phase space. The recurrence of the trajectory to similar states, after some time of divergence, is one of the key features of deterministic dynamical systems. To draw a recurrence plot, one needs to define when trajectories are considered as ‘nearby’ (i.e., when they pass through roughly the same area). For this purpose, a ‘neighbourhood’ of radius r is defined in phase space and two trajectories are assigned as ‘nearby’ if they both pass through the same neighbourhood. Unfortunately, in retrospect, the size of the neighbourhood in Dippner et al. (2002) was chosen much too large. For calanoid copepods, for instance, Dippner et al. (2002, p. 33) used a neighbourhood with radius of $r=5 \text{ mg L}^{-1}$. However, this radius is about 30% of the maximum biomass measured in the calanoid time series. Moreover, population abundances of the calanoids remained below 5 mg L^{-1} for long stretches of time. In fact, the complete population dynamics of the calanoids from $t=400$ to 600 days (index=110 to 170), and also from $t=850$ to 1250 days (index=250 to 350) vanished within the same neighbourhood (this yielded the large black areas in their recurrence plots; compare Figure 1C and Figure 5 in Dippner et al. (2002)). Thus, in retrospect, many of the interesting ups and downs in the population dynamics of the calanoids remained undetected in their recurrence quantification analysis, and, hence, their resolution was too coarse to detect rapid chaotic fluctuations with a predictability of only 15-30 days. The same comment applies to their analysis of the other phytoplankton and zooplankton species.

A.3 Transformation of the time series

We transformed the original time series, shown in Figure 2.1b-g, to obtain stationary time series with equidistant data and homogeneous units of measurement. The transformation steps are illustrated for the bacteria (Figure A.1).

First, the time series were interpolated using cubic hermite interpolation, to obtain data with equidistant time intervals of 3.35 days (Figure A.1a).

Next, because the original time series showed many sharp spikes, the time series were rescaled using a fourth-root power transformation (Figure A.1b). The sharp spikes bias “direct method” estimates of the Lyapunov exponent, because nearby pairs of reconstructed state vectors mostly occurred in the troughs between spikes. The average rate of subsequent trajectory divergence from these pairs is therefore an estimate of the local Lyapunov exponent in the troughs, which may be very different from the global Lyapunov exponent. By making spikes and troughs more nearly symmetric, the power transformation resulted in a much more even spread of nearby state vector pairs across the full range of the data for all functional groups in the food web. The transformation is also useful for fitting nonlinear models of the deterministic skeleton (used for nonlinear predictability and indirect method estimates of the Lyapunov exponent), which was done by least squares and therefore is most efficient when error variances are stabilized. Fourth-root transformation

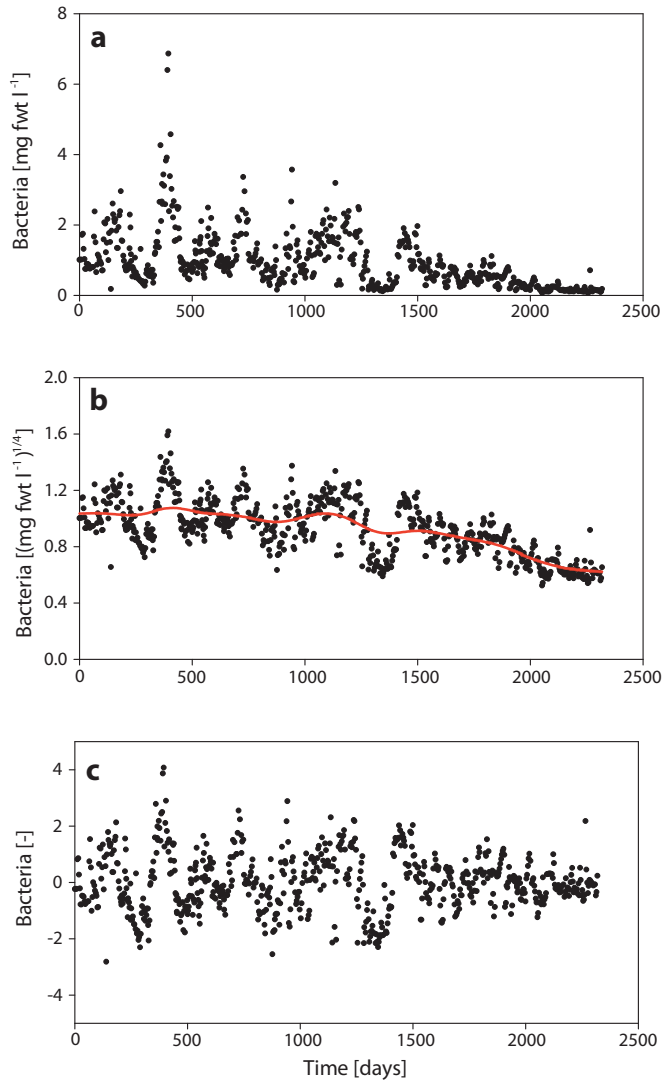


Figure A.1: Data treatment of the time series of bacteria. **a**, First, the time series was interpolated to obtain equidistant intervals of 3.35 days. **b**, Next, the time series was transformed by a fourth-root power transformation to suppress large spikes in the data, and the trend (red line) was calculated by a Gaussian kernel window with a bandwidth of 300 days. **c**, Finally, the time series was detrended, and subsequently normalized to obtain a stationary time series with mean zero and standard deviation of 1.

is intermediate between the square-root transformation that would approximately stabilize the measurement error variance in count data from random subsamples, and the log transformation that is usually recommended for stabilizing process noise variance due to stochastic variation in birth and death rates.

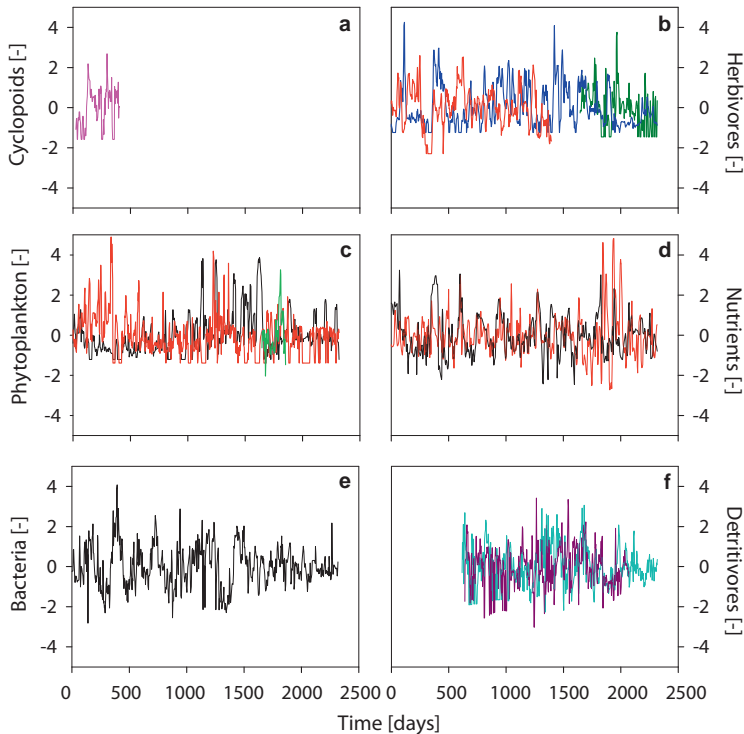


Figure A.2: Stationary time series of the functional groups in the food web, after data treatment. **a**, Cyclopoid copepods; **b**, calanoid copepods (red), rotifers (blue), and protozoa (dark green); **c**, picophytoplankton (black), nanophytoplankton (red), and filamentous diatoms (green); **d**, dissolved inorganic nitrogen (red) and soluble reactive phosphorus (black); **e**, heterotrophic bacteria; **f**, harpacticoid copepods (violet) and ostracods (light blue).

The time series were then detrended using a Gaussian kernel with a bandwidth of 300 days (red line in Figure A.1b), to obtain stationary time series. Most species did not show long-term trends, except for the bacteria, detritivores (ostracods and harpacticoid copepods), dissolved inorganic nitrogen and soluble reactive phosphorus. One possible explanation for these trends in the microbial loop could be the

slow accumulation of refractory organic material in the mesocosm, but we have not measured this component.

Finally, the time series were linearly rescaled to have zero mean and a standard deviation of 1 (Figure A.1c).

The time series of cyclopoid copepods, protozoa, filamentous diatoms, harpacticoid copepods and ostracods contained long sequences of zero values. This does not imply that these species were absent from the food web during these periods, but that their concentrations were below the detection limit. Time series dominated by many zeros can bias the statistical analysis. Therefore, these time series were shortened to remove long sequences of zero values, before the data transformation.

The transformed data of all species in the food web are shown in Figure A.2.

A.4 Spectral analysis

We applied spectral analysis to obtain a better understanding of the predominant periodicities in the species fluctuations. The discrete Fourier transform X for a time series of length N , with observations x_0, \dots, x_{N-1} , is:

$$X(k) = \frac{1}{\sqrt{N}} \sum_{j=0}^{N-1} x_j e^{-\frac{2\pi i j k}{N}} \quad (\text{A.1})$$

where $k = 0, \dots, N - 1$ is the frequency index. The power spectrum is defined as:

$$P(k) = X(k)X^*(k) \quad (\text{A.2})$$

where $X^*(k)$ is the complex conjugate of $X(k)$.

We present both raw power spectra (Figure A.3) and smoothed power spectra (Figure A.4). The raw periodogram is not a consistent estimator of the spectral density, as its variance does not converge to zero when increasing the length of a time series (Percival and Walden 1993). Consistent estimators can be derived by smoothing the raw periodogram. However, smoothing might introduce substantial bias at frequencies near spectral peaks by spreading and flattening the signal. Thus, there is a tradeoff between bias and variance. We smoothed the power spectrum using the modified Welch periodogram (Welch 1967). This method splits the time series in overlapping segments, called Hamming windows, and calculates the periodogram for each window separately. The Welch periodogram is then obtained by averaging the resulting periodograms. This yields a smooth periodogram, which is a consistent and asymptotically unbiased estimator of the spectral density. Visual inspection of the raw power spectra and Welch periodograms indicated that we obtained good results using 5 Hamming windows with 50% overlap.

All species in the food web showed reddened power spectra (i.e., decreasing power with increasing frequency; Figure A.3, A.4), indicating some persistence in the data. Therefore, the power spectra of the species were compared with the power spectrum

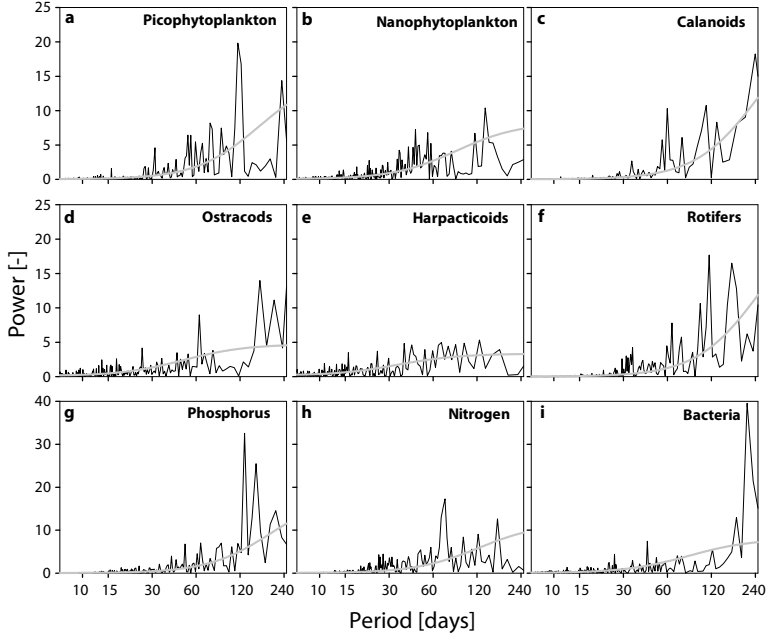


Figure A.3: Raw power spectra of the species. **a**, Picophytoplankton; **b**, nanophytoplankton; **c**, calanoid copepods; **d**, ostracods; **e**, harpacticoid copepods; **f**, rotifers; **g**, soluble reactive phosphorus; **h**, dissolved inorganic nitrogen; **i**, bacteria. For comparison, the grey line shows the red-noise spectrum calculated from an AR1-process. Note the different scale of the y-axes in panels **g-i**.

of red noise. A simple model for red noise is the univariate lag-1 autoregressive [AR(1)] process (e.g., Torrence and Compo 1998):

$$x_t = \alpha x_{t-1} + z_t \quad (\text{A.3})$$

where α is the lag-1 autocorrelation calculated from the time series under investigation, $x_0 = 0$, and z_t is taken from Gaussian white noise. Following Gilman et al. (1963), the power spectrum of red noise calculated from Eq. A.3 is:

$$P(k) = \frac{1 - \alpha^2}{1 + \alpha^2 - 2\alpha \cos \frac{2\pi k}{N}} \quad (\text{A.4})$$

where $k = 0, \dots, N - 1$ is the frequency index.

Both the raw spectra and Welch periodograms show that picophytoplankton, rotifers, and calanoid copepods fluctuated with periodicities of ≈ 30 days, and its

possible harmonics at ≈ 60 and ≈ 120 days (Figure A.3, A.3). This is consistent with earlier studies reporting periodicities of ≈ 30 days for phytoplankton-zooplankton oscillations (Scheffer and Rinaldi 2000; Fussmann et al. 2000).

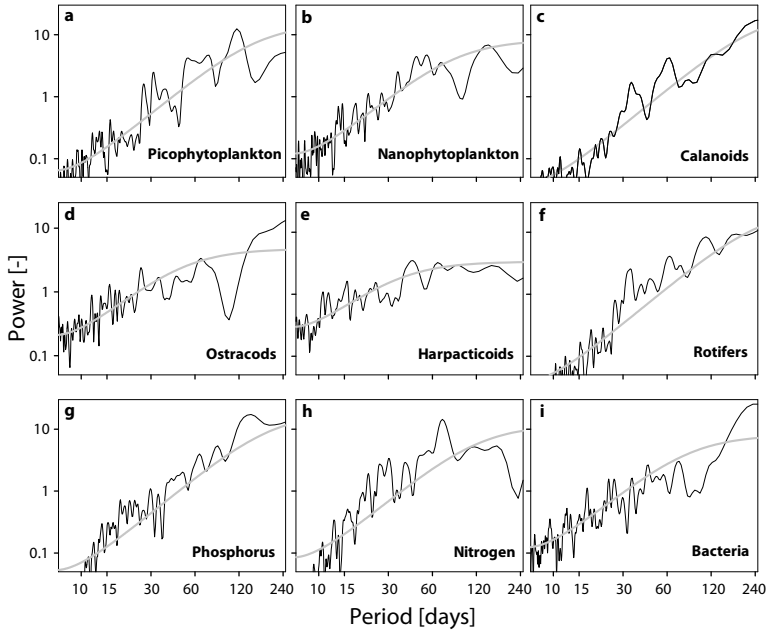


Figure A.4: Welch periodogram of the species. **a**, Picophytoplankton; **b**, nanophytoplankton; **c**, calanoid copepods; **d**, ostracods; **e**, harpacticoid copepods; **f**, rotifers; **g**, soluble reactive phosphorus; **h**, dissolved inorganic nitrogen; **i**, bacteria. For comparison, the grey line shows the red-noise spectrum calculated from an AR1-process. Please note that the power in this graph is plotted on a log scale.

The raw spectra further suggest that ostracods and harpacticoid copepods, which are connected to bacterial activity, may have fluctuated with periodicities of ≈ 15 days (Figure A.3). Other periodicities in the raw spectra can be observed at ≈ 25 days (bacteria, dissolved inorganic nitrogen, ostracods, harpacticoid copepods), ≈ 75 days (dissolved inorganic nitrogen), ≈ 150 days (soluble reactive phosphorus, ostracods), and ≈ 225 days (bacteria), which points at intriguing linkages between nutrients and the microbial loop at a range of commensurate frequencies (Figure A.3). However, many of these periodicities are evident only in the raw spectra and less in the Welch periodogram. For this reason we cannot tell with certainty whether these periodicities of the nutrients and microbial loop are real features of the food web.

A.5 Predictability

A.5.1 Neural network

To investigate the predictability of the food-web dynamics, we employed a neural network model for each species in the food web. The neural network model assumes that the population dynamics of the focal species is a (complex nonlinear) function of the population abundances of this focal species and the species that have a direct link to this focal species (cf. Eq. 2.1 in chapter 2):

$$N_{i,t+T} = f_{i,T}(N_{i,t}, N_{1,t}, N_{2,t}, \dots, N_{m,t}) \quad (\text{A.5})$$

where $N_{i,t}$ is the population abundance (or nutrient concentration) of species i at time t , the subscripts 1 to m indicate all species directly linked to species i , T is the prediction time (i.e., the number of days that we want to predict in advance), and $f_{i,T}$ is an unknown function estimated by the neural network model.

The architecture of the neural network model is shown in Figure A.5. The input of the network is received by input units, which monitor the population abundances of the focal species and the species linked to this focal species. The input values are passed on to a layer of hidden units. Each connection between input unit j and hidden unit k (indicated by an arrow in Figure S5) performs a linear transformation determined by the connection strength γ_{kj} . Hence, the total input for hidden unit k at time t is given by:

$$in_k = \gamma_{ki}N_{i,t} + \sum_{j=1}^m \gamma_{kj}N_{j,t} + \alpha_k \quad (\text{A.6})$$

where the first term on the right-hand side describes the neuron's activity due to input from the focal species i , the second term describes the neuron's activity due to input from the connected species, and the third term, α_k , describes the neuron's intrinsic activity level. In other words, each hidden unit receives its own input, depending on its connection strengths to the input units and its intrinsic activity level.

The hidden unit performs a non-linear transformation on its total input, defined by the activation function ψ . This activation function is the same for all hidden units. Typically, the activation function is a sigmoid function, which approaches zero if the total input is very negative, while it approaches 1 if the total input is very positive. Following Nychka et al. (1992), we used the following activation function:

$$\psi(in_k) = \frac{in_k(1 + |\frac{in_k}{2}|)}{2 + |in_k| + \frac{in_k^2}{2}} \quad (\text{A.7})$$

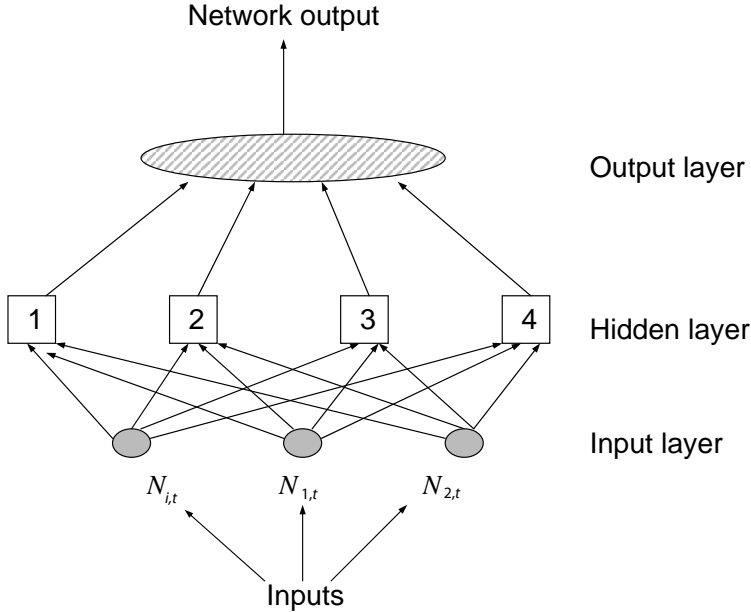


Figure A.5: Architecture of the neural network model. In this example, the input layer consists of 3 input units representing the population abundances of focal species i and two connected species at time t , the hidden layer consists of 4 hidden units, and the output layer predicts the new population abundance of focal species i at time $t+T$.

The activation signals from the hidden units are collected by a single output unit, which performs a linear transformation on the activation signals to present the output of the neural network. The network output can therefore be written as:

$$Out = \beta_0 + \sum_{k=1}^n \beta_k \psi(in_k) \quad (\text{A.8})$$

where β_0 is the intrinsic output level, the β_k 's are the weights given to the activation signals from different hidden units, and n is the total number of hidden units. This output represents the model prediction, by the neural network, of the population abundance of the focal species. The total number of hidden units, n , should be sufficiently large to avoid inaccurate predictions, but should not be too large either as a large number of hidden units increases the computation time substantially. We selected the total number of hidden units by minimizing a generalized cross-validation statistic (GCV_2) with 2-fold overweighting of model degrees of freedom to avoid overfitting (Nychka et al. 1992). This yielded an estimate of 4 hidden

units for bacteria, nanophytoplankton and protozoa, 5 hidden units for cyclopid and calanoid copepods, rotifers, picophytoplankton, phosphorus, nitrogen, ostracods and harpacticoid copepods, and 6 hidden units for filamentous diatoms. The parameters ($\alpha_k, \beta_i, \gamma_{ij}$) of the neural network models were estimated using the software package LENNS (Ellner et al. 1992; Nychka et al. 1992), which fits neural networks to data using a least-squares approach.

A.5.2 Testing for differences between the nonlinear and linear model

We tested whether the nonlinear neural network model yielded significantly higher predictabilities than the corresponding linear model. For this purpose, we calculated the Pearson product-moment correlation coefficient (r) between predicted and observed values, for both the nonlinear model (r_1) and the linear model (r_2). These correlation coefficients are simply the square roots of the coefficients of determination (R^2) shown in Figure 2.2 of the main text.

For each prediction time, we tested the null hypothesis that the linear model and nonlinear model yielded the same predictability (i.e., $r_1=r_2$) against the alternative hypothesis that the nonlinear model yielded better predictions than the linear model (i.e., $r_1>r_2$). The two correlation coefficients were both transformed with the Fisher z-transformation ((Sokal and Rohlf 1995)):

$$z_i = \frac{1}{2} \ln \left(\frac{1 + r_i}{1 - r_i} \right) \tag{A.9}$$

The sampling distribution of the z statistic is known to be approximately normal, with a standard error of

$$\sigma_z = \frac{1}{\sqrt{N-3}} \tag{A.10}$$

where N is the number of observations. We note that, in our case, N is the same for both correlation coefficients, since they are calculated for the same time series. Accordingly, we calculated the difference

$$\Delta z = \frac{z_1 - z_2}{\sqrt{\frac{2}{N-3}}} \tag{A.11}$$

Under the null hypothesis, the sampling distribution of Δz has a standard normal distribution with mean of 0 and standard deviation of 1. Hence, in view of the alternative hypothesis, we rejected the null hypothesis if the calculated value of Δz exceeded the 95th percentile of the standard normal distribution. The results show that, already after one time step, the nonlinear model yielded significantly better predictions than the linear model for all species (Table A.1).

Species	Prediction time			
	1	2	3	>3
Bacteria	< 0.02	< 0.001	< 0.001	< 0.001
Harpacticoids	< 0.001	< 0.001	< 0.001	< 0.001
Ostracods	< 0.001	< 0.001	< 0.001	< 0.001
Nitrogen	<i>n.s.</i>	< 0.02	< 0.001	< 0.001
Phosphorus	<i>n.s.</i>	< 0.005	< 0.001	< 0.001
Picophytoplankton	< 0.05	< 0.001	< 0.001	< 0.001
Nanophytoplankton	<i>n.s.</i>	< 0.01	< 0.001	< 0.001
Filamentous diatoms	< 0.02	< 0.001	< 0.001	< 0.001
Rotifers	< 0.05	< 0.001	< 0.001	< 0.001
Protozoa	<i>n.s.</i>	< 0.01	< 0.005	< 0.005
Calanoids	<i>n.s.</i>	< 0.01	< 0.001	< 0.001
Cyclopoids	<i>n.s.</i>	< 0.05	< 0.05	< 0.02

Table A.1: Statistical evaluation of differences between the predictability of the nonlinear neural network model and the predictability of the best-fitting linear model. Data entries show p values, for each species and each prediction time (measured in time steps, where one time step equals 3.35 days). If $p < 0.05$, the nonlinear model had a significantly higher predictability than the linear model. *n.s.* = not significant.

A.6 Methods for estimating Lyapunov exponents

Numerous methods have been proposed and studied for estimating Lyapunov exponents from time series data. Essentially, these methods can be classified into two types of approaches, *direct methods* and *indirect methods* (the latter are also called *Jacobian methods*); we applied both approaches.

A.6.1 Direct method by time-delay embedding

Direct methods descend from Guckenheimer (1982) and Wolf et al. (1985). The data are searched to find nearby pairs of state vectors (or reconstructed state vectors). In other words, the data are searched for different points in the time series at which all species abundances in the food web are in a similar state. The rate of trajectory divergence at subsequent times, averaged over many such pairs, is an estimate of the dominant Lyapunov exponent λ .

All calculations to estimate the Lyapunov exponent by the direct method were performed using the software of the Tisean package (Hegger et al. 1999). We chose the procedure of Rosenstein et al. (1993), because it was specifically developed and tested for short, noisy time series (which ours are by the standards of theoretical physics). This method uses attractor reconstruction by time-delay embedding (Takens 1981; Strogatz 1994; Kantz and Schreiber 1997), so that separate estimates could be obtained for each species in the food web, providing an additional check on the robustness of our conclusions.

Time-delay embedding requires a suitable choice of time delay and embedding

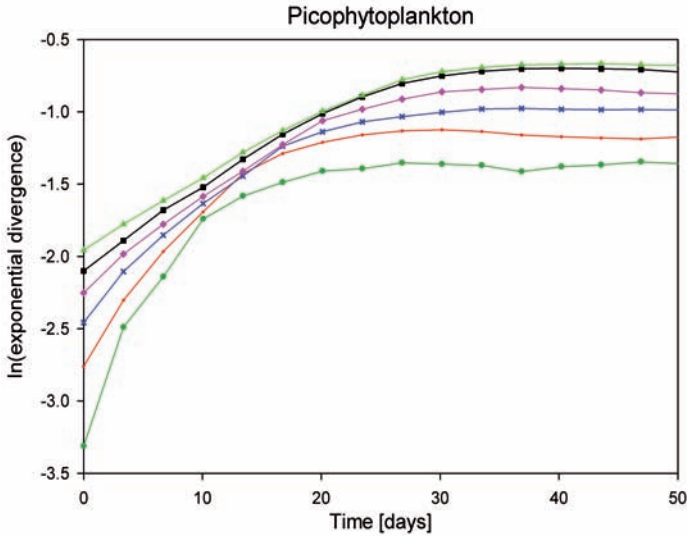


Figure A.6: Exponential divergence of the trajectories of picophytoplankton as a function of time, calculated with different embedding dimensions ($m=3$, dark green; $m=4$, red; $m=5$, blue; $m=6$, pink; $m=7$, black; $m=8$, light green). Exponential divergence is plotted on a natural-logarithmic scale. Robust estimates of the Lyapunov exponent require that the initial slope of the exponential divergence is independent of the exact value of the embedding dimension. This requirement is fulfilled with an embedding dimension of $m \geq 6$.

dimension. Since all data are from the same dynamical system, we chose a single value of the time delay and embedding dimension representative for the entire food web. Rosenstein et al. (1993) suggested that a good choice of time delay is the time lag where the autocorrelation function drops to a fraction $1 - \frac{1}{e}$ (i.e., 63%) of its initial value. Following this criterion, we estimated time delays ranging from 1 to 4 time steps, depending on the species (where 1 time step equals 3.35 days). Turchin (2003) suggested a time delay of 1 time step for organisms with generation times less than the unit time interval. In our food web, several species have a generation time equal or less than ≈ 3.35 days (e.g., bacteria, picophytoplankton, nanophytoplankton, filamentous diatoms, ostracods, rotifers). Hence, a time delay of 1 time step would seem suitable. A time delay of 1 also gave robust results in terms of the linear scaling region in the exponential divergence which is used to calculate the Lyapunov exponent. Accordingly, we chose a time delay of 1 time step.

Theory suggests that the embedding dimension, m , can be estimated by the value

where the number of false nearest neighbours drops to zero (Kantz and Schreiber 1997). Following this criterion, we estimated embedding dimensions ranging from $m=4$ to $m=9$, depending on the species. At embedding dimensions of 6 and higher, the initial slope of the exponential divergence became independent of embedding dimension (Figure A.6). Hence, we chose an embedding dimension of $m=6$.

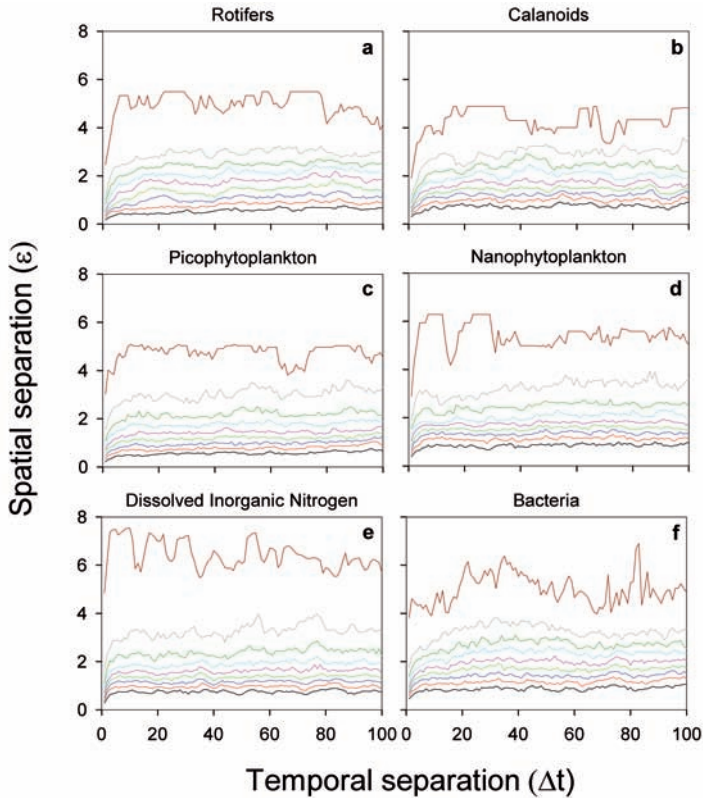


Figure A.7: Space time separation plots of the functional groups. **a**, Rotifers; **b**, calanoid copepods; **c**, picophytoplankton; **d**, nanophytoplankton; **e**, dissolved inorganic nitrogen; **f**, bacteria. The plots indicate how the temporal distance between pairs of data points from the time series affects their spatial distance on the reconstructed attractor. Contour lines are shown at the spatial distance ε where for a given temporal separation Δt (in time steps) a fraction of $1/10$, $2/10$, (lines from below) of pairs are found.

Estimates of trajectory divergence, and therefore of the Lyapunov exponent, may be distorted if nearby state vectors (in state space) are also near in time. For example, the time-delay state vector consisting of samples 101-106 is near to

that consisting of samples 102-107, and their future histories never diverge very far. The Theiler window offers a classical and effective solution to this problem (Theiler 1986; Kantz and Schreiber 1997). A Theiler window removes temporally nearby data points from the set of pairs used to estimate trajectory divergence. We estimated a suitable size of the Theiler window by visual inspection of space time separation plots (Provenzale et al. 1992). Space time separation plots show how the temporal distance between pairs of data points affects their spatial distance on the reconstructed attractor (Figure A.7). The Theiler window should be sufficiently large to exclude those data points for which the spatial distance on the attractor is affected by their temporal distance. For our species, the effect of temporal distance on spatial distance vanished when data points were separated by more than 10 to 20 time steps (Figure A.7). To be on the safe side, we therefore introduced a Theiler window of 50 time steps (≈ 170 days) for each species in the food web.

A.6.2 Jacobian method: a neural network food web model

Jacobian methods descend from Eckmann et al. (1986). These are based on the development of a deterministic model of the underlying dynamics of the system. This deterministic model will henceforth be called the ‘*deterministic skeleton*’. The deterministic skeleton is differentiated to estimate the Jacobian matrices. The Lyapunov exponent is then defined in terms of the sequence of Jacobian matrices of the deterministic skeleton, evaluated at the time series of observed or reconstructed state vectors. Thus, Jacobian methods require the preliminary step of estimating the deterministic skeleton, either locally or by fitting a global map to the time series. For theoretical properties of Jacobian methods, see McCaffrey et al. (1992); Bailey et al. (1997); Lu and Smith (1997).

The length of our time series and the high dimensionality of the system (i.e., the relatively large number of interlinked species in the food web) favour the use of a neural network regression model to estimate the deterministic skeleton, as discussed by Ellner and Turchin (1995). However, our analysis here incorporates some subsequent developments. In particular, follow-up studies have shown that semi-mechanistic (also called semi-parametric) models should be preferred over state space reconstruction in time-delay coordinates (Ellner et al. 1998; Smith et al. 2000). “Semi-mechanistic” means that the structure of the model is based on biological knowledge about the system (when that is available), as are any process rate equations for which independent data are available, while nonparametric methods are used to fit aspects about which little is known. Here we used the food web structure (Figure 2.1a) to dictate the structure of the model, exactly as in the estimates of nonlinear predictability. Hence, functional relationships in the model include only those species that have a direct link in the food web to the focal species. So for example, the deterministic skeleton for rotifers is assumed a priori to have the form

$$rot(t+1) = f_{rot}[rot(t), cyclo(t), pico(t), nano(t), bact(t)] \quad (\text{A.12})$$

where t is the time measured in time steps of 3.35 days. The omission of other dependencies (e.g., absence of nutrients on the right-hand side of the last equation) leads to structural zeros in the fitted Jacobians, which avoids “fitting the noise” or incorporating functional relationships in the model that are absent in the real system. Another advantage of adopting the food web structure is that it eliminates the potential problem of spurious exponents in Jacobian-based estimates using state space reconstruction (Sauer et al. 1998).

As in the direct method estimates, the forecasting interval (one sample time) is chosen on mechanistic grounds (generation time) rather than a statistical rule-of-thumb. However, the skeleton maps f were estimated by fitting a neural network regression model with no a priori limits on the number of hidden units, so that any model shape and complexity can be fitted, if there is evidence for it in the data.

Hence, the final issue is selecting the complexity (number of hidden units) of the skeleton map for each species in the food web. This has no simple resolution. To avoid overfitting we need a conservative criterion. Ellner and Turchin (1995), following Nychka et al. (1992), used GCV_2 , a modification of the Generalized Cross Validation criterion in which model degrees of freedom are overweighted by a factor of 2. Subsequent work suggested that twofold overweighting may be excessive. With short, noisy time series Kendall (2001) found that GCV_2 model selection had a substantial risk of drastically underfitting, leading to spurious strongly negative estimates of λ . For longer and less noisy data sets, McCaffrey et al. (1992) and Nychka et al. (1992) obtained good results using the Bayesian Information Criterion (BIC) with neural network models. Assuming Gaussian errors and using the maximum likelihood estimate of the error variance (i.e. the mean squared residual error, MSE), the BIC criterion is equivalent to choosing the model that minimizes $\log(MSE) + P \frac{\log(N)}{N}$, where P is the number of model parameters and N is the sample size. GCV_2 is equivalent to selecting the model that minimizes $\log(MSE) - 2 \log(1 - \frac{2P}{N})$. For our time series length, the BIC criterion is more conservative.

Based on these considerations, we applied both the GCV_2 and BIC criteria to estimate the number of hidden units. However, in our case, both criteria gave rather similar results. Depending on the species, we obtained skeleton maps f with up to 8 hidden units, which was sufficient for model selection under all criteria.

All calculations to estimate the Lyapunov exponent by the Jacobian method were performed using the LENNS software (Ellner et al. 1992; Nychka et al. 1992). An R (R Development Core Team 2006) version of LENNS for the Windows operating system is available on request from S.P.E. or can be downloaded from <http://www.eeb.cornell.edu/ellner/software>.

To place confidence limits on the estimate of λ we used bootstrapping in particular the “resampling errors” approach to bootstrapping regression models (Davison and Hinkley 1997), as follows. For each functional group i in the food web, let $\hat{f}_i(X_i)$ denote the fitted deterministic skeleton map, where X_i is the vector of all functional groups linked with species i , including itself. From this we obtain a time series of forecasting errors $e_i(t) = x_i(t) - \hat{f}_i(X_i(t-1))$. Each bootstrap sample for

functional group i was generated by first sampling with replacement from $\{e_i(t)\}_{t=2}^N$ to generate a series $\{e_i^*(t)\}_{t=2}^N$. These reshuffled error terms were subsequently used to create a new time series consisting of fictitious “one step ahead” data

$$x_i^*(t) = \hat{f}_i(X_i(t-1)) + e_i^*(t) \quad (\text{A.13})$$

For each such “data set” we then refitted the neural network model (with x_i^* as the response variable, and the real data series $X_i(t-1)$ as the predictors), including selection of model complexity by the BIC criterion. Due to the high computational time required for fitting neural network models reliably, we limited the complexity of the refitted networks to at most 1 more hidden unit than the number selected by BIC for the real data. Because more complex models have a tendency to lead to more strongly positive estimates of λ , this limitation is conservative for our purposes (assessing the strength of evidence that $\lambda > 0$). Obtaining 1000 bootstrap replicates required about one month on a current desktop PC.

Based on these 1000 bootstraps, a one-sided confidence interval at the 95% confidence level yielded a lower bound of $\lambda = 0.03 \text{ d}^{-1}$. This confirms that the Lyapunov exponent was significantly positive. We also report the two-sided confidence interval at the 95% confidence level, which yielded $0.025 < \lambda < 0.109 \text{ d}^{-1}$.

We also assessed the robustness of the Jacobian estimates informally in several different ways (these were done individually, not in all possible combinations).

- We modified the food web by completely removing the detritivores (ostracods and harpacticoid copepods), and subsequent refitting of the neural network model to the remaining time series.
- We eliminated the first 500 days of the time series, during which the temperature was slightly higher than 20°C.
- Instead of a neural network we used a generalized additive model (GAM) with spline ridge functions (Wood 2006, package **mgcv** package in R). The model for functional group i included a univariate self-limitation spline term $s(x_i)$, a univariate spline term $s(x_j)$ for each group j linked to group i , and a bivariate spline term $s(x_i, x_j)$ for each group j linked directly to group i (i.e., indirect links via the microbial loop were not represented by bivariate spline terms). A spline GAM can be fitted quickly and reliably, including selecting model complexity by GCV criteria, but it cannot include higher-order interactions (for example, all possible 3-way interactions between rotifers and all groups linked to them) due to the large number of basis functions required for such a model. We fitted the GAM to the shortened time series mentioned just above.

All of these modifications produced similar results, in particular they all yielded a positive value for the dominant Lyapunov exponent. For the GAM model, we obtained a Lyapunov exponent of $\lambda = 0.08 \text{ d}^{-1}$, and an application of our bootstrap procedure (using 200 replicates) resulted in a positive lower bound of the Lyapunov

exponent at the 95% confidence level of 0.024 d^{-1} . Analyses of the shorter time series (without the first 500 days) produced a slightly larger estimate of the dominant Lyapunov exponent, of $\lambda=0.097 \text{ d}^{-1}$, with a positive lower bound at the 95% confidence level of 0.02 d^{-1} .

A.7 Temperature fluctuations

The mesocosm was placed in a 15°C climate room, and heated by an aquarium thermostat to maintain a constant water temperature. During the entire period of investigation, for 2,319 days, the temperature of the mesocosm was $\approx 20^\circ\text{C}$ (mean= 20.28°C , s.d.= 1.07°C , $n=688$). Nevertheless, some temperature fluctuations were unavoidable (Figure A.8a), either by failure of the climate room or by failure of the aquarium thermostat. For instance, accidental failures of the thermostat resulted in a fast temperature increase on April 3, 1992 (day 292), June 17, 1993 (day 732), May 18, 1995 (day 1432), and September 4, 1997 (day 2272).

One might argue that the chaotic behavior of the food web could have been driven by the temperature fluctuations. There are actually two hypotheses: (1) the temperature itself fluctuated chaotically, and/or (2) the temperature was not chaotic, but temperature variability pushed the species dynamics into a chaotic regime.

To investigate these hypotheses, we carried out several analyses. For this purpose, the temperature data were transformed in exactly the same way as the species in the food web (i.e., interpolation, fourth-root power transformation, detrending, and normalization of the time series). This yielded a stationary time series with equidistant data and homogeneous units of measurements (Figure A.8b).

First, we investigated whether the observed species variability was associated with temperature variability, by calculation of the product-moment correlation coefficient between the species abundances and temperature. This revealed that bacteria and rotifers showed significantly positive correlations with temperature, whereas the other species did not show a significant relationship (Table A.2). Visual inspection of the data suggested that the positive correlations of bacteria and rotifers could be attributed to the slightly elevated temperatures from day 300 to day 475 (Figure A.8a; mean= 21.55°C ; s.d.= 0.96°C , $n=47$). Indeed, when we shortened the time series by removal of the first 500 days, none of the species in the food web showed significant correlations with temperature anymore (Table A.2). Hence, we conclude that the temperature fluctuations may have had some effect on the species abundances, but that this effect was relatively minor and mainly concentrated in the first 500 days of the time series.

Second, we investigated the predictability of the temperature fluctuations by developing a neural network model using the same methodology as for the species in the food web. However, we could of course not exploit the food web structure to predict temperature, and instead we predicted the temperature by time-delay embedding of the time series. We used a time delay of $d=1$ time step, which cor-

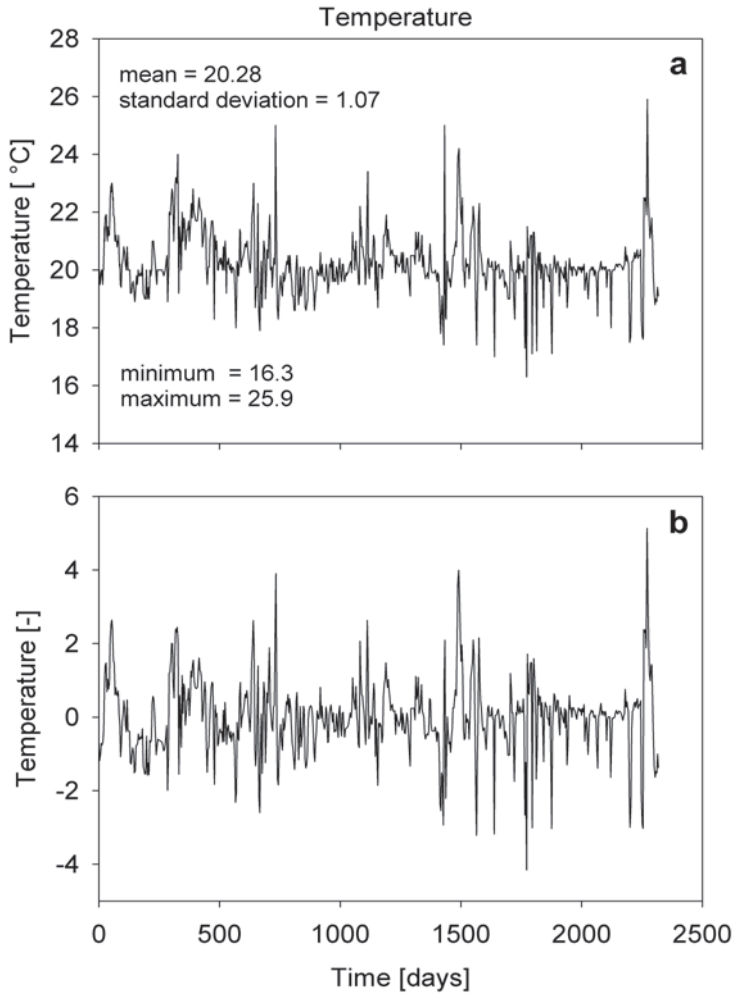


Figure A.8: Time series of the temperature in the mesocosm experiment. **a**, Original time series. **b**, Stationary time series after data transformation.

responded to the value where the autocorrelation function dropped to $1 - \frac{1}{e}$. We used an embedding dimension of $m=3$, corresponding to the first minimum of the GCV_2 statistics as a function of the embedding dimension. The results showed that the predictability of temperature was already low for a prediction time of only one time step ($R^2=0.14$), and was further reduced from the second time step onwards ($R^2<0.08$). Hence, the temperature signal was noise dominated, with only a very

Species	Correlation coefficient	
	complete time series	shortened time series
Bacteria	0.11*	0.11
Harpacticoids	0.09	0.09
Ostracods	0.10	0.11
Nitrogen	0.02	0.03
Phosphorus	0.07	-0.11
Picophytoplankton	-0.12	-0.04
Nanophytoplankton	-0.07	-0.07
Rotifers	0.11*	0.08
Protozoa	-0.01	0.00
Calanoids	-0.11	0.05

Table A.2: Correlations between species abundances and temperature. Table entries show the product-moment correlation coefficients, after transformation of the data to stationary time series (see Methods section). In the shortened time series, the first 500 days were removed from the data set. Significance tests were corrected for multiple hypothesis testing by calculation of adjusted p-values using the false discovery rate (Benjamini and Hochberg 1995). Significant correlations are indicated in bold: *** $p < 0.001$, ** $p < 0.01$; * $p < 0.05$. Filamentous diatoms and cyclopoid copepods were not included in the correlation analysis, because their time series contained too many zeros.

weak deterministic component.

Third, we estimated the Lyapunov exponent using both direct and indirect methods. In the direct method, the Lyapunov exponent was estimated using attractor reconstruction by time-delay embedding, following exactly the same approach as for the species. We used a time delay of $d=1$ time step, an embedding dimension of $m=3$, and a Theiler window of 70 time steps (about 235 days). This yielded a strongly positive Lyapunov exponent ($\lambda=0.151 \text{ d}^{-1}$). Does this imply that the temperature fluctuations were driven by chaotic dynamics? Not necessarily. The direct method may yield positive Lyapunov exponents when the dynamics are chaotic, but also when the dynamics are not chaotic but dominated by noise (Ellner and Turchin 1995). Moreover, the predictability results above had indicated that the temperature fluctuations were noise dominated.

The indirect method is specifically designed for noisy data sets; it avoids the noise signal by investigation of the deterministic skeleton underlying the time series. For this purpose, we used again a neural network model to estimate the deterministic skeleton, and subsequently calculated the Lyapunov exponent by evaluation of the Jacobian matrices. The methodology was as described previously (see the earlier section on the Jacobian method). However, because we could not exploit the food web structure, we used time-delay embedding with a time delay of $d=1$ time step and an embedding dimension of $m=3$ to generate the neural network model. This yielded a strongly negative Lyapunov exponent ($\lambda=-0.091 \text{ d}^{-1}$). In fact, a negative Lyapunov exponent should have been expected, because the temperature was regulated by a thermostat system (i.e., the temperature trajectories should all converge

to the same point attractor at 20°C). The contrasting results from the direct and indirect method emphasize once more that assessment of the chaotic nature of noisy time series (i.e., many ecological time series) requires investigation of the underlying deterministic skeleton.

Thus, we conclude that the temperature fluctuations were not driven by chaotic dynamics, but reflected a stable thermostat system disturbed by noise.

Finally, could the temperature fluctuations have pushed the species dynamics into a chaotic regime? In principle, this could have been the case. However, the species abundances showed at best only a very weak relationship with temperature (Table A.2). Moreover, the positive Lyapunov exponent of the entire food web, estimated by the indirect method (see main text), points out that the underlying population dynamics were chaotic. Hence, we conclude that the chaotic nature of this food web was not driven by external forcing, but by the food web interactions themselves.

Appendix B

Supplementary information to chapter 3

B.1 Introduction

Time series play a prominent role in ecology and environmental management. They usually consist of a series of observations of species abundances and other relevant ecological variables, gathered at regular intervals over a long period of time. Time series are widely used to monitor long-term changes in the species composition of freshwater, terrestrial and marine ecosystems, for instance to investigate impacts of eutrophication, fisheries, or global warming. Time series are also commonly used to study regular or irregular fluctuations in species abundances, as in the famous hare-lynx cycles of northern Canada (Elton and Nicholson 1942; Stenseth et al. 1997), in disease dynamics (Grenfell et al. 2001; Rodó et al. 2002), or in studies of algal bloom dynamics (Smetacek and Cloern 2008).

Several statistical techniques are available to extract information from ecological time series. Traditionally, periodic signals in time series are analyzed by means of spectral analysis (Platt and Denman 1975; Chatfield 1989). Spectral analysis, also known as Fourier analysis, decomposes the fluctuations of a time series into different oscillating components with different frequencies (periods). Spectral analysis produces a periodogram or power spectrum. Peaks in the power spectrum indicate which frequencies (periods) occur most dominant, which enables detection of characteristic periodicities in time series.

However, spectral analysis requires that time series are stationary. That is, spectral techniques assume that the statistical properties of time series do not vary over time. This makes it difficult to apply spectral analysis to ecological time series, because many ecological time series are not stationary. The non-stationarity of ecological time series may originate from many sources. For instance, the expansion of human populations is known to have major impacts on ecosystems, resulting in large changes in species composition and loss of biodiversity in response to, e.g., environmental pollution, urbanization and other changes in land use, or deforestation and local harvesting. Ecosystems may also switch from one relatively stable state to another state through regime shifts, which manifest themselves as abrupt reorgani-

zations of entire ecosystems often in response to gradual changes in climate or other environmental conditions (Hare and Mantua 2000; Scheffer and Carpenter 2003). Non-stationarity of time series may also result from intrinsic processes, generated by complex dynamics within natural ecosystems (Hastings et al. 1993; Benincà et al. 2008). The chaotic dynamics in our experimental food web provides an example. In all these cases, one would like to apply a method that can capture the observed changes in the periodic signal of these non-stationary time series.

During recent years a new methodology has been developed, called wavelet analysis. In contrast to spectral analysis, wavelet analysis is particularly suitable for non-stationary time series. In essence, wavelet analysis decomposes local fluctuations observed during a small stretch of time into different frequencies (periods). Thus, wavelet analysis characterizes periodic signals in terms of both frequency and time. Through this approach, wavelet analysis can keep track of changes in the periodic signal of fluctuations. This makes wavelet analysis a very attractive tool for the analysis of ecological time series (Grenfell et al. 2001; Keitt and Fisher 2006; Ménard et al. 2007; Keitt 2008). Moreover, wavelet techniques have been further extended to compare fluctuations in two time series, through a method known as cross-wavelet analysis. Cross-wavelet analysis aims at the detection of similar periodicities in the fluctuations of two time series, and also estimates the phase angles between these periodicities. Cross-wavelet analysis is therefore a quite natural and very interesting technique for the analysis of predator-prey oscillations and other forms of coupled oscillations.

In this appendix, we first present a simple example to illustrate the basic ideas of wavelet analysis. Next, we discuss the theory underlying wavelet analysis and explain our significance tests. Finally, we move on to introduce cross-wavelet analysis and a related method known as wavelet coherence. Excellent reviews on wavelet analysis are provided in Torrence and Compo (1998), Grinsted et al. (2004), Cazelles et al. (2008).

B.2 A simple example

In Figure B.1, we have presented two time series to illustrate the interpretation of wavelet power spectra. Both time series contain two periodic components: fast fluctuations with a period of 1 day and slow fluctuations with a period of 5 days. Figure B.1a shows a stationary time series; the two periodic components are present throughout the entire time series. Figure B.1b presents an example of a non-stationary time series. The fast fluctuations are present only during the first half of the time series, and are then replaced by slow fluctuations during the second half of the time series. Spectral analysis yields exactly the same power spectra for both time series (Figure B.1c and Figure B.1d), with peaks at the dominant periods of 1 and 5 days.

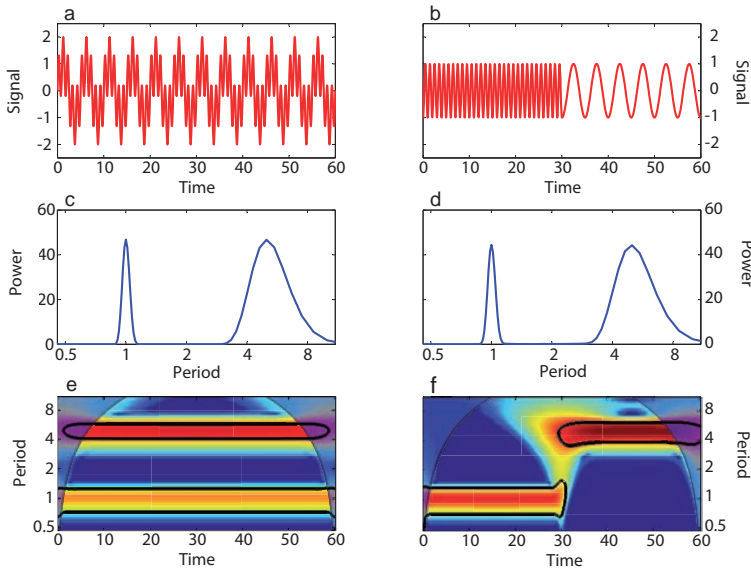


Figure B.1: A simple example illustrating the interpretation of wavelet power spectra. **a**, Time series consisting of a fast and a slow periodic signal that are both present during the entire time series. **b**, Time series that begins with a fast periodic signal, but shifts towards a slow periodic signal. **c**, **d**, Power spectra obtained by classic spectral analysis, for the time series shown in **a** and **b**, respectively. The power spectra are smoothed using the modified Welch periodogram. **e**, **f**, Wavelet power spectra obtained by wavelet analysis, for the time series shown in **a** and **b**, respectively. Wavelet power spectra are presented as contour plots, where the y-axis plots the periodicities detected in the time series, and the x-axis plots how these periodicities change over time. Colour coding indicates the wavelet power, ranging from low power in blue to high power in red. Black contour lines enclose significant regions in the wavelet power spectra. Shaded areas on both sides of the contour plots represent the cone of influence, where edge effects might distort the signal.

However, wavelet power spectra of the two time series are different (Figure B.1e and Figure B.1f). The contour plots show how the wavelet power spectra change during time. High wavelet power is indicated by red and orange colours, surrounded by black contour lines indicating significant regions in the wavelet power spectrum. Figure S1e identifies two dominant periodicities, of 1 and 5 days, which are both significant throughout the entire time series, consistent with the original time series data in Figure B.1a. Conversely, Figure B.1f shows that the fluctuations are dominated by a significant periodicity of 1 day during the first half of the time series, but then shift to a significant periodicity of 5 days during the second half of the experiment, which matches the original time series in Figure B.1b. Thus, wavelet power spectra provide information on the dominant periodicities in time series, as

well as the exact timing during which these dominant periodicities are present.

B.3 Theory of wavelet analysis

Wavelet analysis makes use of a wavelet function, which is a periodic function resembling a local wave. By definition, wavelet functions have zero mean and are localized in frequency and time. One particular wavelet function, called the Morlet wavelet, consists of the product of a sine wave and a Gaussian bell-shaped curve (Figure B.2):

$$\psi_0(\eta) = \pi^{-\frac{1}{4}} e^{i\omega_0\eta} e^{-\frac{\eta^2}{2}} \tag{B.1}$$

where i is the imaginary number, ω_0 is dimensionless frequency, and η is dimensionless time. The Morlet wavelet is particularly useful to analyse periodicities in time series. Therefore, we chose the Morlet wavelet for our analysis, assuming the standard value of $\omega_0=6$ to satisfy the admissibility condition for wavelet functions (Farge 1992).

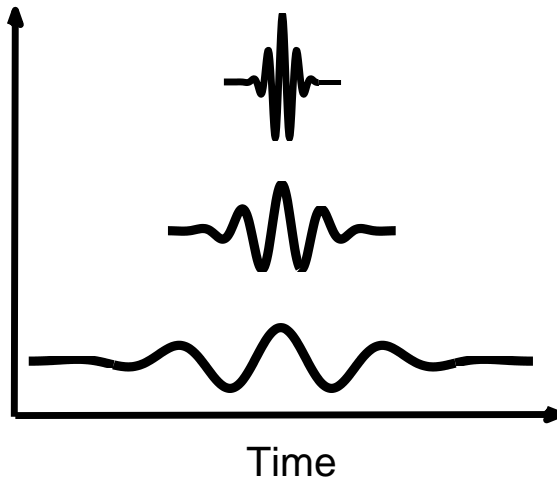


Figure B.2: Three examples of the Morlet wavelet, a local wave function that can be characterized by the frequency and timing of its oscillations. The three examples differ in wavelet scale.

We consider a time series x_n , consisting of observations $n = 1, \dots, N$ that are equally spaced in time at intervals δt . The continuous wavelet transform, $W_n(s)$, of our discrete time series x_n is defined as the convolution of x_n with the scaled and normalized wavelet. This can be written as (Grinsted et al. 2004):

$$W_n(s) = \sqrt{\frac{\delta t}{s}} \sum_{m=1}^N x_m \psi_0 \left[\frac{(m-n)\delta t}{s} \right] \quad (\text{B.2})$$

The wavelet transform is stretched in time by varying the wavelet scale s . The wavelet transform is normalized to ensure that wavelet transforms at different scales s are comparable. The local wavelet power spectrum is defined as $|W_n(s)|^2$, whereas the complex argument of $W_n(s)$ can be interpreted as the local phase (Torrence and Compo 1998; Grinsted et al. 2004). The word ‘local’ indicates that the wavelet power spectrum and its phase depend on the local time n . Thus, results from wavelet analysis can be visualized in contour plots in which the local wavelet power spectrum is plotted as a function of time.

We define the global wavelet spectrum as the time-average of all local wavelet spectra:

$$\overline{W^2}(s) = \frac{1}{N} \sum_{n=1}^N |W_n(s)|^2 \quad (\text{B.3})$$

The global wavelet spectrum provides a consistent and unbiased estimation of the total power spectrum of a time series (Percival 1995).

When the wavelet transform is applied to a real finite length time series, errors will occur at the beginning and end of the wavelet spectra. To limit these edge effects, the beginning and end of the time series can be padded with zeroes before calculating the wavelet transform (and removing these added data afterwards). However, this procedure still introduces discontinuities and decreases the amplitudes at the edges. The cone of influence (COI) is the region of the wavelet spectrum where this edge effect is important. Following Torrence and Compo (1998), we define the COI as the area in which the wavelet power caused by a discontinuity at the edge has dropped by a factor e^{-2} . Results falling in the COI are not included in our further analysis.

The statistical significance of the wavelet power can be assessed by comparison against an appropriate null hypothesis. Our null hypothesis is that the wavelet power spectrum is generated by a background signal, such as white noise or red noise. Many ecological time series show a high degree of temporal autocorrelation. That is, ecological time series often have distinctive red noise characteristics, and this also applied to our experimental time series. Red noise can be modeled by a first-order autoregressive process (AR1). The power spectrum, P_k , of an AR1 process is (Gilman et al. 1963):

$$P_k = \frac{1 - \alpha^2}{1 + \alpha^2 - 2\alpha \cos\left(\frac{2\pi k}{N}\right)} \quad (\text{B.4})$$

where the autocorrelation coefficient α at a time lag of 1 is estimated from the observed time series, and $k = 0, \dots, N/2$ is the frequency index.

The measured local wavelet power spectrum can be tested against the power spectrum of a red noise process using a chi-square test. More precisely, under the null hypothesis of red noise, the distribution of the local wavelet power spectrum is given by Torrence and Compo (1998):

$$\frac{|W_n(s)|^2}{\sigma^2} \Rightarrow \frac{1}{2} P_k \chi_2^2 \tag{B.5}$$

where σ^2 is the variance of the time series, the symbol “ \Rightarrow ” indicates “is distributed as”, and χ_2^2 is the chi-square distribution with two degrees of freedom. The value of P_k in Eq. B.5 is the mean power spectrum at the frequency index k that corresponds to the wavelet scale s (Torrence and Compo 1998). Thus, one can construct 95% confidence contour lines by evaluating Eq. B.5 at each scale using the 95th percentile value of the chi-square distribution. The software for our wavelet analysis was kindly provided by C. Torrence and G. Compo, and is available at <http://atoc.colorado.edu/research/wavelets/>.

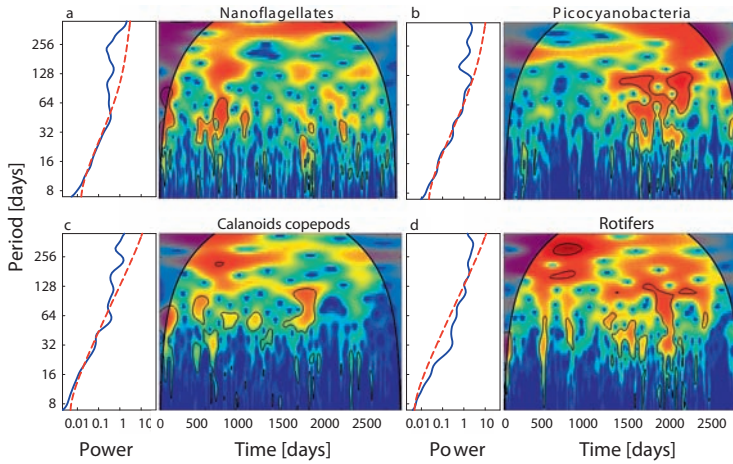


Figure B.3: Wavelet power spectra of the experimental data. **a**, Nanoflagellates; **b**, picocyanobacteria; **c**, calanoid copepods; **d**, rotifers. Colour coding indicates the local power of the species fluctuations. Black contour lines enclose regions of greater than 95% confidence that the observed local power exceeds red noise. Shaded areas on both sides of the contour plots represent the cone of influence, where edge effects might distort the signal. Line graphs show the global wavelet power spectra of the experimental data (blue lines) and of red noise (red lines).

We applied wavelet analysis to the time series of picocyanobacteria, nanoflagellates, rotifers and calanoid copepods. The results are plotted as contour plots in Figure B.3. The colour coding in the contour plots indicates the local wavelet power.

Black contour lines enclose regions of greater than 95% confidence that the observed local wavelet power exceeds the wavelet power that would have been generated by red noise. Shaded areas on either end of the contour plots represent the cone of influence, where edge effects might distort the signal. The contour plots show several significant regions in the local wavelet power spectra of all four species, primarily at periodicities in the range of 32-128 days (Figure B.3). This is further confirmed by global wavelet power spectra of the four species, which show significant periodicities at 32-64 days (line graphs in Figure B.3).

B.4 Cross-wavelet analysis

In predator-prey studies, as well as in many other applications, one would like to know whether the ups and downs of two time series are related with each other. This can be investigated by cross-wavelet analysis (Grinsted et al. 2004). Cross-wavelet analysis compares the wavelet power spectra of two time series. This enables detection of similarities in the local ups and downs of these two time series, and also allows an estimation of the phase angle between these fluctuations.

The cross-wavelet transform of two time series, x_n and y_n , is defined as $W_{xy,n}(s) = W_{x,n}(s) \cdot W_{y,n}^*(s)$, where the superscript * denotes complex conjugation. The local cross-wavelet power spectrum is defined as $|W_{xy,n}(s)|$, while the complex argument $\arg(W_{xy,n}(s))$ can be interpreted as the local phase angle between fluctuations in the two time series x_n and y_n . The phase angle can be visualized graphically by arrows in the cross-wavelet plots.

To assess the significance of the observed phase angles, we investigated whether the cross-wavelet spectra were significantly different (at the 0.05 level) from the cross-wavelet spectra of two independent red-noise processes with the same first-order autoregression coefficients as the original time series. Under the null hypothesis that both time series are generated by red noise, with background power spectra $P_{x,k}$ and $P_{y,k}$, the distribution of the cross-wavelet power spectrum of the two time series is given by Torrence and Compo (1998):

$$\frac{|W_{xy,n}(s)|}{\sigma_x \sigma_y} \Rightarrow \frac{1}{2} \sqrt{P_{x,k} P_{y,k}} V_2(p) \quad (\text{B.6})$$

where $V_2(p)$ is the value associated with the p^{th} percentile of a probability density function defined by the square root of the product of two chi-square distributions with two degrees of freedom. In our applications, we chose 95% confidence levels (i.e., $V_2(0.95)=3.999$) to evaluate Eq. B.6 at each scale. Software for cross-wavelet analysis was kindly provided by A. Grinsted, and is available at <http://www.pol.ac.uk/home/research/waveletcoherence/>.

B.5 Wavelet Coherence

To investigate the robustness of our findings, we also applied a related method called wavelet coherence (Grinsted et al. 2004; Maraun and Kurths 2004). Cross-wavelet analysis and wavelet coherence provide two different perspectives on the coupled fluctuations of two time series. Cross-wavelet spectra describe the common power of two time series, but without normalization of the wavelet power spectra of the two time series. This might lead to spurious results. For instance, if the wavelet power spectrum of one of the two time series is locally flat while the other wavelet power spectrum exhibits strong peaks, this can produce peaks in the cross-wavelet power spectrum even without any relationship between the two time series (Maraun and Kurths 2004). This problem is overcome by wavelet coherence. Wavelet coherence investigates how much the ups and downs in two time series are correlated (i.e., it investigates the coherence of fluctuations).

More specifically, the wavelet coherence of two time series is defined as the square of the cross-wavelet power spectrum normalized by the two single wavelet power spectra (Torrence and Webster 1999; Grinsted et al. 2004):

$$R_n^2(s) = \frac{|S(s^{-1}W_{xy,n}(s))|^2}{S(s^{-1}|W_{x,n}(s)|^2) \cdot S(s^{-1}|W_{y,n}(s)|^2)} \quad (\text{B.7})$$

where S is a smoothing operator. We note that this definition resembles that of a traditional correlation coefficient. It is thus useful to think of the wavelet coherence as a localized correlation coefficient. The smoothing operator is defined as:

$$S(W) = S_{scale}(S_{time}(W_n(s))) \quad (\text{B.8})$$

with S_{scale} denoting smoothing along the wavelet scale axis and S_{time} smoothing along the wavelet time axis. Smoothing in wavelet scale was based on a boxcar filter with a width of 0.6, which is the empirically determined scale decorrelation length for the Morlet wavelet (Torrence and Compo 1998). Smoothing in time was based on a Gaussian filter with the width of the smoothing kernel in the same order as the wavelength.

The statistical significance of the wavelet coherence can be tested against red noise using Monte Carlo methods (Grinsted et al. 2004). We generated 1000 pairs of surrogate time series with the same first-order autoregression coefficients as the original time series. For each pair, we calculated the wavelet coherence. We then estimated the significance level for each scale from the ensemble of Monte Carlo results, again using 95% confidence levels. The resulting wavelet coherence plots are shown in Figure B.4, and the phase angles of the significant regions are summarized in Table B.1.

Cross-wavelet analysis and wavelet coherence analysis both have their limitations. Cross-wavelet analysis has the disadvantage that the wavelet power spectra of the two time series are not normalized. A disadvantage of wavelet coherence is that

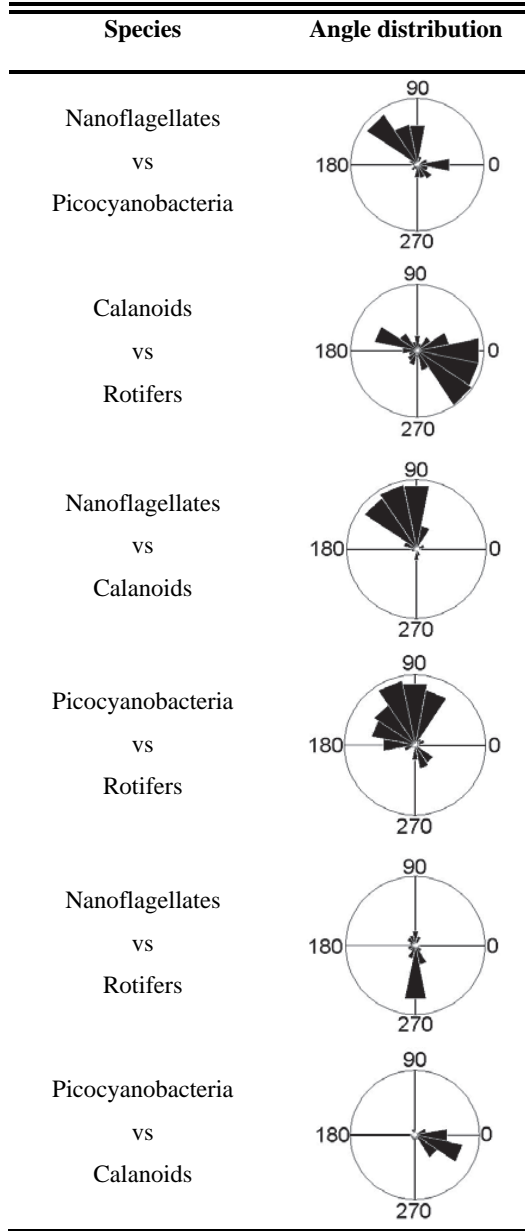


Table B.1: Relative frequency distributions of the phase angles between the fluctuating species, as determined by wavelet coherence analysis of the experimental data. The relative frequency distributions are based on all phase angles located within significant regions of the wavelet coherence spectra, but outside the cone of influence.

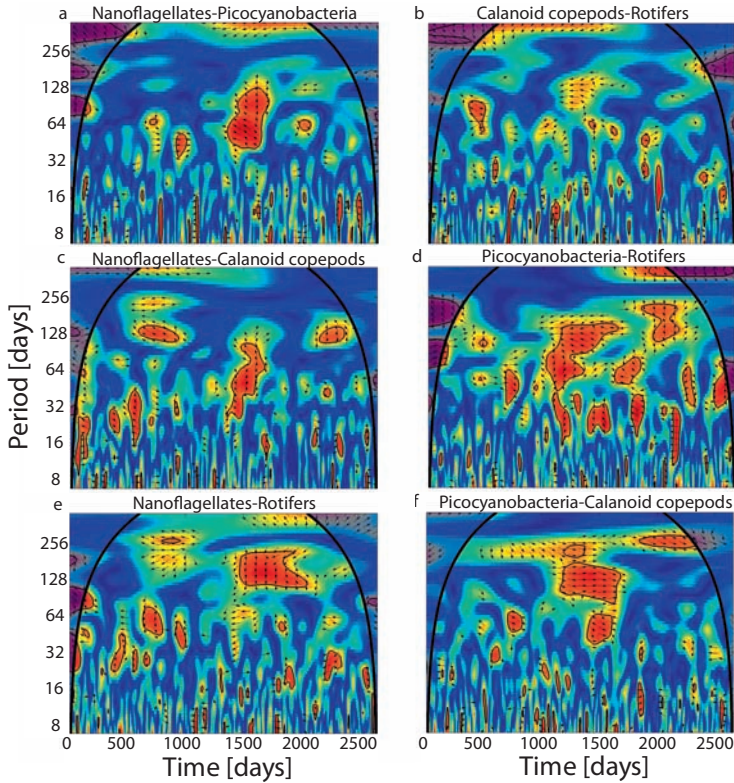


Figure B.4: Wavelet coherence spectra of the experimental data. **a**, Nanoflagellates versus picocyanobacteria (P_1 vs P_2); **b**, Calanoid copepods versus rotifers (Z_1 vs Z_2); **c**, Nanoflagellates versus calanoid copepods (P_1 vs Z_1); **d**, Picocyanobacteria versus rotifers (P_2 vs Z_2); **e**, Nanoflagellates versus rotifers (P_1 vs Z_2); **f**, Picocyanobacteria versus calanoid copepods (P_2 vs Z_1). Colour coding indicates the wavelet coherence in the fluctuations of the two time series. Arrows indicate the phase angles, where arrows pointing to the right represent in-phase oscillations (0°), while arrows pointing to the left represent anti-phase oscillations (180°). Black contour lines enclose regions of greater than 95% confidence that the wavelet coherence of the two time series exceeds red noise. Shaded areas on both sides of the contour plots represent the cone of influence, where edge effects might distort the signal.

the results are sensitive to the smoothing procedure, and that smoothing decreases the localization in space and time (Grinsted et al. 2004). It is thus recommendable to apply both approaches and to compare their results. In our case, cross-wavelet spectra and wavelet coherence yielded similar patterns for almost all species combinations (compare Figure 3.4 and Figure B.4). The only exception is the species

combination of nanoflagellates versus rotifers, where the significant areas were differently spread across the time-frequency domain. For this species combination, the phase angles obtained by wavelet coherence suggest a three-quarter delay, whereas the phase angles obtained by cross-wavelet analysis were more widely distributed. For all other species combinations, both approaches yielded similar distributions of the phase angles (compare the last columns in Table 3.1 and Table B.1). Thus, the two approaches yield largely consistent results.

Appendix C

Supplementary information to chapter 4

C.1 Model attractors and Lyapunov exponents

C.1.1 The different attractors

We used several criteria to distinguish between stationary equilibria, limit cycles, complex periodic cycles, quasiperiodicity and chaos. We visually checked every simulation result. In parallel, we calculated the Lyapunov exponent for each simulation, and we developed a simple algorithm to count the number of different local maxima ('peaks') of the dominant plankton species during the simulations. Stationary equilibria had no peaks, limit cycles had one peak, complex periodic cycles had more than one peak, whereas quasiperiodicity and chaos had numerous peaks (usually more than 10). The Lyapunov exponents were used to distinguish between non-chaotic and chaotic behavior. In several cases, to confirm the existence of chaos, we constructed Poincaré maps by sampling the model communities once per year for many consecutive years. Quasiperiodic solutions produced a torus manifold (i.e., a circle; Figure 4.3a) on the Poincaré map, whereas chaotic solutions produced a complex fractal Figure (Figure 4.3b).

Figure C.1 shows how often the different dynamical behaviors were displayed by the model communities. For this purpose, we simulated 100 randomly generated model communities at each different level of seasonal forcing (a) and productivity (K). The results show that, at low productivity ($K=2$), most of the model communities displayed cyclic behavior while only a few displayed chaotic dynamics. In contrast, at intermediate productivity ($K=5$, $K=10$), many of the model communities displayed chaotic dynamics.

C.1.2 Lyapunov exponent

The Lyapunov exponent measures the exponential divergence (or convergence) of nearby trajectories (Strogatz 1994; Sprott 2003). A positive Lyapunov exponent indicates divergence of the trajectories, and hence chaos. Conversely, a negative

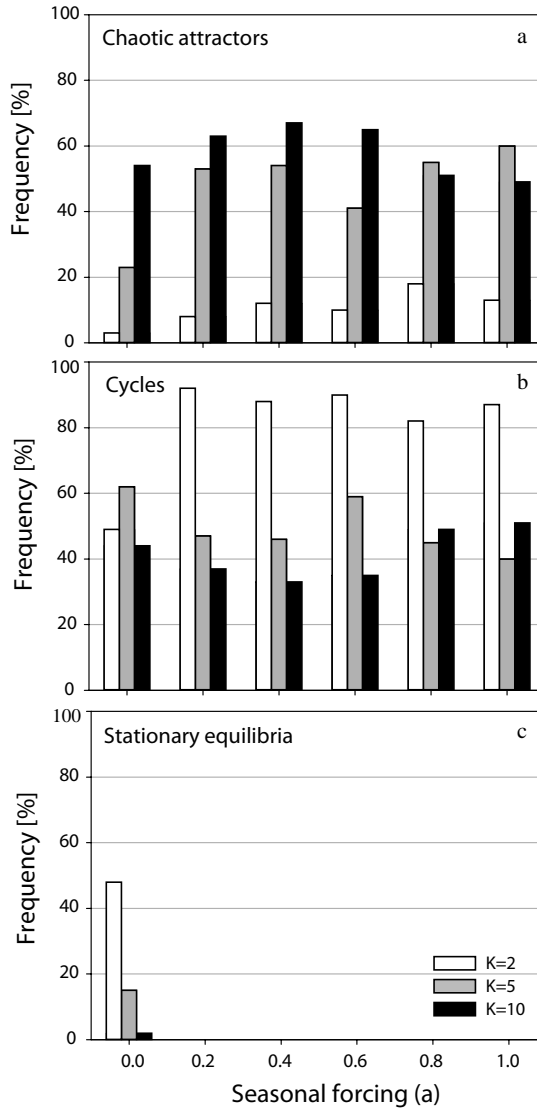


Figure C.1: Frequency of occurrence of the different dynamical behaviors as a function of seasonal forcing. The results are shown for model communities at low productivity ($K=2 \text{ mg L}^{-1}$) and intermediate productivity ($K=5 \text{ mg L}^{-1}$, $K=10 \text{ mg L}^{-1}$). **a**, chaotic attractors, **b**, cycles (including simple cycles, complex cycles and quasiperiodicity), **c**, stationary equilibria. Data are based on 100 randomly generated model communities at each level of productivity and seasonal forcing.

Lyapunov exponent indicates convergence of the trajectories, for instance towards a stable point equilibrium or a stable periodic cycle. We first ran each model simulation for 1,000 years to ensure that the system had reached an attractor. Thereafter, we continued the model simulations to calculate the Lyapunov exponent. In total, there were 16 dynamic variables in the model (10 phytoplankton species and 6 zooplankton species), which means that there were actually 16 Lyapunov exponents to calculate (Wolf et al. 1985). However, instead of calculating the complete Lyapunov spectrum, we focused on the dominant Lyapunov exponent only. For this purpose, we tracked two nearby trajectories that differed infinitesimally in initial conditions by $\delta_0=10^{-8}$. We allowed these two trajectories to run for 100,000 time steps to sample the entire attractor as much as possible. The Euclidean distance, $\delta(t)$, of the two trajectories was calculated at each time step. The Lyapunov exponent, λ , quantifies the exponential divergence (or convergence) of the trajectories, as described by $\|\delta(t)\| \approx \|\delta_0\|e^{\lambda t}$ (Strogatz 1994). Accordingly, we calculated λ by linear regression, as the slope of the ln-transformed divergence over time.

Several model communities showed signs of intermittent chaos, especially at intermediate productivity. These communities followed complex periodic trajectories but were repeatedly interrupted by outbursts of chaotic motion. Still these model simulations were considered chaotic if they yielded positive Lyapunov exponents.

C.2 Interpretation in terms of the Paradox of Enrichment

The results show that the occurrence of chaos is affected by productivity (Table 4.2; Figure 4.5), which agrees with previous observations on simpler tritrophic models (Yodzis and Innes 1992; McCann and Yodzis 1994). This is confirmed by a bifurcation analysis, using the productivity K as bifurcation parameter. In this bifurcation analysis, we consider a multispecies community without seasonal forcing. At low productivity, the dynamics of the multispecies model converge to a stable equilibrium point. With increasing productivity, at $K=4$, the equilibrium point becomes unstable, and the dynamics bifurcate into a limit cycle. When productivity is increased further, more bifurcations accumulate and the system is led through a quasiperiodicity route into chaos (Figure C.2).

The destabilization of predator-prey systems with increasing productivity has been termed the ‘Paradox of Enrichment’ (Rosenzweig 1971). This paradox may help to understand why seasonal forcing had qualitatively different effects on inter-annual variability at different levels of productivity. Our intuitive argument can be illustrated by phase-plane analysis of a simple two-species version of our predator-prey model (Figure C.3). The vertical line in the phase plane is the zooplankton isocline. Ignoring the small immigration term (u), it is straightforward to derive from Eq. 4.2 in the main text that the position of the zooplankton isocline is affected neither by productivity nor by seasonal forcing. The hump-shaped curve is

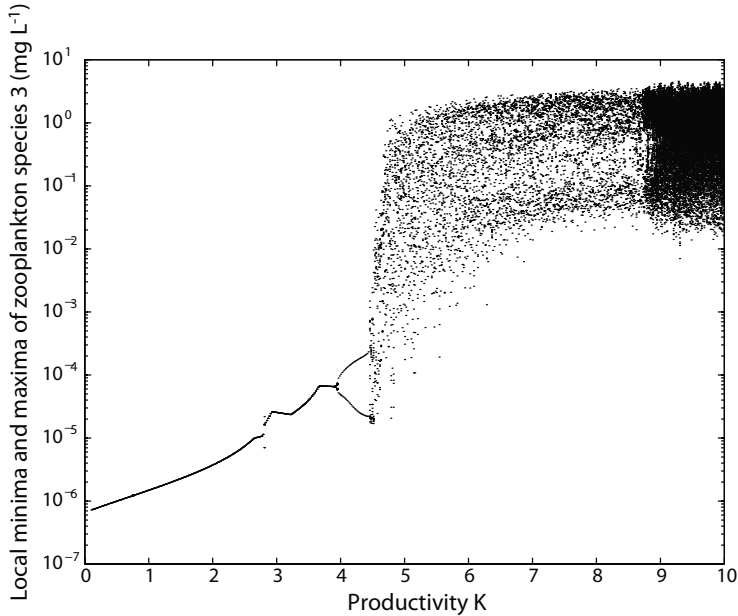


Figure C.2: Bifurcation diagram plotting the local maxima and minima of one of the zooplankton species in the model community as a function of productivity K . The bifurcation diagram is presented for a model community without seasonal forcing, and illustrates the transition of the community dynamics from a stable equilibrium, to a limit cycle, to chaos.

the phytoplankton isocline, and its location in the phase plane does vary with both productivity and seasonal forcing. It is well known that this two-species predator-prey model is stable, if the maximum (the ‘hump’) of the phytoplankton isocline is located on the left-hand side of the vertical zooplankton isocline (Rosenzweig and MacArthur 1963; Rosenzweig 1971). At low productivity ($K=2$), the maximum of the phytoplankton isocline is indeed located on the left-hand side of the zooplankton isocline (Figure C.3a). Accordingly, the equilibrium is a stable node. With seasonal forcing, the position of the phytoplankton isocline may vary, but essentially the hump will remain on the left-hand side of the zooplankton isocline, and the equilibrium will track the seasonal variation.

At intermediate productivity ($K=5$), the hump in the phytoplankton isocline is close to the zooplankton isocline (Figure C.3b). Moreover, seasonal forcing shifts the position of the phytoplankton isocline (indicated by the gray lines in Figure C.3). Every now and then, this may bring the hump in the phytoplankton isocline to the other side of the zooplankton isocline, thereby destabilizing the equilibrium. In the two-species system, destabilization of the predator-prey interaction through

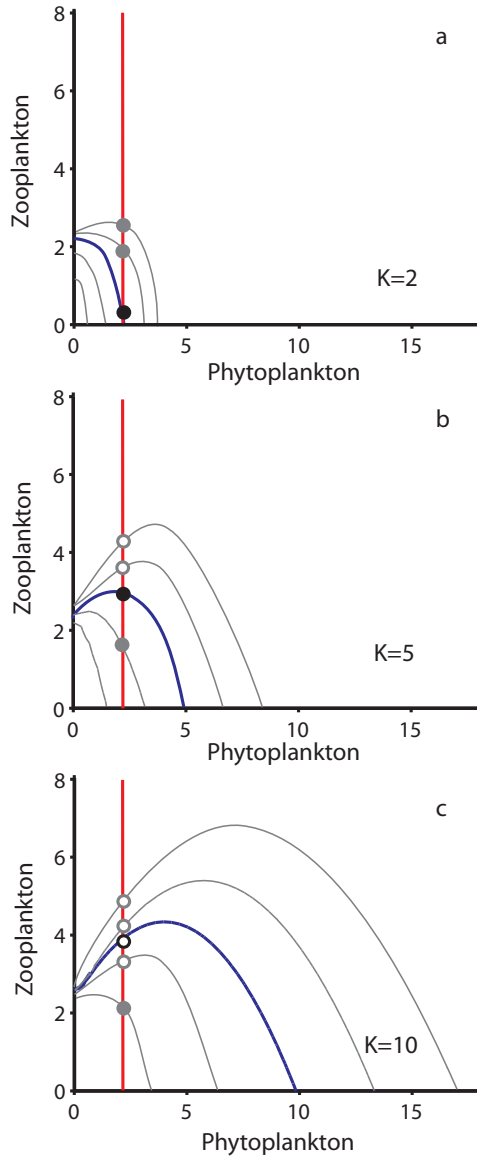


Figure C.3: Phase-plane diagrams with the phytoplankton isocline (blue line) and zooplankton isocline (red line), for a simple two-species version of our predator-prey model. The diagrams show three levels of productivity: **a**, $K=2$ mg L^{-1} ; **b**, $K=5$ mg L^{-1} ; **c**, $K=10$ mg L^{-1} . Open circles: unstable equilibria; closed circles: stable equilibria. Grey lines indicate variation of the phytoplankton isocline due to seasonal forcing.

this Hopf bifurcation yields a limit cycle. In our multispecies model, destabilization of multiple predator-prey interactions raises the probability that the community dynamics shift into a chaotic regime. Thus, at intermediate productivity, seasonal forcing pushes the equilibrium back and forth between stability and instability. This may explain the observation of intermittent chaos at intermediate productivity.

At somewhat higher productivity ($K=10$), the hump in the phytoplankton isocline is nearly always on the right-hand side of the zooplankton isocline (Figure C.3c). In this case, the internal equilibrium is unstable, which enables a limit-cycle solution in the two-species model and chaos in the analogous multispecies model.

At very high productivity ($K=20$ and $K=50$), the hump in the phytoplankton isocline is far to the right of the zooplankton isocline. In a multispecies context, this will induce rather similar large-amplitude cycles for all phytoplankton-zooplankton pairs. We speculate that this similarity in the cyclic dynamics of the different predator-prey interactions increases the likelihood of periodic dynamics in the full model community. This, then, would provide a possible explanation for the shift from predominantly chaotic dynamics to predominantly cyclic dynamics at very high productivity.

C.3 Parameter values

This section presents the parameter values used in the simulations. The simulations were based on Eq. 4.1, 4.2, 4.3 presented in the main text, and parameterized for phytoplankton and zooplankton species with a timescale of days. In Figure 4.2 and Figure C.1 we used the default values $r_i=0.5 \text{ d}^{-1}$ for all phytoplankton species, and $g_k=0.4 \text{ d}^{-1}$, $H_k=0.6 \text{ mg L}^{-1}$, $e_k=0.6$, and $m_k=0.15 \text{ d}^{-1}$ for all zooplankton species. In Figures 4 and 5, we sampled a broad range of values for these parameters (specified in Table 4.1). We introduced a small level of immigration, $u=10^{-7} \text{ mg L}^{-1} \text{ d}^{-1}$ for all plankton species. Phytoplankton intraspecific competition was set to unity ($\alpha_{ii}=1$ for all i), while the interspecific competition coefficients (α_{ij}) were drawn randomly from the interval (0.5, 1.5). The selectivity coefficients S_{ik} were drawn randomly from the interval (0, 1). Below we provide the initial conditions of the phytoplankton and zooplankton species in the vectors \mathbf{P}_0 and \mathbf{Z}_0 . Selectivity coefficients are given in the matrix \mathbf{S} , where rows represent phytoplankton species and columns represent zooplankton species. Competition coefficients are given in the matrix \mathbf{A} , where the entries α_{ij} describe the competitive effect of phytoplankton species j on phytoplankton species i .

In Figure 4.2a, we assumed intermediate productivity ($K=5 \text{ mg L}^{-1}$) without seasonal forcing ($a=0$). Vectors \mathbf{P}_0 , \mathbf{Z}_0 and matrices \mathbf{S} , \mathbf{A} were given by:

$$P_0 = \begin{pmatrix} 3.63536 \\ 5.63899 \\ 0.926864 \\ 1.12498 \\ 5.27325 \\ 7.78813 \\ 1.36785 \\ 1.42816 \\ 5.69949 \\ 9.33256 \end{pmatrix} \quad Z_0 = \begin{pmatrix} 3.69388 \\ 7.77147 \\ 8.36731 \\ 1.92747 \\ 1.57839 \\ 2.29056 \end{pmatrix}$$

$$S = \begin{pmatrix} 0.29066 & 0.34137 & 0.32241 & 0.32266 & 0.32654 & 0.34656 \\ 0.32898 & 0.39781 & 0.37396 & 0.36588 & 0.34053 & 0.37233 \\ 0.37539 & 0.33605 & 0.36242 & 0.35330 & 0.35269 & 0.26154 \\ 0.29321 & 0.38711 & 0.36405 & 0.36109 & 0.34945 & 0.29957 \\ 0.38581 & 0.30817 & 0.34383 & 0.29069 & 0.39209 & 0.34397 \\ 0.37598 & 0.31852 & 0.29804 & 0.36015 & 0.37608 & 0.29163 \\ 0.25377 & 0.25485 & 0.29822 & 0.38126 & 0.37246 & 0.36031 \\ 0.29771 & 0.35155 & 0.27249 & 0.37407 & 0.26834 & 0.30395 \\ 0.26983 & 0.39634 & 0.31168 & 0.33042 & 0.25705 & 0.34062 \\ 0.34774 & 0.33646 & 0.26717 & 0.36551 & 0.25712 & 0.33537 \end{pmatrix}$$

$$A = \begin{pmatrix} 1.00000 & 0.93529 & 1.09800 & 1.01780 & 1.01970 & 0.94738 \\ 1.09910 & 0.91660 & 0.98330 & 0.91521 & & \\ 1.08960 & 1.00000 & 1.01660 & 1.09940 & 1.05640 & 1.04370 \\ 0.94900 & 0.98847 & 0.91656 & 1.06600 & & \\ 0.95871 & 1.08950 & 1.00000 & 1.05290 & 1.05250 & 1.09370 \\ 0.96018 & 1.00550 & 0.93843 & 0.95333 & & \\ 0.99044 & 1.02270 & 1.00290 & 1.00000 & 0.95653 & 0.91140 \\ 1.07130 & 0.91366 & 0.96024 & 1.07650 & & \\ 0.92558 & 0.94945 & 0.99425 & 1.01580 & 1.00000 & 1.04160 \\ 1.01740 & 0.99802 & 0.99003 & 1.09370 & & \\ 1.05950 & 0.95095 & 1.01410 & 1.04660 & 0.92574 & 1.00000 \\ 0.91697 & 0.98950 & 1.02470 & 1.07470 & & \\ 0.93503 & 0.93194 & 1.02140 & 1.00820 & 0.90720 & 1.01870 \\ 1.00000 & 1.02720 & 0.95704 & 0.99208 & & \\ 1.03540 & 0.92333 & 1.08330 & 1.04220 & 1.06620 & 0.99684 \\ 0.99463 & 1.00000 & 1.01960 & 1.02390 & & \\ 0.92517 & 0.92813 & 0.98473 & 1.04920 & 0.95651 & 0.97612 \\ 0.96988 & 1.06700 & 1.00000 & 0.94958 & & \\ 0.96589 & 1.06430 & 1.04800 & 0.92050 & 1.07460 & 0.92459 \\ 1.04750 & 1.08260 & 0.95875 & 1.00000 & & \end{pmatrix}$$

In Figure 4.2b, we assumed intermediate productivity ($K=5 \text{ mg L}^{-1}$) without seasonal forcing ($a=0$). Vectors \mathbf{P}_0 , \mathbf{Z}_0 and matrices \mathbf{S} , \mathbf{A} were given by:

$$\mathbf{P}_0 = \begin{pmatrix} 7.70527 \\ 1.40047 \\ 9.73707 \\ 4.092 \\ 1.04469 \\ 7.26438 \\ 6.52615 \\ 6.76509 \\ 7.51183 \\ 5.64357 \end{pmatrix} \quad \mathbf{Z}_0 = \begin{pmatrix} 9.32981 \\ 1.27736 \\ 9.39732 \\ 7.13483 \\ 1.49748 \\ 2.00112 \end{pmatrix}$$

$$\mathbf{S} = \begin{pmatrix} 0.369460 & 0.378060 & 0.390170 & 0.330240 & 0.351780 & 0.338660 \\ 0.284680 & 0.290930 & 0.259610 & 0.336330 & 0.301050 & 0.258100 \\ 0.324250 & 0.332030 & 0.323780 & 0.314200 & 0.343040 & 0.383740 \\ 0.362280 & 0.394840 & 0.379420 & 0.355100 & 0.367740 & 0.302460 \\ 0.365300 & 0.255900 & 0.286870 & 0.291240 & 0.388680 & 0.370970 \\ 0.294050 & 0.385170 & 0.289640 & 0.312490 & 0.267070 & 0.304720 \\ 0.308260 & 0.343080 & 0.382880 & 0.314170 & 0.261270 & 0.284470 \\ 0.341270 & 0.359480 & 0.340710 & 0.363480 & 0.398210 & 0.306090 \\ 0.323800 & 0.396260 & 0.303930 & 0.331770 & 0.313480 & 0.306740 \\ 0.341080 & 0.294930 & 0.307330 & 0.291120 & 0.317310 & 0.321990 \end{pmatrix}$$

$$\mathbf{A} = \begin{pmatrix} 1.00000 & 1.06810 & 1.09250 & 0.90593 & 0.93300 & 0.94678 \\ 0.92708 & 0.93491 & 1.00540 & 1.03190 & & \\ 0.91815 & 1.00000 & 1.04980 & 0.95780 & 1.04690 & 0.90456 \\ 0.93093 & 0.93165 & 0.95471 & 1.09410 & & \\ 0.98000 & 0.96840 & 1.00000 & 1.01280 & 1.08830 & 1.04070 \\ 1.09570 & 1.08530 & 0.96473 & 0.93196 & & \\ 1.03820 & 0.90094 & 1.08400 & 1.00000 & 0.91844 & 0.92753 \\ 0.95868 & 1.03980 & 1.03620 & 0.98015 & & \\ 1.09810 & 1.09890 & 0.93642 & 1.00060 & 1.00000 & 0.94410 \\ 1.05680 & 1.06680 & 1.01840 & 0.95244 & & \\ 1.06500 & 0.94160 & 1.01160 & 1.08820 & 0.97381 & 1.00000 \\ 1.03520 & 0.95863 & 0.96214 & 1.04210 & & \\ 1.03910 & 0.93183 & 0.98489 & 1.03360 & 1.08770 & 1.04660 \\ 1.00000 & 1.01950 & 1.05890 & 1.03150 & & \\ 1.07120 & 1.00040 & 1.03280 & 0.90156 & 1.00330 & 0.97390 \\ 1.09260 & 1.00000 & 0.93127 & 0.91351 & & \\ 1.02750 & 1.08410 & 0.93845 & 1.05780 & 0.92050 & 0.98527 \\ 1.09440 & 0.90141 & 1.00000 & 0.98681 & & \\ 0.96586 & 0.90094 & 0.95552 & 0.93032 & 1.04240 & 0.91469 \\ 1.07990 & 0.93056 & 1.09060 & 1.00000 & & \end{pmatrix}$$

In Figure 4.2c, we assumed intermediate productivity ($K=5 \text{ mg L}^{-1}$) without seasonal forcing ($a=0$). Vectors \mathbf{P}_0 , \mathbf{Z}_0 and matrices \mathbf{S} , \mathbf{A} were given by:

$$\mathbf{P}_0 = \begin{pmatrix} 5.7592 \\ 0.00672887 \\ 6.11753 \\ 7.46021 \\ 3.44718 \\ 7.19126 \\ 0.681792 \\ 6.33776 \\ 4.87448 \\ 2.5065 \end{pmatrix} \quad \mathbf{Z}_0 = \begin{pmatrix} 7.63593 \\ 7.18401 \\ 5.00864 \\ 9.96982 \\ 0.49456 \\ 1.6149 \end{pmatrix}$$

$$\mathbf{S} = \begin{pmatrix} 0.35645 & 0.25911 & 0.25599 & 0.25540 & 0.37147 & 0.34333 \\ 0.38235 & 0.35224 & 0.36569 & 0.27879 & 0.36060 & 0.28062 \\ 0.31936 & 0.32580 & 0.30852 & 0.36343 & 0.25057 & 0.35436 \\ 0.31883 & 0.36660 & 0.33324 & 0.32782 & 0.25176 & 0.36090 \\ 0.37799 & 0.29458 & 0.28562 & 0.25347 & 0.25830 & 0.33710 \\ 0.34292 & 0.25465 & 0.38898 & 0.27298 & 0.28282 & 0.30612 \\ 0.34073 & 0.28625 & 0.26579 & 0.34103 & 0.25826 & 0.36782 \\ 0.29506 & 0.28847 & 0.27941 & 0.35595 & 0.28382 & 0.28470 \\ 0.29987 & 0.29349 & 0.38515 & 0.33480 & 0.30321 & 0.38924 \\ 0.31410 & 0.33482 & 0.28590 & 0.31797 & 0.34107 & 0.34043 \end{pmatrix}$$

$$\mathbf{A} = \begin{pmatrix} 1.00000 & 1.05790 & 0.97426 & 1.00740 & 0.94092 & 1.09990 \\ 0.90903 & 1.05330 & 1.08520 & 0.92133 & & \\ 1.00800 & 1.00000 & 0.97564 & 0.96529 & 0.92472 & 0.93132 \\ 1.06050 & 1.01340 & 0.93058 & 1.01850 & & \\ 1.05830 & 1.02460 & 1.00000 & 0.90137 & 1.09590 & 1.05280 \\ 1.03850 & 0.99204 & 1.03740 & 0.90772 & & \\ 0.96101 & 0.97340 & 1.05390 & 1.00000 & 0.96059 & 0.94482 \\ 1.00150 & 0.95437 & 1.05070 & 0.91310 & & \\ 1.05070 & 1.07380 & 0.97477 & 1.08530 & 1.00000 & 1.09730 \\ 1.01080 & 1.08880 & 1.08520 & 0.97148 & & \\ 0.92899 & 0.90022 & 1.02250 & 1.01170 & 1.01910 & 1.00000 \\ 1.09950 & 1.07590 & 1.09130 & 1.01620 & & \\ 0.95827 & 0.94281 & 1.08610 & 0.99913 & 0.96210 & 0.90316 \\ 1.00000 & 1.08490 & 0.91968 & 1.02780 & & \\ 1.07950 & 0.96716 & 0.94957 & 1.00020 & 0.97495 & 1.04280 \\ 0.96887 & 1.00000 & 1.09510 & 0.94234 & & \\ 0.90156 & 0.93505 & 1.02880 & 0.96737 & 1.04400 & 1.01660 \\ 1.03190 & 1.07240 & 1.00000 & 0.98084 & & \\ 0.94354 & 0.98360 & 1.03910 & 1.03120 & 0.96599 & 0.97693 \\ 1.09450 & 1.03180 & 0.94039 & 1.00000 & & \end{pmatrix}$$

In Figure 4.2d, we assumed intermediate productivity ($K=5 \text{ mg L}^{-1}$) without seasonal forcing ($a=0$). Vectors \mathbf{P}_0 , \mathbf{Z}_0 and matrices \mathbf{S} , \mathbf{A} were given by:

$$\mathbf{P}_0 = \begin{pmatrix} 5.46925 \\ 4.08658 \\ 3.94005 \\ 5.75499 \\ 5.70258 \\ 6.47918 \\ 3.70245 \\ 5.28271 \\ 3.17896 \\ 0.259128 \end{pmatrix} \quad \mathbf{Z}_0 = \begin{pmatrix} 4.8726 \\ 3.96219 \\ 6.69961 \\ 6.0902 \\ 1.67571 \\ 7.68037 \end{pmatrix}$$

$$\mathbf{S} = \begin{pmatrix} 0.25096 & 0.28766 & 0.31457 & 0.35247 & 0.39975 & 0.26367 \\ 0.30954 & 0.36659 & 0.31202 & 0.29266 & 0.39689 & 0.28135 \\ 0.25247 & 0.38632 & 0.37334 & 0.39992 & 0.29728 & 0.26864 \\ 0.27276 & 0.25480 & 0.25624 & 0.35366 & 0.37262 & 0.38621 \\ 0.27708 & 0.30285 & 0.34715 & 0.27772 & 0.29860 & 0.35856 \\ 0.35184 & 0.30223 & 0.33853 & 0.39829 & 0.26348 & 0.38859 \\ 0.30563 & 0.29752 & 0.38819 & 0.35284 & 0.39792 & 0.29081 \\ 0.33811 & 0.27008 & 0.29145 & 0.29599 & 0.32123 & 0.29531 \\ 0.28847 & 0.38878 & 0.25455 & 0.28204 & 0.32032 & 0.28840 \\ 0.38221 & 0.32273 & 0.27457 & 0.33139 & 0.30382 & 0.37318 \end{pmatrix}$$

$$\mathbf{A} = \begin{pmatrix} 1.00000 & 0.98904 & 0.98967 & 0.96012 & 1.01940 & 1.05710 \\ 0.95028 & 1.07300 & 1.06550 & 1.00600 & & \\ 0.93047 & 1.00000 & 0.94060 & 0.93359 & 0.99974 & 1.02800 \\ 1.01540 & 1.02930 & 1.08940 & 0.91925 & & \\ 0.98235 & 0.93034 & 1.00000 & 1.05760 & 0.99245 & 0.96100 \\ 0.90099 & 0.92003 & 1.08520 & 0.91460 & & \\ 0.99105 & 0.95057 & 0.91751 & 1.00000 & 1.00140 & 0.98971 \\ 1.00730 & 1.00990 & 0.92243 & 1.03310 & & \\ 1.01000 & 1.06150 & 1.04160 & 1.01620 & 1.00000 & 1.09420 \\ 1.01970 & 1.02420 & 0.96354 & 0.96942 & & \\ 1.09950 & 0.92310 & 0.91790 & 1.09960 & 0.99412 & 1.00000 \\ 1.07700 & 0.98083 & 0.98945 & 1.01660 & & \\ 0.90976 & 0.92729 & 0.91977 & 1.05940 & 1.06380 & 1.09790 \\ 1.00000 & 1.03980 & 0.94122 & 1.07660 & & \\ 1.09370 & 1.05770 & 1.09210 & 1.04830 & 0.93232 & 1.09860 \\ 0.96215 & 1.00000 & 1.07030 & 1.03070 & & \\ 0.97206 & 1.06230 & 0.90409 & 1.01970 & 1.08000 & 1.01810 \\ 0.93359 & 0.98099 & 1.00000 & 0.96620 & & \\ 0.92105 & 1.09950 & 0.99182 & 1.03560 & 0.93059 & 1.07920 \\ 0.95261 & 1.07890 & 1.09990 & 1.00000 & & \end{pmatrix}$$

In Figure 4.2e, we assumed intermediate productivity ($K=5 \text{ mg L}^{-1}$) with very strong seasonal forcing ($a=0.999$). Vectors \mathbf{P}_0 , \mathbf{Z}_0 and matrices \mathbf{S} , \mathbf{A} were given by:

$$\mathbf{P}_0 = \begin{pmatrix} 1.35022 \\ 2.17904 \\ 5.83062 \\ 9.16413 \\ 0.0916846 \\ 4.6438 \\ 4.09236 \\ 9.88841 \\ 8.19372 \\ 9.88152 \end{pmatrix} \quad \mathbf{Z}_0 = \begin{pmatrix} 5.87321 \\ 7.06241 \\ 2.87903 \\ 2.17233 \\ 2.78354 \\ 5.65313 \end{pmatrix}$$

$$\mathbf{S} = \begin{pmatrix} 0.39865 & 0.30829 & 0.32136 & 0.39892 & 0.25554 & 0.38321 \\ 0.32633 & 0.37665 & 0.36584 & 0.27568 & 0.33179 & 0.33371 \\ 0.39992 & 0.30389 & 0.38274 & 0.25890 & 0.37922 & 0.32362 \\ 0.25016 & 0.25118 & 0.30628 & 0.33729 & 0.38902 & 0.32366 \\ 0.25536 & 0.27644 & 0.27915 & 0.39927 & 0.26037 & 0.32143 \\ 0.32427 & 0.36610 & 0.36934 & 0.31307 & 0.37736 & 0.31577 \\ 0.33226 & 0.36876 & 0.31494 & 0.36511 & 0.29199 & 0.38403 \\ 0.39815 & 0.34108 & 0.29649 & 0.26011 & 0.33128 & 0.25436 \\ 0.38152 & 0.35705 & 0.25678 & 0.39816 & 0.31040 & 0.30565 \\ 0.28345 & 0.28799 & 0.28468 & 0.26485 & 0.35382 & 0.37778 \end{pmatrix}$$

$$\mathbf{A} = \begin{pmatrix} 1.00000 & 1.01010 & 1.01190 & 1.05760 & 0.95627 & 1.08580 \\ 1.09130 & 0.92674 & 0.91477 & 1.09910 & & \\ 1.02750 & 1.00000 & 1.09200 & 1.08710 & 0.98821 & 0.99870 \\ 0.96925 & 0.97137 & 0.91290 & 1.06450 & & \\ 0.96447 & 1.04140 & 1.00000 & 1.08660 & 0.92022 & 0.95105 \\ 0.91928 & 1.01810 & 0.90255 & 1.04450 & & \\ 1.03220 & 0.98655 & 1.06450 & 1.00000 & 1.09600 & 1.09050 \\ 1.09900 & 0.95522 & 0.92495 & 1.06090 & & \\ 0.99499 & 0.99424 & 1.00640 & 1.05330 & 1.00000 & 0.93234 \\ 1.01290 & 1.08020 & 0.92839 & 0.99257 & & \\ 1.04130 & 0.97710 & 0.94098 & 1.01260 & 1.07340 & 1.00000 \\ 0.93333 & 1.09200 & 0.98503 & 0.93855 & & \\ 0.97753 & 1.09290 & 0.98456 & 1.02730 & 1.05260 & 0.96266 \\ 1.00000 & 1.04380 & 1.02290 & 1.02320 & & \\ 0.98529 & 0.90061 & 1.09550 & 0.98408 & 0.93780 & 0.99902 \\ 1.08720 & 1.00000 & 0.98880 & 0.91732 & & \\ 0.90328 & 0.96697 & 1.05240 & 1.05310 & 1.04040 & 0.93419 \\ 1.05520 & 1.09770 & 1.00000 & 0.94580 & & \\ 0.92449 & 1.05200 & 1.09650 & 0.91481 & 0.94793 & 0.95781 \\ 0.98937 & 0.96963 & 0.93559 & 1.00000 & & \end{pmatrix}$$

In Figure 4.2f, we assumed intermediate productivity ($K=10 \text{ mg L}^{-1}$) with very strong seasonal forcing ($a=0.999$). Vectors \mathbf{P}_0 , \mathbf{Z}_0 and matrices \mathbf{S} , \mathbf{A} were given by:

$$\mathbf{P}_0 = \begin{pmatrix} 4.16377 \\ 4.84055 \\ 5.94447 \\ 6.62461 \\ 5.29555 \\ 3.65465 \\ 3.12409 \\ 9.63348 \\ 0.50302 \\ 7.18931 \end{pmatrix} \quad \mathbf{Z}_0 = \begin{pmatrix} 6.57662 \\ 5.48389 \\ 6.42695 \\ 2.56577 \\ 2.04671 \\ 8.6042 \end{pmatrix}$$

$$\mathbf{S} = \begin{pmatrix} 0.283857 & 0.372463 & 0.290207 & 0.373357 & 0.355053 & 0.378232 \\ 0.26072 & 0.27255 & 0.277528 & 0.313199 & 0.316006 & 0.389759 \\ 0.347154 & 0.362965 & 0.273746 & 0.341199 & 0.377318 & 0.371781 \\ 0.399823 & 0.298206 & 0.324793 & 0.374443 & 0.28278 & 0.357781 \\ 0.334821 & 0.252581 & 0.308743 & 0.266602 & 0.326801 & 0.39519 \\ 0.35126 & 0.286861 & 0.280053 & 0.278262 & 0.344288 & 0.33747 \\ 0.367837 & 0.295083 & 0.337205 & 0.35588 & 0.253831 & 0.300378 \\ 0.286979 & 0.254326 & 0.389331 & 0.279495 & 0.363212 & 0.354572 \\ 0.28763 & 0.328498 & 0.27909 & 0.288631 & 0.302239 & 0.357728 \\ 0.391896 & 0.259821 & 0.307517 & 0.30207 & 0.250141 & 0.391685 \end{pmatrix}$$

$$\mathbf{A} = \begin{pmatrix} 1.00000 & 0.985761 & 0.963661 & 1.02766 & 1.04015 & 1.01678 \\ 1.06449 & 0.902599 & 0.94197 & 1.00091 & & \\ 1.07192 & 1.000000 & 0.986204 & 0.915673 & 1.08432 & 1.09222 \\ 1.0175 & 0.908832 & 0.952354 & 1.06094 & & \\ 1.02466 & 1.01656 & 1.000000 & 1.02295 & 1.01378 & 0.95793 \\ 1.06178 & 1.02433 & 1.00002 & 1.07753 & & \\ 0.93733 & 1.06949 & 0.953364 & 1.000000 & 1.05311 & 1.04462 \\ 0.92502 & 0.923436 & 1.02989 & 0.980133 & & \\ 0.956111 & 0.908995 & 1.08516 & 0.951834 & 1.00000 & 0.911134 \\ 1.04295 & 0.956939 & 0.975999 & 0.970241 & & \\ 0.972238 & 1.00404 & 0.951228 & 0.976466 & 1.08144 & 1.000000 \\ 0.934735 & 1.00448 & 0.985677 & 1.01317 & & \\ 1.00235 & 0.962066 & 0.929795 & 1.02865 & 1.06561 & 0.954257 \\ 1.000000 & 0.992102 & 0.937234 & 1.09479 & & \\ 0.945243 & 1.04171 & 1.06076 & 1.08768 & 0.919391 & 0.976771 \\ 1.03821 & 1.000000 & 0.915 & 0.962707 & & \\ 0.913016 & 1.05948 & 1.07459 & 0.950775 & 0.973166 & 1.02252 \\ 1.01513 & 0.915069 & 1.000000 & 0.92413 & & \\ 0.930614 & 1.01939 & 1.08068 & 1.0372 & 0.937767 & 0.954307 \\ 1.00749 & 0.948873 & 1.041 & 1.00000 & & \end{pmatrix}$$

In Figure 4.2g, we assumed intermediate productivity ($K=10 \text{ mg L}^{-1}$) with moderate seasonal forcing ($a=0.4$). Vectors \mathbf{P}_0 , \mathbf{Z}_0 and matrices \mathbf{S} , \mathbf{A} were given by:

$$\mathbf{P}_0 = \begin{pmatrix} 4.10477 \\ 2.81403 \\ 9.10236 \\ 4.83123 \\ 4.41213 \\ 0.0614716 \\ 8.0491 \\ 5.71316 \\ 0.406246 \\ 3.10672 \end{pmatrix} \quad \mathbf{Z}_0 = \begin{pmatrix} 4.53639 \\ 2.70974 \\ 0.523771 \\ 0.147228 \\ 2.09257 \\ 7.2228 \end{pmatrix}$$

$$\mathbf{S} = \begin{pmatrix} 0.315775 & 0.375235 & 0.368958 & 0.352066 & 0.276252 & 0.329779 \\ 0.252791 & 0.296686 & 0.320735 & 0.379944 & 0.369076 & 0.399898 \\ 0.305393 & 0.268981 & 0.314635 & 0.336644 & 0.322805 & 0.329775 \\ 0.372249 & 0.384677 & 0.324383 & 0.35038 & 0.355527 & 0.287814 \\ 0.371079 & 0.261451 & 0.267947 & 0.351081 & 0.313239 & 0.287255 \\ 0.38034 & 0.327614 & 0.287563 & 0.319867 & 0.252655 & 0.285626 \\ 0.388058 & 0.376138 & 0.312235 & 0.265859 & 0.313237 & 0.354579 \\ 0.351709 & 0.315101 & 0.271029 & 0.380018 & 0.365342 & 0.256062 \\ 0.258677 & 0.392012 & 0.332469 & 0.340307 & 0.397981 & 0.355939 \\ 0.371127 & 0.305727 & 0.347293 & 0.25696 & 0.296807 & 0.359825 \end{pmatrix}$$

$$\mathbf{A} = \begin{pmatrix} 1.00000 & 1.01572 & 0.961557 & 0.956827 & 1.06387 & 1.03968 \\ 0.957823 & 1.09485 & 0.932573 & 0.939896 & & \\ 1.00629 & 1.00000 & 0.961619 & 1.03137 & 0.994312 & 0.936902 \\ 1.03503 & 1.01267 & 1.08975 & 0.967337 & & \\ 0.949632 & 1.03345 & 1.000000 & 1.03934 & 0.916193 & 0.936613 \\ 0.902708 & 0.969061 & 1.02978 & 1.07123 & & \\ 1.01177 & 0.972276 & 1.01985 & 1.000000 & 0.903534 & 1.09485 \\ 0.952337 & 0.957572 & 1.04925 & 0.94649 & & \\ 0.947522 & 1.08278 & 1.05456 & 1.0142 & 1.000000 & 1.08988 \\ 0.930929 & 1.03527 & 1.02583 & 1.03548 & & \\ 1.05684 & 0.944364 & 1.06856 & 1.01075 & 0.904244 & 1.000000 \\ 0.943427 & 1.01604 & 1.05913 & 1.06444 & & \\ 0.936893 & 1.08735 & 1.06614 & 1.09557 & 0.96127 & 1.04325 \\ 1.000000 & 1.00426 & 0.977152 & 0.923501 & & \\ 1.00697 & 0.908474 & 1.01724 & 1.03262 & 0.950694 & 1.03784 \\ 1.00362 & 1.000000 & 0.977461 & 0.92729 & & \\ 1.08731 & 0.927108 & 0.943043 & 0.992167 & 1.03755 & 1.04617 \\ 1.02253 & 0.961301 & 1.000000 & 1.06604 & & \\ 1.09304 & 0.921416 & 1.04479 & 1.06258 & 0.972632 & 0.986827 \\ 1.09111 & 1.04673 & 0.98218 & 1.00000 & & \end{pmatrix}$$

In Figure 4.3a, we assumed intermediate productivity ($K=10 \text{ mg L}^{-1}$) with moderate seasonal forcing ($a=0.3$). We used the same value of $g_k=0.4 \text{ d}^{-1}$ for all zooplankton species, but gave different values of r_i , H_k , e_k , and m_k to different species. More specifically:

$$r = \begin{pmatrix} 0.64665 \\ 0.73128 \\ 1.09515 \\ 0.24008 \\ 1.97589 \\ 1.3165 \\ 0.45302 \\ 0.78771 \\ 0.72965 \\ 0.50729 \end{pmatrix} \quad H = \begin{pmatrix} 1.18118 \\ 0.920836 \\ 1.18118 \\ 0.920836 \\ 1.17589 \\ 1.37788 \\ 1.43905 \\ 1.02976 \end{pmatrix} \quad e = \begin{pmatrix} 0.8391 \\ 0.8535 \\ 0.78746 \\ 0.87448 \\ 0.87566 \\ 0.74493 \end{pmatrix} \quad m = \begin{pmatrix} 0.16785 \\ 0.1913 \\ 0.10878 \\ 0.12509 \\ 0.11267 \\ 0.17558 \end{pmatrix}$$

Vectors P_0 , Z_0 and matrices r , m , e , S , A were given by:

$$P_0 = \begin{pmatrix} 5.6033 \\ 3.7343 \\ 2.9252 \\ 9.5756 \\ 1.3244 \\ 6.6919 \\ 0.5373 \\ 4.0248 \\ 9.7121 \\ 3.1616 \end{pmatrix} \quad Z_0 = \begin{pmatrix} 2.5483 \\ 0.4711 \\ 7.3076 \\ 4.7199 \\ 8.6046 \\ 3.9517 \end{pmatrix}$$

$$S = \begin{pmatrix} 0.2739 & 0.3692 & 0.7245 & 0.8688 & 0.8239 & 0.7317 \\ 0.8734 & 0.0925 & 0.6020 & 0.3653 & 0.0612 & 0.5319 \\ 0.3627 & 0.4512 & 0.7672 & 0.7366 & 0.5831 & 0.3031 \\ 0.1146 & 0.2210 & 0.0088 & 0.7630 & 0.6388 & 0.1579 \\ 0.2838 & 0.0599 & 0.0094 & 0.6393 & 0.3668 & 0.2917 \\ 0.8561 & 0.9374 & 0.2962 & 0.9456 & 0.5268 & 0.5625 \\ 0.6497 & 0.9486 & 0.5343 & 0.3542 & 0.0289 & 0.4778 \\ 0.0115 & 0.4202 & 0.3704 & 0.2416 & 0.1949 & 0.3004 \\ 0.0279 & 0.8689 & 0.2471 & 0.9396 & 0.9559 & 0.7904 \\ 0.7885 & 0.5857 & 0.1170 & 0.6928 & 0.3288 & 0.4700 \end{pmatrix}$$

$$A = \begin{pmatrix} 1.0000 & 1.0961 & 0.5490 & 0.5034 & 1.0724 & 0.9110 \\ 0.9208 & 1.3619 & 1.0463 & 0.7324 & & \\ 1.4645 & 1.0000 & 0.7008 & 1.1112 & 1.2020 & 0.7292 \\ 0.5634 & 0.7309 & 1.2020 & 1.4881 & & \\ 1.4564 & 0.5321 & 1.0000 & 1.0015 & 0.6147 & 0.8651 \\ 1.0998 & 0.8082 & 1.0616 & 0.8880 & & \\ 1.0383 & 1.3350 & 1.2496 & 1.0000 & 0.5553 & 0.8010 \\ 0.5817 & 0.7524 & 1.2584 & 0.6846 & & \\ 0.6634 & 1.2818 & 1.0817 & 1.1604 & 1.0000 & 0.9473 \\ 0.6999 & 0.7931 & 0.7071 & 1.1986 & & \\ 1.0415 & 1.0303 & 0.5901 & 0.8202 & 0.5466 & 1.0000 \\ 0.8536 & 0.6567 & 1.0201 & 0.7779 & & \\ 1.3418 & 1.2713 & 0.6140 & 0.5881 & 1.4340 & 1.2514 \\ 1.0000 & 0.8507 & 1.3627 & 0.7733 & & \\ 1.3741 & 1.4933 & 1.1073 & 0.6776 & 0.8548 & 0.5546 \\ 0.8700 & 1.0000 & 1.1961 & 1.3775 & & \\ 0.9202 & 1.4680 & 0.6642 & 0.5577 & 1.2664 & 1.3027 \\ 0.6061 & 0.9352 & 1.0000 & 0.8912 & & \\ 1.1962 & 0.6250 & 0.5699 & 1.0464 & 1.3721 & 1.0575 \\ 1.4082 & 1.4656 & 0.7015 & 1.0000 & & \end{pmatrix}$$

In Figure 4.3b, we assumed intermediate productivity ($K=10 \text{ mg L}^{-1}$) with moderate seasonal forcing ($a=0.4$). $g_k=0.4 \text{ d}^{-1}$, $H_k=0.6 \text{ mg L}^{-1}$, $e_k=0.6$, and $m_k=0.15 \text{ d}^{-1}$, and $u=10^{-7} \text{ mg L}^{-1} \text{ d}^{-1}$ for all plankton species. Vectors P_0 , Z_0 and matrices S , A were given by:

$$P_0 = \begin{pmatrix} 1.75155 \\ 8.86987 \\ 8.65678 \\ 0.344306 \\ 3.05737 \\ 6.19159 \\ 0.793746 \\ 2.82526 \\ 6.02323 \\ 4.73876 \end{pmatrix} \quad Z_0 = \begin{pmatrix} 6.27295 \\ 1.82754 \\ 7.16044 \\ 3.04619 \\ 7.5931 \\ 6.42452 \end{pmatrix}$$

$$S = \begin{pmatrix} 0.29850 & 0.27860 & 0.34527 & 0.37445 & 0.34266 & 0.32663 \\ 0.31940 & 0.35693 & 0.31036 & 0.28472 & 0.36201 & 0.35804 \\ 0.31993 & 0.29126 & 0.25304 & 0.31508 & 0.38415 & 0.34650 \\ 0.27725 & 0.37420 & 0.39575 & 0.27723 & 0.37798 & 0.29580 \\ 0.26970 & 0.27078 & 0.27360 & 0.34278 & 0.39206 & 0.26376 \\ 0.31529 & 0.38120 & 0.37441 & 0.34481 & 0.34716 & 0.39626 \\ 0.25364 & 0.30899 & 0.31042 & 0.27531 & 0.29503 & 0.38262 \\ 0.30948 & 0.29572 & 0.37126 & 0.38137 & 0.36730 & 0.39064 \\ 0.28607 & 0.36875 & 0.28077 & 0.38314 & 0.35655 & 0.28498 \\ 0.38015 & 0.31553 & 0.28367 & 0.26540 & 0.34975 & 0.33271 \end{pmatrix}$$

$$A = \begin{pmatrix} 1.00000 & 0.99475 & 0.97958 & 0.95910 & 1.03280 & 0.92700 \\ 0.98234 & 0.96638 & 1.08750 & 0.95666 & & \\ 1.06560 & 1.00000 & 0.95634 & 1.08220 & 0.95074 & 1.00540 \\ 1.09620 & 1.08420 & 0.93489 & 0.91330 & & \\ 0.91709 & 0.92685 & 1.00000 & 1.04790 & 0.99072 & 0.98929 \\ 0.96196 & 0.91312 & 1.07330 & 0.92231 & & \\ 1.06590 & 1.03800 & 1.01530 & 1.00000 & 0.94733 & 1.04940 \\ 1.01340 & 1.07910 & 0.95883 & 1.04470 & & \\ 1.01210 & 0.92515 & 0.93053 & 1.09910 & 1.00000 & 0.98273 \\ 0.95250 & 1.02730 & 0.91475 & 1.09590 & & \\ 1.02820 & 1.09840 & 0.98001 & 1.00150 & 0.97731 & 1.00000 \\ 1.09980 & 0.90727 & 1.04890 & 1.09850 & & \\ 1.03300 & 0.98970 & 1.09570 & 1.06060 & 0.94573 & 0.98086 \\ 1.00000 & 0.90866 & 0.94027 & 1.04700 & & \\ 0.91563 & 1.01030 & 0.91116 & 0.90763 & 0.98071 & 0.90113 \\ 1.08920 & 1.00000 & 1.05080 & 1.04510 & & \\ 1.07190 & 0.90280 & 0.95476 & 0.90458 & 1.01090 & 1.09010 \\ 1.03770 & 1.03020 & 1.00000 & 0.98129 & & \\ 0.96522 & 0.95182 & 1.01380 & 1.01840 & 0.95030 & 1.05550 \\ 1.09230 & 0.99024 & 0.93853 & 1.0000 & & \end{pmatrix}$$

In Figure 4.4, we assumed intermediate productivity ($K=5 \text{ mg L}^{-1}$) with strong seasonal forcing ($a=0.8$). We used the same value of $g_k=0.4 \text{ d}^{-1}$ for all zooplankton species, but gave different values of r_i , H_k , e_k , and m_k to different species. More specifically, the vectors \mathbf{r} (d^{-1}), \mathbf{H} (mg L^{-1}), \mathbf{e} , and \mathbf{m} (d^{-1}) were given by:

$$\mathbf{r} = \begin{pmatrix} 1.54861 \\ 0.227021 \\ 1.00078 \\ 1.55148 \\ 1.99442 \\ 1.96711 \\ 0.354273 \\ 0.721033 \\ 0.615612 \\ 0.20288 \end{pmatrix} \quad \mathbf{H} = \begin{pmatrix} 1.13726 \\ 1.15042 \\ 1.46427 \\ 0.907053 \\ 0.958407 \\ 1.14154 \end{pmatrix} \quad \mathbf{e} = \begin{pmatrix} 0.760409 \\ 0.88252 \\ 0.834658 \\ 0.666893 \\ 0.843236 \\ 0.606695 \end{pmatrix} \quad \mathbf{m} = \begin{pmatrix} 0.122999 \\ 0.127312 \\ 0.164034 \\ 0.183516 \\ 0.163904 \\ 0.107039 \end{pmatrix}$$

Vectors \mathbf{P}_0 , \mathbf{Z}_0 and matrices \mathbf{S} , \mathbf{A} were given by:

$$\mathbf{P}_0 = \begin{pmatrix} 0.00117804 \\ 6.30557e^{-07} \\ 5.75243e^{-07} \\ 0.785067 \\ 1.29333e^{-06} \\ 2.41034e^{-06} \\ 6.65038e^{-07} \\ 4.0123e^{-06} \\ 1.54209e^{-06} \\ 9.22919e^{-07} \end{pmatrix} \quad \mathbf{Z}_0 = \begin{pmatrix} 1.39431 \\ 2.05514 \\ 4.05325e^{-06} \\ 3.28186e^{-06} \\ 0.257369 \\ 3.94753e^{-06} \end{pmatrix}$$

$$S = \begin{pmatrix} 0.08698 & 0.52533 & 0.17573 & 0.64005 & 0.66433 & 0.65032 \\ 0.73321 & 0.60993 & 0.42224 & 0.11952 & 0.74602 & 0.18858 \\ 0.55316 & 0.97766 & 0.99446 & 0.79080 & 0.07369 & 0.00642 \\ 0.39041 & 0.24748 & 0.45050 & 0.37535 & 0.41623 & 0.14282 \\ 0.19733 & 0.74224 & 0.98730 & 0.16071 & 0.63454 & 0.37086 \\ 0.49605 & 0.57411 & 0.91880 & 0.61654 & 0.14503 & 0.29152 \\ 0.70794 & 0.83863 & 0.65944 & 0.27091 & 0.96533 & 0.10926 \\ 0.38644 & 0.22721 & 0.70474 & 0.11154 & 0.31407 & 0.23903 \\ 0.59253 & 0.13447 & 0.03458 & 0.52474 & 0.89346 & 0.86357 \\ 0.74268 & 0.34403 & 0.63889 & 0.12762 & 0.65188 & 0.36374 \end{pmatrix}$$

$$A = \begin{pmatrix} 1.00000 & 0.846013 & 0.61694 & 0.54086 & 1.08818 & 1.32430 \\ 1.07503 & 1.41741 & 1.06555 & 0.93454 & & \\ 0.88426 & 1.00000 & 1.04436 & 1.23063 & 1.03164 & 0.51144 \\ 0.76902 & 0.96793 & 1.07259 & 1.25264 & & \\ 0.55652 & 0.77579 & 1.00000 & 1.22768 & 0.54063 & 1.39338 \\ 0.65997 & 1.41046 & 1.01110 & 1.38066 & & \\ 1.12062 & 0.76347 & 1.31129 & 1.00000 & 0.58935 & 1.15726 \\ 0.51551 & 0.71593 & 0.55077 & 1.41190 & & \\ 1.13481 & 1.40532 & 0.61007 & 1.07318 & 1.00000 & 1.33831 \\ 1.00879 & 1.40002 & 0.86743 & 0.68890 & & \\ 0.81958 & 1.14729 & 1.12559 & 0.95518 & 1.36336 & 1.00000 \\ 0.86975 & 1.38648 & 0.78592 & 1.44744 & & \\ 0.73085 & 0.89928 & 0.79923 & 0.50769 & 0.67607 & 0.84860 \\ 1.00000 & 1.23217 & 0.87494 & 1.29477 & & \\ 0.88884 & 1.21369 & 0.91026 & 0.69580 & 0.82509 & 1.14056 \\ 0.81636 & 1.00000 & 0.62630 & 1.44856 & & \\ 0.79612 & 1.17477 & 0.60108 & 0.94745 & 0.66530 & 1.36991 \\ 0.75158 & 0.86824 & 1.00000 & 0.50631 & & \\ 0.59113 & 0.83081 & 1.45812 & 0.63744 & 0.56553 & 0.91114 \\ 1.42703 & 0.84536 & 0.78182 & 1.00000 & & \end{pmatrix}$$

In Figure 4.5, we ran 100 simulations per data point. For each simulation, new parameter values were drawn randomly from the ranges indicated in Table 4.1.

In Figure C.1, we ran 100 simulations per data point. For each simulation, new parameter values were drawn randomly from the ranges indicated in Table 4.1.

In Figure C.2, we assumed no seasonal forcing ($a=0$). Vectors \mathbf{P}_0 , \mathbf{Z}_0 and matrices \mathbf{S} , \mathbf{A} were given by:

$$P_0 = \begin{pmatrix} 0.00117804 \\ 6.30557e^{-07} \\ 5.75243e^{-07} \\ 0.785067 \\ 1.29333e^{-06} \\ 2.41034e^{-06} \\ 6.65038e^{-07} \\ 4.0123e^{-06} \\ 1.54209e^{-06} \\ 9.22919e^{-07} \end{pmatrix} \quad Z_0 = \begin{pmatrix} 1.39431 \\ 2.05514 \\ 4.05325e^{-06} \\ 3.28186e^{-06} \\ 0.257369 \\ 3.94753e^{-06} \end{pmatrix}$$

$$S = \begin{pmatrix}
 0.39688 & 0.34169 & 0.33293 & 0.27692 & 0.36566 & 0.29518 \\
 0.29508 & 0.38791 & 0.35051 & 0.26846 & 0.39198 & 0.38191 \\
 0.25412 & 0.26443 & 0.26618 & 0.25863 & 0.27739 & 0.34430 \\
 0.36514 & 0.31579 & 0.29553 & 0.27960 & 0.30566 & 0.29690 \\
 0.37799 & 0.39630 & 0.33657 & 0.31228 & 0.30683 & 0.32668 \\
 0.39557 & 0.26548 & 0.27360 & 0.30007 & 0.31975 & 0.28773 \\
 0.38807 & 0.39995 & 0.34352 & 0.28910 & 0.32468 & 0.35178 \\
 0.39374 & 0.33758 & 0.35297 & 0.34044 & 0.31643 & 0.25621 \\
 0.25841 & 0.34850 & 0.28327 & 0.33934 & 0.29598 & 0.27393 \\
 0.32442 & 0.34733 & 0.33914 & 0.29485 & 0.38918 & 0.30345
 \end{pmatrix}$$

$$A = \begin{pmatrix}
 1.00000 & 1.00410 & 1.01700 & 0.91726 & 0.99183 & 0.94602 \\
 1.00830 & 0.99112 & 1.03780 & 0.92279 & & \\
 0.99627 & 1.00000 & 0.95722 & 0.97682 & 1.00170 & 1.06080 \\
 0.98161 & 0.91644 & 1.02540 & 0.99051 & & \\
 1.02610 & 1.02860 & 1.00000 & 0.94895 & 0.93013 & 1.06750 \\
 0.96058 & 0.93244 & 1.04050 & 1.03700 & & \\
 0.95701 & 1.02430 & 1.05220 & 1.00000 & 1.09760 & 0.95281 \\
 1.08510 & 1.05120 & 0.94871 & 1.06190 & & \\
 0.92834 & 1.05650 & 1.04300 & 0.91381 & 1.00000 & 1.00990 \\
 1.05440 & 1.05860 & 1.08530 & 1.00310 & & \\
 1.01440 & 1.02030 & 1.03400 & 1.02710 & 1.06360 & 1.00000 \\
 0.99833 & 0.92670 & 1.08860 & 1.00100 & & \\
 0.92927 & 1.05900 & 0.93177 & 1.06990 & 1.06180 & 1.07350 \\
 1.00000 & 0.95214 & 1.02190 & 0.95715 & & \\
 0.98737 & 0.91678 & 1.04950 & 1.08330 & 0.95171 & 0.95582 \\
 1.07160 & 1.00000 & 0.95818 & 0.97624 & & \\
 0.90661 & 0.97521 & 0.97198 & 0.94045 & 1.08230 & 0.92413 \\
 0.95609 & 1.06650 & 1.00000 & 1.05470 & & \\
 1.01010 & 1.07520 & 0.94364 & 1.02940 & 0.98052 & 0.93263 \\
 0.94588 & 0.93248 & 1.04440 & 1.00000 & &
 \end{pmatrix}$$

Appendix D

Supplementary information to chapter 5

D.1 Sources of the temperature data

The time series of water temperature analyzed in this paper were obtained from different sources. The data for Lake IJsselmeer were obtained from the Dutch Governmental Water Institute (Rijkswaterstaat) and are available at <http://www.waterbase.nl/>. The data for U.S lakes were obtained from the U.S. Geological Survey (USGS) and can be downloaded at the following link: <http://waterdata.usgs.gov/nwis>. The ocean data were obtained from the National Data Buoy Center and can be downloaded at the following link <http://www.ndbc.noaa.gov/>. For all time series, the water temperature was sampled daily, except for the buoy data, where the water temperature was sampled every hour. To make the buoy data comparable with the other time series, we calculated the daily mean for all buoy time series. To estimate the mean annual temperature cycle, temperature data measured on February 29 were removed from the leap years. Missing data were interpolated using cubic hermite interpolation. Table D.1 provides additional information on the time series data.

Water body	Time interval	Status of the data	Number of data points	Maximum number of consecutive missing data	Total number of missing data	Type of measurement
Atlantic Ocean Mid Atlantic Station N° 41041 14.357 N 46.008 W	28/05/2005-30/11/2007	Approved	917	8	8	Daily mean
IJsselmeer (The Netherlands)	01/01/1972-31/12/1993	Approved	8030	0	0	Instantaneous measurement (at 8:00 AM)
Crater Lake (Oregon, USA)	28/7/1998-07/07/2003	Provisory	1806	6	52	Daily mean
Pacific Ocean (Southwest of Hilo, Hawaii, USA) Station N° 51002 17.094 N 157.808 W	22/03/2006-28/02/2009	Approved	1074	0	0	Daily mean
Cedar Lake (Wisconsin, USA)	09/05/1974-28/11/1976	Approved	934	5	15	Daily mean
Bee Lake (Mississippi, USA)	27/9/2005-30/9/2009	Approved	1464	1	2	Daily mean
Gulf of Mexico (South of Freeport, Texas, USA) Station N° 42019 27.913 N 95.353 W	23/06/2000-10/06/2006	Approved	2146	16	16	Daily mean
Pacific Ocean (Shumagin Islands, Alaska, USA) Station N° 46075 53.911 N 160.806 W	01/01/2005-31/12/2009	Approved	1825	0	0	Daily mean
Caillou lake (Louisiana, USA)	22/05/1997-10/02/2002	Approved	1960	12	52	Daily mean

Continued on Next Page...

Tarpon Lake (Florida, USA)	01/10/1964-20/9/1968	Approved	1450	2	10	Instantaneous measurement
Atlantic Ocean (Southeast of Nantucket, Massachusetts, USA) Station N ^o 44008 40.502 N 69.247 W	01/01/2005-01/10/2008	Approved	1369	0	0	Daily mean
Lake Meredith (Colorado, USA)	06/05/2004-20/09/2009	Approved	1963	10	38	Average (max/min)
Lake Champlain (New York, USA)	11/01/2005-08/03/2010	Provisory	1882	3	40	Daily mean

Table D.1: Additional information on the time series of surface temperature analyzed in this paper.

D.2 Power spectral density of the temperature fluctuations

First, the seasonal variation was removed from the temperature time series. This was done by calculating the mean temperature for each particular day of the year (averaged over all years in the time series), and subsequently subtracting this seasonal pattern from the time series.

As a next step, we estimated the power spectral density of the seasonally detrended time series. The discrete Fourier transform X for a time series of length N , with observations x_0, \dots, x_{N-1} , is:

$$X(k) = \frac{1}{\sqrt{N}} \sum_{j=0}^{N-1} x_j e^{-\frac{2\pi i j k}{N}} \quad (\text{D.1})$$

where $k = 0, \dots, N - 1$ is the frequency index. The periodogram is defined as:

$$P(k) = X(k) X^*(k) \quad (\text{D.2})$$

where $X^*(k)$ is the complex conjugate of $X(k)$.

The raw periodogram as expressed in Eq. D.2 is not a consistent estimator of the power spectral density, because its variance does not converge to zero when increasing the length of a time series (Percival and Walden 1993). Consistent estimators can be derived by smoothing the raw periodogram. We smoothed the periodogram using the modified Welch periodogram (Welch 1967). This method splits the time series in overlapping segments, called Hamming windows, and calculates the periodogram for each window separately. The Welch periodogram is then obtained by averaging the resulting periodograms. This yields a smooth periodogram, which is a consistent and asymptotically unbiased estimator of the power spectral density. The power spectral density estimate (black line in Figure 5.6c of the main text) was calculated using 5 Hamming windows with 50% overlap.

D.3 Power spectral density of red noise

For each time series, the power spectral density of the seasonally detrended temperature data was compared against the power spectral density of red noise. A simple model for red noise is the first-order autoregressive AR(1) process (Box and Jenkins 1970):

$$n_{t+1} = \alpha n_t + \epsilon_t \quad (\text{D.3})$$

where α is the lag-1 autocorrelation coefficient and ϵ_t is white noise drawn from a Gaussian distribution with zero mean and standard deviation σ_ϵ . The power spectral density of red noise for a finite time series of length N generated by equation D.3

can be calculated using the following approximation (Gilman et al. 1963):

$$P_k = \frac{1 - \alpha^2}{1 + \alpha^2 - 2\alpha \cos(\frac{2\pi k}{N})} \quad (\text{D.4})$$

where $K = 0, \dots, N$ is the frequency index.

For each time series, we calculated the autocorrelation coefficient α from the product-moment correlation between the temperature at day t and at day $t+1$. Subsequently, we inserted this value of α into equation D.4 to estimate the corresponding power spectral density of red noise (red line in Figure 5.6c of the main text).

D.4 Growth rates of zooplankton

Taxonomic group	Species name	Maximum specific growth rate (d^{-1})	References
Heterotrophic flagellates (green)	<i>Paraphysomonas vestita</i> (Δ)	5.5	Fenchel 1982
	<i>Ochromonas</i> sp. (\square)	4.6	Fenchel 1982
	<i>Monosiga</i> sp. (\circ)	4.1	Fenchel 1982
	<i>Pleuromonas jaculans</i> (\triangleleft)	3.8	Fenchel 1982
Ciliates (red)	<i>Balanion</i> sp. (Δ)	2.9	Stoecker et al. 1983
	<i>Strombidium</i> sp. (\square)	2.7	Ohman and Snyder 1991
	<i>Urotricha furcata</i> (∇)	1.7	Müller and Geller 1993

Continued on Next Page...

Appendix D

	<i>Eutintinnus pectinis</i> (○)	1.4	Heinbokel 1978
	<i>Tintinnopsis cf. acuminata</i> (○)	1.4	Heinbokel 1978
	<i>Plagostrombidium flallax</i> (▷)	0.9	Müller and Geller 1993
Rotifers (gray)	<i>Brachionus rubens</i> (○)	1.25	Rothhaupt 1990
	<i>Synchaeta pectinata</i> (▷)	0.9	Kirk and Gilbert 1990
	<i>Ascomorpha ecaudis</i> (▽)	0.7	Stemberger 1987
	<i>Polyarthra vulgaris</i> (◁)	0.29	Kirk and Gilbert 1990
	<i>Keratella cochlearis</i> (□)	0.25	Kirk and Gilbert 1990
	<i>Keratella crassa</i> (◇)	0.245	Kirk and Gilbert 1990
Salps (violet)	<i>Thalia democratica</i> (○)	2.5	Heron 1972
Cladocerans (black)	<i>Daphnia magna</i> ¹ (△)	0.24	Rose et al. 1988
	<i>Ceriodaphnia dubia</i> (△)	0.23	Kirk and Gilbert 1990
	<i>Daphnia pulex</i> (○)	0.18	Kirk and Gilbert 1990

Continued on Next Page...

	<i>Daphnia ambigua</i> (◁)	0.16	Kirk and Gilbert 1990
	<i>Bosmina longirostris</i> (□)	0.1	Kirk and Gilbert 1990
Copepods (orange)	<i>Acartia tonsa</i> (○)	0.45	Berggreen et al. 1988
	<i>Calanus pacificus</i> (□)	0.18	Banse 1982
	<i>Pseudocalanus</i> sp. (◁)	0.11	Banse 1982
	<i>Nitocra spinipes</i> (▽)	0.09	Breitholtz and Wol- lenberger 2003
	<i>Metridia gerlachei</i> (▷)	0.06	Schnack et al. 1985
	<i>Pseudocalanus newmani</i> (◁)	0.04	Jonasdottir 1989
	<i>Pleuromamma abdominalis</i> (◇)	0.02	Petipa et al. 1975
Euphasiids (light blue)	<i>Euphausia superba</i> (○)	0.002	Mori and Butter- worth 2006

¹ This value corresponds to a medium size individual.

Table D.2: Maximum specific growth rates of the zooplankton species used in Figure 5.7 of the main text.

References

- Abrams, P. A. and Matsuda, H. (1997). Prey adaptation as a cause of predator-prey cycles. *Evolution*, 51:1742–1750.
- Adrian, R., Walz, N., Hintze, T., Hoeg, S., and Rusche, R. (1999). Effects of ice duration on plankton succession during spring in a shallow polymictic lake. *Freshwater Biology*, 41:1–12.
- Allen, J. C., Schaffer, W. M., and Rosko, D. (1993). Chaos reduces species extinction by amplifying local population noise. *Nature*, 364:229–232.
- Arhonditsis, G. B., Winder, M., Brett, M. T., and Schindler, D. E. (2004). Patterns and mechanisms of phytoplankton variability in Lake Washington (USA). *Water Research*, 38:4013–4027.
- Armstrong, R. A. and McGehee, R. (1980). Competitive exclusion. *American Naturalist*, 115:151–170.
- Bailey, B. A., Ellner, S., and Nychka, D. W. (1997). Chaos with confidence: asymptotics and applications of local Lyapunov exponents. In Cutler, C. D. and Kaplan, D. T., editors, *Nonlinear Dynamics and Time Series: Building a Bridge Between the Natural and Statistical Sciences*, volume 110, pages 115–133. American Mathematical Society, Providence, RI.
- Banse, K. (1982). Mass-scaled rates of respiration and intrinsic growth in very small invertebrates. *Marine Ecology Progress Series*, 9:281–297.
- Becks, L., Hilker, F. M., Malchow, H., Jürgens, K., and Arndt, H. (2005). Experimental demonstration of chaos in a microbial food web. *Nature*, 435:1226–1229.
- Begon, M., Townsend, C. R., and Harper, J. L. (2006). *Ecology: From Individuals to Ecosystems*. Blackwell Publishing, Oxford, UK, 4th edition.
- Benincà, E., Huisman, J., Heerkloss, R., Jöhnk, K. D., Branco, P., van Nes, E. H., et al. (2008). Chaos in a long-term experiment with a plankton community. *Nature*, 451:822–825.
- Benincà, E., Jöhnk, K. D., Heerkloss, R., and Huisman, J. (2009). Coupled predator-prey oscillations in a chaotic food web. *Ecology Letters*, 12:1367–1378.

- Benjamini, Y. and Hochberg, Y. (1995). Controlling the false discovery rate - a practical and powerful approach to multiple testing. *Journal of the Royal Statistical Society Series B-Methodological*, 57:289–300.
- Bennett, M., Schatz, M. F., Rockwood, H., and Wiesenfeld, K. (2002). Huygens's clocks. *Proceedings of the Royal Society of London A*, 458:563–579.
- Berg, M. P., Kniese, J. P., Bedaux, J. J. M., and Verhoef, H. A. (1998). Dynamics and stratification of functional groups of micro- and mesoarthropods in the organic layer of a Scots pine forest. *Biology and Fertility of Soils*, 26:268–284.
- Berggreen, U., Hansen, B., and Kiørboe, T. (1988). Food size spectra, ingestion and growth of the copepod *Acartia tonsa* during development: implications for determination of copepod production. *Marine Biology*, 99:341–352.
- Berman, T., Yacobi, Y. Z., and Pollinger, U. (1992). Lake Kinneret phytoplankton: stability and variability during 20 years (1970-1989). *Aquatic Sciences*, 54:104–127.
- Berryman, A. A. and Millstein, J. A. (1989). Are ecological systems chaotic - and if not, why not? *Trends in Ecology & Evolution*, 4:26–28.
- Billings, L. and Schwartz, I. B. (2002). Exciting chaos with noise: unexpected dynamics in epidemic outbreaks. *Journal of Mathematical Biology*, 44:31–48.
- Bjørnstad, O. N. and Grenfell, B. T. (2001). Noisy clockwork: time series analysis of population fluctuations in animals. *Science*, 293:638–643.
- Bohannan, B. J. M. and Lenski, R. E. (1997). Effect of resource enrichment on a chemostat community of bacteria and bacteriophage. *Ecology*, 78:2303–2315.
- Box, G. E. P. and Jenkins, G. M. (1970). *Time Series Analysis: Forecasting and Control*. Holden-Day, San Francisco.
- Brassil, C. E. (2006). Can environmental variation generate positive indirect effects in a model of shared predation? *American Naturalist*, 167:43–54.
- Breitholtz, M. and Wollenberger, L. (2003). Effects of three PBDEs on development, reproduction and population growth rate of the harpacticoid copepod *Nitocra spinipes*. *Aquatic Toxicology*, 64:85–96.
- Brose, U. (2008). Complex food webs prevent competitive exclusion among producer species. *Proceedings of the Royal Society of London B*, 275:2507–2514.
- Cazelles, B., Chavez, M., Berteaux, D., Ménard, F., Vik., J. O., Jenouvrier, S., et al. (2008). Wavelet analysis of ecological time series. *Oecologia*, 156:287–304.

- Chatfield, J. R. (1989). *The Analysis of Time Series: an Introduction*. Chapman & Hall, London.
- Chesson, J. (1978). Measuring preference in selective predation. *Ecology*, 59:211–215.
- Chesson, P. (2000). Mechanisms of maintenance of species diversity. *Annual Review of Ecology and Systematics*, 31:343–366.
- Connell, J. H. (1978). Diversity in tropical rain forests and coral reefs. *Science*, 199:1302–1310.
- Costantino, R. F., Desharnais, R. A., Cushing, J. M., and Dennis, B. (1997). Chaotic dynamics in an insect population. *Science*, 275:389–391.
- Coulson, T., Rohani, P., and Pascual, M. (2004). Skeletons, noise and population growth: the end of an old debate? *Trends in Ecology and Evolution*, 19:359–364.
- Dakos, V., Benincà, E., van Nes, E. H., Philippart, C. J. M., Scheffer, M., and Huisman, J. (2009). Interannual variability in species composition explained as seasonally entrained chaos. *Proceedings of the Royal Society of London B*, 276:2871–2880.
- Davison, A. C. and Hinkley, D. V. (1997). *Bootstrap Methods and their Application*. Cambridge University Press, Cambridge.
- De Roos, A. M., Diekmann, O., and Metz, J. A. J. (1992). Studying the dynamics of structured population models: a versatile technique and its application to *Daphnia*. *American Naturalist*, 139:123–147.
- De Roos, A. M., Persson, L., and McCauley, E. (2003). The influence of size-dependent life-history traits on the structure and dynamics of populations and communities. *Ecology Letters*, 6:473–487.
- Descamps-Julien, B. and Gonzalez, A. (2005). Stable coexistence in a fluctuating environment: an experimental demonstration. *Ecology*, 86:2815–2824.
- Dippner, J. W., Heerkloss, R., and Zbilut, J. P. (2002). Recurrence quantification analysis as a tool for characterization of non-linear mesocosm dynamics. *Marine Ecology-Progress Series*, 242:29–37.
- Doveri, F., Scheffer, M., Rinaldi, S., Muratori, S., and Kuznetsov, Y. (1993). Seasonality and chaos in a plankton fish model. *Theoretical Population Biology*, 43:159–183.
- Easterling, D. R., Evans, J. L., Groisman, P. Y., Karl, T. R., Kunkel, P. E., and Ambenje, P. (2000). Observed variability and trends in extreme climate events: a brief review. *Bulletin of the American Meteorological Society*, 81:417–425.

- Ebenhöh, W. (1992). Temporal organization in a multi-species model. *Theoretical Population Biology*, 42:152–171.
- Eckmann, J. P., Kamphorst, S. O., and Ruelle, D. (1987). Recurrence plots of dynamical systems. *Europhysics Letters*, 4:973–977.
- Eckmann, J. P., Kamphorst, S. O., Ruelle, D., and Ciliberto, S. (1986). Liapunov exponents from time-series. *Physical Review A*, 34:4971–4979.
- Ellner, S. P., Bayley, B. A., Bobashev, G. V., Gallant, A. R., Grenfell, B. T., and Nychka, D. W. (1998). Noise and nonlinearity in measles epidemics: combining mechanistic and statistical approaches to population modeling. *American Naturalist*, 151:425–440.
- Ellner, S. P., Nychka, D. W., and Gallant, A. R. (1992). LENNS, a program to estimate the dominant Lyapunov exponent of noisy nonlinear systems from time series data. *Institute of Statistics Mimeo Series # 2235, Statistics Department, North Carolina State University, Raleigh NC 27695-8203*.
- Ellner, S. P. and Turchin, P. (1995). Chaos in a noisy world: new methods and evidence from time-series analysis. *American Naturalist*, 145:343–375.
- Elton, C. and Nicholson, M. (1942). The ten-year cycle in numbers of the lynx in Canada. *Journal of Animal Ecology*, 11:215–244.
- Elton, C. S. (1924). Periodic fluctuations in the number of animals: their causes and effects. *British Journal of Experimental Biology*, 2:119–163.
- Erwin, T. L. (1982). Tropical forests: their richness in Coleoptera and other arthropod species. *The Coleopterists Bulletin*, 36:74–75.
- Farge, M. (1992). Wavelet transforms and their applications to turbulence. *Annual Review of Fluid Mechanics*, 24:395–457.
- Fasham, M. J. R., Ducklow, H. W., and McKelvie, S. M. (1990). A nitrogen-based model of plankton dynamics in the oceanic mixed layer. *Journal of Marine Research*, 48:591–639.
- Feike, M. and Heerkloss, R. (2008). Long-term stability of the seasonal succession of different zooplankton species in a brackish water lagoon (southern Baltic Sea). *Hydrobiologia*, 611:17–28.
- Fenchel, T. (1982). Ecology of heterotrophic microflagellates. II. Bioenergetics and growth. *Marine Ecology Progress Series*, 8:225–231.
- Flöder, S. and Sommer, U. (1999). Diversity in planktonic communities: an experimental test of the intermediate disturbance hypothesis. *Limnology and Oceanography*, 44:1114–1119.

- Franks, P. J. S. (2002). NPZ models of plankton dynamics: their construction, coupling to physics, and application. *Journal of Oceanography*, 58:379–387.
- Fussmann, G. F., Ellner, S. P., Shertzer, K. W., and Hairston, N. G., Jr. (2000). Crossing the hopf bifurcation in a live predator-prey system. *Science*, 290:1358–1360.
- Gaedeke, A. and Sommer, U. (1986). The influence of the frequency of periodic disturbances on the maintenance of phytoplankton diversity. *Oecologia*, 71:25–28.
- Gause, G. F. (1934). *The Struggle for Existence*. Williams & Wilkins, Baltimore.
- Giller, P. S. and Doube, B. M. (1994). Spatial and temporal co-occurrence of competitors in southern african dung beetle communities. *Journal of Animal Ecology*, 63:629–643.
- Gilman, D. L., Fuglister, F. J., and Mitchell, J. M., Jr. (1963). On the power of red noise. *Journal of the Atmospheric Sciences*, 20:182–184.
- Gilpin, M. E. (1979). Spiral chaos in a predator-prey model. *American Naturalist*, 113:306–308.
- Gliwicz, Z. M. and Wrzosek, D. (2008). Predation-mediated coexistence of large- and small- bodied *Daphnia* at different food levels. *American Naturalist*, 172:358–374.
- Golubitsky, M., Stewart, I., Buono, P. L., and Collins, J. J. (1999). Symmetry in locomotor central pattern generators and animal gaits. *Nature*, 401:693–695.
- Graham, D. W., Knapp, C. W., Van Vleck, E. S., Bloor, K., Lane, T. B., and Graham, C. E. (2007). Experimental demonstration of chaotic instability in biological nitrification. *ISME Journal*, 1:385–393.
- Grasshoff, K., Ehrhardt, M., and Kremling, K. (1983). *Methods of Seawater Analysis*. Verlag Chemie, Weinheim, 2nd edition.
- Greenman, J. V. and Benton, T. G. (2003). The amplification of environmental noise in population models: causes and consequences. *American Naturalist*, 161:225–239.
- Greenman, J. V. and Benton, T. G. (2005). The impact of environmental fluctuations on structured discrete time population models: resonance, synchrony and threshold behaviour. *Theoretical Population Biology*, 68:217–235.
- Grenfell, B. T., Bjørnstad, O. N., and Kappey, J. (2001). Travelling waves and spatial hierarchies in measles epidemics. *Nature*, 414:716–723.

- Grinsted, A., Moore, J. C., and Jevrejeva, S. (2004). Application of cross wavelet transform and wavelet coherence to geophysical time series. *Nonlinear Processes in Geophysics*, 11:561–566.
- Grover, J. P. (1991). Resource competition in a variable environment: phytoplankton growing according to the variable-internal-stores model. *American Naturalist*, 136:811–835.
- Guckenheimer, J. (1982). Noise in chaotic systems. *Nature*, 298:358–361.
- Guo, Q. F., Brown, J. H., and Valone, T. J. (2002). Long-term dynamics of winter and summer annual communities in the Chihuahuan desert. *Journal of Vegetation Science*, 13:575–584.
- Hanski, I., Turchin, P., Korpimäki, E., and Henttonen, H. (1993). Population oscillations of boreal rodents: regulation by mustelid predators leads to chaos. *Nature*, 364:232–235.
- Hare, S. R. and Mantua, N. J. (2000). Empirical evidence for North Pacific regime shifts in 1997 and 1989. *Progress in Oceanography*, 47:103–145.
- Harris, G. P. and Baxter, G. (1996). Interannual variability in phytoplankton biomass and species composition in a subtropical reservoir. *Freshwater Biology*, 35:545–560.
- Hassell, M. P., Lawton, J. H., and May, R. M. (1976). Patterns of dynamical behaviour in single-species populations. *Journal of Animal Ecology*, 45:471–486.
- Hastings, A., Hom, C. L., Ellner, S., Turchin, P., and Godfray, H. C. J. (1993). Chaos in ecology: is mother nature a strange attractor? *Annual Review of Ecology and Systematics*, 24:1–33.
- Hastings, A. and Powell, T. P. (1991). Chaos in a three-species food chain. *Ecology*, 72:896–903.
- Heerkloss, R. and Klinkenberg, G. (1993). Chaotic dynamics of a plankton community in a species-depleted mesocosmos. *Verhandlungen Internationaler Verein für Limnologie*, 25:995–1000.
- Heerkloss, R. and Klinkenberg, G. (1998). A long-term series of a planktonic foodweb: a case of chaotic dynamics. *Verhandlungen Internationaler Verein für Theoretische und Angewandte Limnologie*, 26:1952–1956.
- Heerkloss, R., Schnese, W., and Adamkiewicz-Chojnacka, B. (1991). Eutrophication induced changes of zooplankton communities in coastal regions of the Baltic Sea. *Internationale revue der gesamten hydrobiologie*, 76:397–404.

- Hegger, R., Kantz, H., and Schreiber, T. (1999). Practical implementation of non-linear time series methods: the Tisean package. *Chaos*, 9:413–435.
- Heinbokel, J. (1978). Studies on the functional role of tintinnids in the Southern California Bight. I. Grazing and growth rates in laboratory cultures. *Marine Biology*, 147:191–197.
- Heron, A. C. (1972). Population ecology of a colonizing species: the pelagic tunicate *Thalia democratica* II. Population growth rate. *Oecologia*, 10:294–312.
- Hochberg, M. E., Hassell, M. P., and May, R. M. (1990). The dynamics of host-parasitoid-pathogen interactions. *American Naturalist*, 135:74–94.
- Hsieh, C. H., Glaser, S. M., Lucas, A. J., and Sugihara, G. (2005). Distinguishing random environmental fluctuations from ecological catastrophes for the North Pacific Ocean. *Nature*, 435:336–340.
- Huffaker, C. B. (1958). Experimental studies on predation: dispersion factors and predator-prey oscillations. *Hilgardia*, 27:795–835.
- Huisman, J., Jonker, R. R., Zonneveld, C., and Weissing, F. J. (1999). Competition for light between phytoplankton species: experimental tests of mechanistic theory. *Ecology*, 80:211–222.
- Huisman, J., Pham Thi, N. N., Karl, D. M., and Sommeijer, B. (2006). Reduced mixing generates oscillations and chaos in the oceanic deep chlorophyll maximum. *Nature*, 439:322–325.
- Huisman, J. and Weissing, F. J. (1999). Biodiversity of plankton by species oscillations and chaos. *Nature*, 402:407–410.
- Huisman, J. and Weissing, F. J. (2001). Biological conditions for oscillations and chaos generated by multispecies competition. *Ecology*, 82:2682–2695.
- Huppert, A., Blasius, B., Olinky, R., and Stone, L. (2005). A model for seasonal phytoplankton blooms. *Journal of Theoretical Biology*, 236:276–290.
- Hutchinson, G. E. (1961). The paradox of the plankton. *American Naturalist*, 95:137–145.
- Irigoien, X., Huisman, J., and Harris, R. P. (2004). Global biodiversity patterns of marine phytoplankton and zooplankton. *Nature*, 429:863–867.
- Ives, A. R., Einarsson, A., Jansen, V. A. A., and Gardarsson, A. (2008). High-amplitude fluctuations and alternative dynamical states of midges in Lake Myvatn. *Nature*, 452:84–87.

- Ives, A. R. and Jansen, V. A. A. (1998). Complex dynamics in stochastic tritrophic models. *Ecology*, 79:1039–1052.
- Jonasdottir, S. (1989). Effects of food concentrations on egg production rates of two species of *Pseudocalanus*: laboratory observations. *Journal of Experimental Marine Biology and Ecology*, 130:33–43.
- Kaitala, V., Ranta, E., and Lindstrom, J. (1996). Cyclic population dynamics and random perturbations. *Ecology*, 65:249–251.
- Kantz, H. and Schreiber, T. (1997). *Nonlinear Time Series Analysis*. Cambridge University Press, Cambridge, UK.
- Keitt, T. H. (2008). Coherent ecological dynamics induced by large scale disturbance. *Nature*, 454:331–334.
- Keitt, T. H. and Fisher, J. (2006). Detection of scale-specific community dynamics using wavelets. *Ecology*, 87:2895–2904.
- Kendall, B. E. (2001). Cycles, chaos, and noise in predator-prey dynamics. *Chaos Solitons & Fractals*, 12:321–332.
- Kendall, B. E., Prendergast, J., and Bjørnstad, O. N. (1998). The macroecology of population dynamics: taxonomic and biogeographic patterns in population cycles. *Ecology Letters*, 1:160–164.
- King, A. A. and Schaffer, W. M. (1999). The rainbow bridge: Hamiltonian limits and resonance in predator-prey dynamics. *Journal of Mathematical Biology*, 39:439–469.
- Király, A., Bartos, I., and Jánosi, I. M. (2006). Correlation properties of daily temperature anomalies over land. *Tellus*, 58 A:593–600.
- Kirk, K. L. and Gilbert, J. J. (1990). Suspended clay and the population dynamics of planktonic rotifers and cladocerans. *Ecology*, 71:1741–1755.
- Kiss, I. Z., Zhai, Y., and Hudson, J. L. (2002). Emerging coherence in a population of chemical oscillators. *Science*, 296:1676–1678.
- Kot, M. and Schaffer, W. M. (1984). The effects of seasonality on discrete models of population growth. *Theoretical Population Biology*, 26:340–360.
- Lekve, K., Bagøien, E., Dahl, E., Edvardsen, B., Skogen, M., and Stenseth, N. C. (2006). Environmental forcing as a main determinant of bloom dynamics of the *Chrysochromulina* algae. *Proceedings of the Royal Society of London B*, 273:3047–3055.

- Lima, I. D., Olson, D. B., and Doney, S. C. (2002). Intrinsic dynamics and stability properties of size-structured pelagic ecosystem models. *Journal of Plankton Research*, 24:533–556.
- Litchman, E. and Klausmeier, C. A. (2001). Competition of phytoplankton under fluctuating light. *American Naturalist*, 157:170–187.
- Longhurst, A. R. (2006). *Ecological geography of the sea*. Academic Press, London, UK, 2nd edition.
- Lorenz, E. N. (1963). Deterministic nonperiodic flow. *Journal of the Atmospheric Sciences*, 20:130–141.
- Lorenz, E. N. (1982). Atmospheric predictability experiments with a large numerical model. *Tellus*, 34:505–513.
- Lotka, A. J. (1925). *Elements of Physical Biology*. Williams & Wilkins, Baltimore.
- Lu, Z. Q. and Smith, R. L. (1997). Estimating local Lyapunov exponents. In Cutler, C. D. and Kaplan, D. T., editors, *Nonlinear Dynamics and Time Series: Building a Bridge Between the Natural and Statistical Sciences*, volume 110, pages 135–151. American Mathematical Society, Providence, RI.
- Luckinbill, L. S. (1973). Coexistence in laboratory populations of *Paramecium aurelia* and its predator *Didinium nasutum*. *Ecology*, 54:1320–1327.
- Maberly, S. C., Hurley, M. A., Butterwick, C., Corry, J. E., Heaney, S. I., Irish, A. E., et al. (1994). The rise and fall of *Asterionella formosa* in the South Basin of Windermere: analysis of a 45-year series of data. *Freshwater Biology*, 31:19–34.
- Mandelbrot, B. B. and Wallis, J. R. (1969). Some long-run properties of geophysical records. *Water Resources Research*, 5:321–340.
- Mankin, R., Laas, T., Sauga, A., and Ainsaar, A. (2006). Colored-noise-induced hopf bifurcations in predator-prey communities. *Physical Review E*, 74:021101–021101–10.
- Maraun, D. and Kurths, J. (2004). Cross wavelet analysis: significance testing and pitfalls. *Nonlinear Processes in Geophysics*, 11:505–514.
- Marcus, N. H. and Boero, F. (1998). The importance of benthic-pelagic coupling and the forgotten role of life cycles in coastal aquatic systems. *Limnology and Oceanography*, 43:763–768.
- Marwan, N., Romano, M. C., Thiel, M., and Kurths, J. (2007). Recurrence plots for the analysis of complex systems. *Physics Reports-Review Section of Physics Letters*, 438:237–329.

- May, R. M. (1973). *Stability and complexity in model ecosystems*. Princeton University Press, Princeton, NJ.
- May, R. M. (1974). Biological populations with nonoverlapping generations: stable points, stable cycles, and chaos. *Science*, 186:645–647.
- May, R. M. (1976). Simple mathematical models with very complicated dynamics. *Nature*, 261:459–467.
- May, R. M. and Hassell, M. P. (1981). The dynamics of multiparasitoid-host interactions. *American Naturalist*, 117:234–261.
- May, R. M. and Leonard, W. J. (1975). Nonlinear aspects of competition between three species. *SIAM Journal on Applied Mathematics*, 29:243–253.
- McCaffrey, D. F., Ellner, S., Gallant, A. R., and Nychka, D. W. (1992). Estimating the Lyapunov exponent of a chaotic system with nonparametric regression. *Journal of the American Statistical Association*, 87:682–695.
- McCann, K., Hastings, A., and Huxel, G. R. (1998). Weak trophic interactions and the balance of nature. *Nature*, 395:794–798.
- McCann, K. and Yodzis, P. (1994). Biological conditions for chaos in a 3-species food-chain. *Ecology*, 75:561–564.
- McCauley, E. and Murdoch, W. W. (1987). Cyclic and stable populations: plankton as paradigm. *American Naturalist*, 129:97–121.
- McCauley, E., Nelson, W. A., and Nisbet, R. M. (2008). Small-amplitude cycles emerge from stage structured interactions in *Daphnia*-algal systems. *Nature*, 455:1240–1243.
- Ménard, F., Marsac, F., Bellier, E., and Cazelles, B. (2007). Climatic oscillations and tuna catch rates in the Indian Ocean: a wavelet approach to time series analysis. *Fisheries Oceanography*, 16:95–104.
- Mori, M. and Butterworth, D. S. (2006). A first step towards modelling the krill-predator dynamics of the Antarctic ecosystem. *CCAMLR Science*, 13:217–277.
- Müller, H. and Geller, W. (1993). Maximum growth rates of aquatic ciliated protozoa: the dependence on body size and temperature reconsidered. *Archiv für Hydrobiologie*, 126:315–327.
- Murdoch, W. W., Nisbet, R. M., McCauley, E., de Roos, A. M., and Gurney, W. S. C. (1998). Plankton abundance and dynamics across nutrient levels: tests of hypotheses. *Ecology*, 79:1339–1356.

- Nelson, W. A., McCauley, E., and Wrona, F. J. (2005). Stage-structured cycles promote genetic diversity in a predator-prey system of *Daphnia* and algae. *Nature*, 433:413–417.
- Neutel, A. M., Heesterbeek, J. A. P., and de Ruiter, P. C. (2002). Stability in real food webs: weak links in long loops. *Science*, 296:1120–1123.
- Nielsen, T. G., Kiørboe, T., and Bjørnsen, P. K. (1990). Effects of a *Chrysochromulina polylepis* subsurface bloom on the planktonic community. *Marine Ecology Progress Series*, 62:21–35.
- Nisbet, R. M. and Gurney, W. S. C. (1976). A simple mechanism for population cycles. *Nature*, 263:319–320.
- Nychka, D., Ellner, S., Gallant, A. R., and McCaffrey, D. (1992). Finding chaos in noisy systems. *Journal of the Royal Statistical Society Series B-Methodological*, 54:399–426.
- Ohman, M. D. and Snyder, R. A. (1991). Growth kinetics of the omnivorous oligotrich ciliate *Strombidium* sp. *Limnology and Oceanography*, 36:922–935.
- Olsen, L. F. and Schaffer, W. M. (1990). Chaos versus noisy periodicity: alternative hypotheses for childhood epidemics. *Science*, 249:499–504.
- Olsen, L. F., Truty, G. L., and Schaffer, W. M. (1988). Oscillations and chaos in epidemics: a nonlinear dynamic study of six childhood diseases in Copenhagen, Denmark. *Theoretical Population Biology*, 33:344–370.
- Pelletier, J. D. (2002). Natural variability of atmospheric temperatures and geomagnetic intensity over a wide range of time scales. *Proceedings of the National Academy of Sciences USA*, 99:2546–2553.
- Percival, D. B. (1995). On estimation of the wavelet variance. *Biometrika*, 82:619–631.
- Percival, D. B. and Walden, A. T. (1993). *Spectral Analysis for Physical Applications*. Cambridge University Press, Cambridge, UK.
- Petchey, O. L., Gonzalez, A., and Wilson, H. B. (1997). Effects on population persistence: the interaction between environmental noise colour, intraspecific competition and space. *Proceedings of the Royal Society of London B*, 264:1841–1847.
- Petipa, T. S., Monakov, A. V., Pavlyutin, A. P., and Sorokin, Y. I. (1975). Nutrition and energy balance of tropical copepods. *Fisheries and Marine service, Canada, Translation series*, 3382.

- Philippart, C. J. M., Cadée, G. C., van Raaphorst, W., and Riegman, R. (2000). Long-term phytoplankton-nutrient interactions in a shallow coastal sea: algal community structure, nutrient budgets, and denitrification potential. *Limnology and Oceanography*, 45:131–144.
- Philippi, T. E., Carpenter, M. P., Case, T. J., and Gilpin, M. E. (1987). *Drosophila* population dynamics: chaos and extinctions. *Ecology*, 68:154–159.
- Platt, T. and Denman, K. L. (1975). Spectral analysis in ecology. *Annual Review of Ecology and Systematics*, 6:189–210.
- Porter, K. G. and Feig, Y. S. (1980). The use of Dapi for identifying and counting aquatic microflora. *Limnology and Oceanography*, 25:943–948.
- Provenzale, A., Smith, L. A., Vio, R., and Murante, G. (1992). Distinguishing between low-dimensional dynamics and randomness in measured time series. *Physica D*, 58:31–49.
- Raimondo, S., Turcani, M., Patoeka, J., and Liebhold, A. M. (2004). Interspecific synchrony among foliage-feeding forest *Lepidoptera* species and the potential role of generalist predators as synchronizing agents. *Oikos*, 107:462–470.
- Raven, J. A. and Geider, R. J. (1988). Temperature and algal growth. *New Phytologist*, 110:441–461.
- Redfield, A. C. (1958). The biological control of chemical factors in the environment. *American Scientist*, 46:205–221.
- Reynolds, C. S. (2006). *Ecology of phytoplankton*. Cambridge University Press, Cambridge, UK.
- Reynolds, C. S. and Bellinger, E. G. (1992). Patterns of abundance and dominance of the phytoplankton of Rostherne Mere, England: evidence from an 18-year dataset. *Aquatic Sciences*, 54:10–36.
- Reynolds, C. S., Padisák, J., and Sommer, U. (1993). Intermediate disturbance in the ecology of phytoplankton and the maintenance of species diversity. *Hydrobiologia*, 249:183–188.
- Rinaldi, S., Muratori, S., and Kuznetsov, Y. (1993). Multiple attractors, catastrophes and chaos in seasonally perturbed predator-prey communities. *Bulletin of Mathematical Biology*, 55:15–35.
- Ripa, J. and Ives, A. R. (2003). Food web dynamics in correlated and autocorrelated environments. *Theoretical Population Biology*, 64:369–384.

- Rodó, X., Pascual, M., Fuchs, G., and Faruque, S. G. (2002). ENSO and cholera: a nonstationary link related to climate change? *Proceeding of the National Academy of Sciences of the United States of America*, 99:12901–12906.
- Rodriguez, E., George, N., Lachaux, J. P., Martinerie, J., Renault, B., and Varela, F. J. (1999). Perception's shadow: long-distance synchronization of human brain activity. *Nature*, 397:430–433.
- Roe, G. (2009). Feedbacks, timescales and seeing red. *Annual Review of Earth and Planetary Sciences*, 37:93–115.
- Rohde, K. H. and Nehring, D. (1979). Ausgewählte methoden zur bestimmung von inhaltsstoffen im meer- und brackwasser. *Geodatische geophysikalische Veröffentlichungen. Reihe 4.*, 27:1–68.
- Rose, K. A., Swartzman, G. L., Kindig, A. C., and Taub, F. B. (1988). Stepwise iterative calibration of a multi-species phytoplankton-zooplankton simulation model using laboratory data. *Ecological Modelling*, 42:1–32.
- Rosenstein, M. T., Collins, J. J., and De Luca, C. J. (1993). A practical method for calculating largest Lyapunov exponents from small data sets. *Physica D*, 65:117–134.
- Rosenzweig, M. L. (1971). Paradox of enrichment: destabilization of exploitation ecosystems in ecological time. *Science*, 171:385–388.
- Rosenzweig, M. L. and MacArthur, R. H. (1963). Graphical representation and stability conditions of predator-prey interactions. *American Naturalist*, 97:209–223.
- Rothhaupt, K. O. (1990). Differences in particle size-dependent feeding efficiencies of closely related rotifer species. *Limnology and Oceanography*, 35:16–23.
- Roughgarden, J. (1975). A simple model for population dynamics in stochastic environments. *American Naturalist*, 109:713–736.
- Ruokolainen, L., Lindén, A., Kaitala, V., and Fowler, M. S. (2009). Ecological and evolutionary dynamics under coloured environmental variation. *Trends in Ecology and Evolution*, 24:555–563.
- Sauer, T. D., Tempkin, J. A., and Yorke, J. A. (1998). Spurious Lyapunov exponents in attractor reconstruction. *Physical Review Letters*, 81:4341–4344.
- Schaffer, W. M. and Kot, M. (1986). Chaos in ecological systems: the coals that Newcastle forgot. *Trends in Ecology & Evolution*, 1:58–63.

- Schaffer, W. M., Olsen, L. F., Truty, G. L., and Fulmer, S. L. (1990). The case for chaos in childhood epidemics. In Krasner, S., editor, *The Ubiquity of Chaos*, pages 139–167. AAAS, Washington, D.C.
- Scheffer, M. (1991). Should we expect strange attractors behind plankton dynamics and if so, should we bother? *Journal of Plankton Research*, 13:1291–1305.
- Scheffer, M., Bascompte, J., Brock, W. A., Brovkin, V., Carpenter, S. R., Dakos, V., et al. (2009). Early warning signals for critical transitions. *Nature*, 461:53–59.
- Scheffer, M., Carpenter, S., Foley, J. A., Folke, C., and Walker, B. (2001). Catastrophic shifts in ecosystems. *Nature*, 413:591–596.
- Scheffer, M. and Carpenter, S. R. (2003). Catastrophic regime shifts in ecosystems: linking theory to observation. *Trends in Ecology & Evolution*, 18:648–656.
- Scheffer, M. and de Boer, R. J. (1995). Implications of spatial heterogeneity for the paradox of enrichment. *Ecology*, 76:2270–2277.
- Scheffer, M. and Rinaldi, S. (2000). Minimal models of top-down control of phytoplankton. *Freshwater Biology*, 45:265–283.
- Scheffer, M., Rinaldi, S., Huisman, J., and Weissing, F. J. (2003). Why plankton communities have no equilibrium: solutions to the paradox. *Hydrobiologia*, 491:9–18.
- Scheffer, M., Rinaldi, S., Kuznetsov, Y. A., and van Nes, E. H. (1997). Seasonal dynamics of *Daphnia* and algae explained as a periodically forced predator-prey system. *Oikos*, 80:519–532.
- Schnack, S. B., Smetacek, V., von Bodungen, B., and Stegmann, P. (1985). Utilization of phytoplankton by copepods in Antarctic waters during spring. In Siegfried, W. R., Condy, P. R., and Laws, R. M., editors, *Antarctic nutrient cycles and food webs*, pages 65–81. Springer, Berlin.
- Smayda, T. J. (1998). Patterns of variability characterizing marine phytoplankton, with examples from Narragansett Bay. *ICES Journal of Marine Science*, 55:562–573.
- Smetacek, V. and Cloern, J. E. (2008). Oceans: on phytoplankton trends. *Science*, 319:1346–1348.
- Smith, R. H., Daniels, S., Simkiss, K., Bell, E. D., Ellner, S. P., and Forrest, M. B. (2000). Blowflies as a case study in non-linear population dynamics. In Perry, J. N., Smith, R. H., Woiwod, I. P., and Morse, D. R., editors, *Chaos in Real Data: Analysis of Non-linear Dynamics from Short Ecological Time Series*, pages 137–172. Kluwer Academic Publishers, Dordrecht, NL.

- Sokal, R. R. and Rohlf, F. J. (1995). *Biometry*. Freeman, New York, 3rd edition.
- Solomon, S., Qin, D., Manning, M., Marquis, M., Averyt, K., Tignor, M. M. B., et al. (2007). *Climate Change 2007: The Physical Science Basis. Contribution of Working Group I to the Fourth Assessment Report of the Intergovernmental Panel on Climate Change*. Cambridge University Press, Cambridge, UK.
- Sommer, U. (1995). An experimental test of the intermediate disturbance hypothesis using cultures of marine phytoplankton. *Limnology and Oceanography*, 40:1271–1277.
- Sommer, U., Gliwicz, Z. M., Lampert, W., and Duncan, A. (1986). The PEG-model of seasonal succession of planktonic events in fresh waters. *Archiv für Hydrobiologie*, 106:433–471.
- Sprott, J. C. (2003). *Chaos and Time Series Analysis*. Oxford University Press, Oxford, UK.
- Steele, J. H. (1985). A comparison of terrestrial and marine ecological systems. *Nature*, 313:355–358.
- Steele, J. H. and Henderson, E. W. (1994). Coupling between physical and biological scales. *Philosophical Transactions of the Royal Society B*, 343:5–9.
- Steffen, E., Malchow, H., and Medvinsky, A. B. (1997). Effects of seasonal perturbations on a model plankton community. *Environmental Modeling & Assessment*, 2:43–48.
- Stemberger, R. (1987). The potential for population growth of *Ascomorpha ecaudis*. *Hydrobiologia*, 147:297–301.
- Stenseth, N. C. (1999). Population cycles in voles and lemmings: density dependence and phase dependence in a stochastic world. *Oikos*, 87:427–461.
- Stenseth, N. C., Falck, W., Bjørnstad, O. N., and Krebs, C. J. (1997). Population regulation in snowshoe hare and Canadian lynx: asymmetric food web configurations between hare and lynx. *Proceeding of the National Academy of Sciences of the United States of America*, 94:5147–5152.
- Stoecker, D., Davis, L. H., and Provan, A. (1983). Growth of *Favella* sp. (Ciliata: Tintinnina) and other microzooplankters in cages incubated in situ and comparison to growth in vitro. *Marine Biology*, 75:293–302.
- Stomp, M., van Dijk, M. A., van Overzee, H. M. J., Wortel, M. T., Sigon, C. A. M., Egas, M., et al. (2008). The time scale of phenotypic plasticity, and its impact on competition in fluctuating environments. *American Naturalist*, 172:E169–E185.

- Straile, D. (2000). Meteorological forcing of plankton dynamics in a large and deep continental European lake. *Oecologia*, 122:44–50.
- Strogatz, S. H. (1994). *Nonlinear Dynamics and Chaos: With Applications to Physics, Biology, Chemistry, and Engineering*. Perseus, Cambridge, MA.
- Strogatz, S. H. and Stewart, I. (1993). Coupled oscillators and biological synchronization. *Scientific American*, 269:102–109.
- Sugihara, G. and May, R. M. (1990). Nonlinear forecasting as a way of distinguishing chaos from measurement error in time-series. *Nature*, 344:734–741.
- Takens, F. (1981). Detecting strange attractors in turbulence. In Rand, D. A. and Young, L. S., editors, *Lecture Notes in Mathematics*, volume 898, pages 366–381. Springer, Berlin.
- Talling, J. F. (1993). Comparative seasonal changes, and interannual variability and stability, in a 26-year record of total phytoplankton biomass in four English lake basins. *Hydrobiologia*, 268:65–98.
- Tanabe, K. and Namba, T. (2005). Omnivory creates chaos in simple food web models. *Ecology*, 86:3411–3414.
- Theiler, J. (1986). Spurious dimension from correlation algorithms applied to limited time-series data. *Physical Review A*, 34:2427–2432.
- Thingstad, T. F. (2000). Elements of a theory for the mechanisms controlling abundance, diversity, and biogeochemical role of lytic bacterial viruses in aquatic systems. *Limnology and Oceanography*, 45:1320–1328.
- Thingstad, T. F. and Lignell, R. (1997). Theoretical models for the control of bacterial growth rate, abundance, diversity and carbon demand. *Aquatic Microbial Ecology*, 13:19–27.
- Tilman, D. (1977). Resource competition between planktonic algae: an experimental and theoretical approach. *Ecology*, 58:338–348.
- Torrence, C. and Compo, G. P. (1998). A practical guide to wavelet analysis. *Bulletin of the American Meteorological Society*, 79:61–78.
- Torrence, C. and Webster, P. J. (1999). Interdecadal changes in the ENSO-monsoon system. *Journal of Climate*, 12:2679–2690.
- Turchin, P. (1993). Chaos and stability in rodent population dynamics: evidence from non-linear time-series analysis. *Oikos*, 68:167–172.
- Turchin, P. (1995). Chaos in microtine populations. *Proceedings of the Royal Society of London B*, 262:357–361.

-
- Turchin, P. (2003). *Complex Population Dynamics: A Theoretical/Empirical Synthesis*. Princeton University Press, Princeton.
- Turchin, P. and Taylor, A. D. (1992). Complex dynamics in ecological time series. *Ecology*, 73:289–305.
- Valdés, L., López-Urrutia, A., Cabal, J., Alvarez-Ossorio, M., Bode, A., Miranda, A., et al. (2007). A decade of sampling in the bay of biscay: what are the zooplankton time series telling us? *Progress in Oceanography*, 74:98–114.
- van Nes, E. H. and Scheffer, M. (2004). Large species shifts triggered by small forces. *American Naturalist*, 164:255–266.
- Vandermeer, J. (1993). Loose coupling of predator-prey cycles: entrainment, chaos, and intermittency in the classic MacArthur consumer-resource equations. *American Naturalist*, 141:687–716.
- Vandermeer, J. (2004). Coupled oscillations in food webs: balancing competition and mutualism in simple ecological models. *American Naturalist*, 163:857–867.
- Vandermeer, J. (2006). Oscillating populations and biodiversity maintenance. *BioScience*, 56:967–975.
- Vandermeer, J., Stone, L., and Blasius, B. (2001). Categories of chaos and fractal basin boundaries in forced predator-prey models. *Chaos Solitons & Fractals*, 12:265–276.
- Vasseur, D. A. (2007). Populations embedded in trophic communities respond differently to coloured environmental noise. *Theoretical Population Biology*, 72:186–196.
- Vasseur, D. A. and Fox, J. W. (2007). Environmental fluctuations can synchronize food web dynamics by increasing synchrony. *Ecology Letters*, Ecology Letters:1066–1074.
- Venter, J. C., Remington, K., Heidelberg, J. F., Halpern, A. L., Rusch, D., Eisen, J. A., et al. (2004). Environmental genome shotgun sequencing of the Sargasso Sea. *Science*, 304:66–74.
- Volterra, V. (1926). Fluctuations in the abundance of a species considered mathematically. *Nature*, 118:558–600.
- von Storch, H. and Zwiers, F. W. (2003). *Statistical Analysis in Climate Research*. Cambridge University Press, Cambridge.
- Vos, M., Kooij, B. W., DeAngelis, D. L., and Mooij, W. M. (2004). Inducible defences and the paradox of enrichment. *Oikos*, 105:471–480.

- Welch, P. D. (1967). The use of Fast Fourier Transform for the estimation of power spectra: A method based on time averaging over short, modified periodograms. *IEEE Transactions on Audio and Electroacoustics*, AU-15:70–73.
- Weyhenmeyer, G. A., Blenckner, T., and Petterson, K. (1999). Changes of the plankton spring outburst related to the North Atlantic Oscillation. *Limnology and Oceanography*, 44:1788–1792.
- Wigley, T. M. L., Smith, R. L., and Santer, B. D. (1998). Anthropogenic influence on the autocorrelation structure of hemispheric-mean temperatures. *Science*, 282:1676–1679.
- Wolda, H. (1988). Insect seasonality: why? *Annual Review of Ecology and Systematics*, 19:1–18.
- Wolf, A., Swift, J. B., Swinney, H. L., and Vastano, J. A. (1985). Determining Lyapunov exponents from a time-series. *Physica D*, 16:285–317.
- Wood, S. N. (2006). *Generalized Additive Models: An Introduction with R*. Chapman and Hall/CRC, Boca Raton, FL.
- Xu, C. and Li, Z. (2002). Populations response to environmental noise: the influence of food web structure. *Ecological Modelling*, 154:193–202.
- Xu, C. and Li, Z. (2003). Population dynamics and the color of environmental noise: a study on a three-species food chain system. *Ecological Research*, 18:145–154.
- Yodzis, P. and Innes, S. (1992). Body size and consumer-resource dynamics. *American Naturalist*, 139:1151–1175.
- Yoshida, T., Jones, L. E., Ellner, S. P., Fussmann, G. F., and Hairston, N. G., Jr. (2003). Rapid evolution drives ecological dynamics in a predator-prey system. *Nature*, 424:303–306.
- Zimmer, C. (1999). Life after chaos. *Science*, 284:83–86.

Summary

Species often show irregular fluctuations in their population abundances. Traditionally, ecologists have thought that external processes (e.g., variability in weather conditions) are the main drivers of these ups and downs. However, recent theoretical work suggests that fluctuations in natural populations may also be driven by internal mechanisms (e.g., the interplay between species). In this thesis I use a combination of time series analysis and modeling to provide more insight into the question to which extent such internally generated chaos might drive the population dynamics of plankton communities under controlled as well as natural conditions.

In **chapter 2** we present a time series analysis of a long-term experiment with a marine plankton community isolated from the Baltic Sea and studied under constant laboratory conditions for nearly 8 years by Dr. Reinhard Heerkloss. The food web consisted of bacteria, several phytoplankton species, herbivorous and predatory zooplankton species and detritivores. Despite constant laboratory conditions, the species abundances showed striking fluctuations over several orders of magnitude. We analysed the dynamics of this complex food web using various statistical techniques. The population dynamics were characterized by positive Lyapunov exponents (the hallmark of chaos) of similar magnitude for each species. Predictability of the species abundances was limited to 15-30 days, only slightly longer than the predictability horizon of the local weather forecast. These results provide the first experimental demonstration of chaos in a complex food web.

Although **chapter 2** shows that the dynamics of the experimental plankton community were caused by internal mechanisms, the approach followed there does not allow identification of the mechanisms driving the chaotic fluctuations. To address this issue we therefore analyzed the experimental time series by means of wavelet and cross-wavelet analysis (**chapter 3**). The analysis revealed that the species fluctuations are dominated by two predator-prey cycles that fluctuated largely in anti-phase. According to theory, such phase differences between the species point at strong competition between the prey species, and little prey overlap among the predators. This finding is consistent with the size structure of the plankton community. Thus, it seems likely that the chaotic dynamics in this experimental food web are caused by the interplay between two predator-prey oscillations.

In **chapter 4** we address the question whether seasonal variation in environmental conditions might suppress chaos in natural communities. For this purpose, we investigated a predator-prey model consisting of multiple phytoplankton and zoo-

plankton species in a seasonal environment. Interestingly, seasonality increased the probability of chaos, but the population dynamics had a somewhat peculiar character as the species fluctuations were locked within the seasonal cycle. On a closer look, the species composition and succession differed profoundly between subsequent years. This suggests that interannual variability in species composition could be an intrinsic property of multi-species communities that does not require year-to-year differences in the weather.

In addition to the regular seasonal cycle, real ecosystems are also subject to stochastic environmental variation such as day-to-day variability in temperature. In **chapter 5** we use a simple predator-prey model to examine how plankton dynamics might respond to such environmental stochasticity. Fluctuations in environmental factors, such as the water temperature of lakes and oceans, can be described by “red noise” when fluctuations are temporally correlated (i.e., the temperature of today resembles that of yesterday). In line with previous work our results show that the effect of red noise is particularly large if the predator-prey system is on the edge of stability. In this case, small temperature fluctuations are magnified by the intrinsic oscillatory nature of the predator-prey interaction. The magnitude of this resonance effect depends critically on the characteristic time scale of the environmental fluctuations relative to that of the predator-prey oscillations. Specifically we show that systems with an intrinsic tendency to oscillate with a period of T are particularly sensitive to environmental noise with a time scale of $t = \frac{T}{2\pi}$. Strikingly, temperature data from lakes and marine systems show that the characteristic time scales of natural temperature fluctuations fall largely within the range to which plankton communities should be most sensitive.

In conclusion, this thesis demonstrates in theory and experiment that species in plankton communities may rise and fall forever in a chaotic way. This implies that short-term predictions of species abundances will be feasible, but long-term prediction is limited. We can at best indicate within which bounds species will fluctuate. Given that many other food webs are structurally similar to our plankton food web it is tempting to speculate that other ecosystems could behave chaotically as well. Our results challenge the traditional view that nature is at equilibrium and that only externally driven processes may disturb this equilibrium. I hope that this thesis will contribute to a better understanding of the species fluctuations in nature, and will stimulate future investigations of complex dynamics in other ecosystems.

Samenvatting

Hoewel vaak wordt gerefereerd naar het ‘natuurlijk evenwicht’, blijken de dichtheden van veel soorten in de natuur juist erg variabel. Sommige jaren nemen soorten toe, en in andere jaren nemen ze weer af. Veel ecologen beschouwen externe processen zoals variaties in de weersomstandigheden als verklaring voor deze schommelingen in aantallen. Uit recent theoretisch werk is echter gebleken dat ook intrinsieke natuurlijke processen, zoals de interacties tussen soorten, verantwoordelijk kunnen zijn voor zulke fluctuaties. Interessant is dat in wiskundige modellen die dit gedrag vertonen, het onregelmatige aantalsverloop extreem gevoelig kan zijn voor kleine variaties. We noemen dit verschijnsel “deterministische chaos”. Onder ecologen is nog altijd veel discussie over de vraag of deterministische chaos in echte ecosystemen van belang kan zijn. Dit proefschrift probeert op deze kwestie een antwoord te geven, door studie van de aantalschommelingen in het plankton.

In **hoofdstuk 2** analyseren we de gegevens van een experiment, uitgevoerd door Dr. Reinhard Heerkloss, waarin plankton werd gesoleerd uit de Oostzee en in het laboratorium gedurende bijna 8 jaar is gevolgd. Het onderzochte voedselweb bestond uit vele soorten bacteriën, fytoplankton, herbivore zoöplanktonsoorten, carnivore zoöplanktonsoorten en detritivoren. Ondanks de constante laboratorium condities fluctueerden de aantallen van deze soorten voortdurend. De fluctuaties werden gekarakteriseerd door positieve Lyapunov exponenten, een overtuigend bewijs voor chaos. Uit de analyse kwam naar voren dat de voorspelbaarheid van het plankton maximaal 15-30 dagen is, niet veel beter dus dan de lokale weersvoorspelling. Dit is de eerste keer dat chaos is aangetoond in een complex voedselweb.

Deze bevinding brengt ons naar de volgende vraag: wat zouden de onderliggende mechanismen kunnen zijn die deze chaotische dynamiek veroorzaken? Om deze vraag te beantwoorden, analyseerden we de fluctuaties in het plankton experiment door middel van wavelet en cross-wavelet analyse (**hoofdstuk 3**). Uit deze analyse kwamen twee dominante predator-prooi cycli naar voren die grotendeels in anti-fase waren. Volgens wiskundige modellen duidt zo’n faseverschil op een sterke concurrentie tussen de prooi-soorten en weinig voedseloverlap van de predatoren. Deze conclusie is in overeenstemming met de grootteverdeling van de planktonsoorten in het experiment. Met andere woorden, het lijkt er op dat het chaotisch gedrag in dit experimentele voedselweb wordt veroorzaakt door de interactie tussen twee predator-prooi systemen die tegen elkaar in fluctueren.

Nu zou het in principe zo kunnen zijn dat in echte ecosystemen de seizoenveran-

deringen zulke chaos teniet kunnen doen. Om het effect van seizoenen op chaos te onderzoeken, hebben we een predator-prooi model met meerdere soorten fytoplankton en zoöplankton blootgesteld aan regelmatige seizoensvariaties (**hoofdstuk 4**). Bij een sterke seizoensdynamiek verdween de chaos niet; integendeel de regelmatige seizoenscycli verhoogden de kans op chaos juist. Wel veranderde de vorm van de fluctuaties doordat de seizoenscyclus de populatieschommelingen als het ware samenknijpt in de winter en uitvergroot in de zomer. Opvallend in de simulaties is dat in opeenvolgende jaren verschillende soorten elkaar afwisselen. Dat suggereert dat jaarlijkse verschillen in soortensamenstelling door interne processen verklaard kunnen worden en dus niet altijd hoeven samen te hangen met jaarlijkse variaties in weersomstandigheden.

Echte ecosystemen staan niet alleen bloot aan seizoensvariatie, maar ook aan stochastische variatie in omgevingsfactoren zoals temperatuur die door het dagelijkse weer worden bepaald. In **hoofdstuk 5** onderzoeken we wat daarvan het effect zou kunnen zijn op een eenvoudig fytoplankton-zooplankton model. Natuurlijke temperatuurschommelingen kunnen worden beschreven als “rode ruis”; dagelijkse schommelingen die in de tijd gecorreleerd zijn (de temperatuur van vandaag lijkt op die van gisteren). We onderzochten vooral de invloed van zulke ruis op het predator-prooi model als het evenwicht nog net stabiel is en de soorten na een verstoring via gedempte oscillaties naar dit evenwicht terug keren. In zo'n systeem kunnen lichte temperatuurfluctuaties verrassend versterkt worden door de interne dynamiek van de predator-prooi interactie en leiden tot relatief grote schommelingen in de populaties. Zoals eerdere werk aangetoond heeft, is de grootte van deze resonantie sterk afhankelijk van de karakteristieke tijdschaal van de omgevingsfluctuaties in relatie tot de eigen tijdschaal van het predator-prooi systeem. Specifiek vinden we dat systemen die een intrinsieke neiging hebben te oscilleren met een bepaalde periode T het gevoeligst zijn voor milieufunctuaties met een tijdschaal van $t = \frac{T}{2\pi}$. Een analyse van temperatuurmetingen in meren en oceanen toont aan dat de karakteristieke tijdschalen van temperatuurfluctuaties grotendeels binnen het bereik vallen waarvoor planktongemeenschappen het gevoeligst zijn.

Samenvattend heb ik in dit proefschrift met een combinatie van wiskundige modellen en experimentele gegevens aangetoond dat soorten in planktongemeenschappen op een chaotische manier kunnen stijgen en dalen. Dit betekent dat korte-termijn voorspellingen mogelijk zijn, maar dat lange-termijn voorspelling van de abundanties van soorten beperkt is en we op zijn best kunnen aangeven binnen welke grenzen soorten zullen fluctueren. Omdat het voedselweb in andere ecosystemen vaak min of meer dezelfde structuur heeft als in onze planktongemeenschap is het verleidelijk om te speculeren dat soorten in andere ecosystemen zich ook chaotisch kunnen gedragen. Deze resultaten maken een einde aan de traditionele opvatting dat de natuur ‘in evenwicht’ is en dat alleen externe processen dit evenwicht kunnen verstoren. Ik hoop dat dit werk een belangrijke stimulans zal zijn voor een beter begrip van de complexe fluctuaties van soorten in ecosystemen.

Sommario

Spesso in natura le specie variano nel loro numero in modo irregolare. Per molto tempo gli ecologi hanno attribuito a processi esterni (come ad esempio alla variabilità delle condizioni meteorologiche) la principale causa di queste fluttuazioni. Recentemente, i risultati emersi da studi teorici hanno aperto la strada all'idea che le irregolari fluttuazioni nel numero delle specie possano anche essere attribuite a meccanismi interni (ad esempio, a meccanismi di interazione tra le specie come competizione e predazione). In questa tesi attraverso l'analisi di serie temporali e all'uso di semplici modelli viene investigata l'ipotesi che le interazioni tra le specie possano generare dinamiche caotiche nelle popolazioni di plancton.

Nel **capitolo 2** viene presentata un'analisi di serie temporali, applicata ai dati risultanti da un esperimento condotto su una comunità marina di plancton. Questa comunità marina planctonica è stata isolata dal Mar Baltico e mantenuta a condizioni esterne costanti in un mesocosmo per circa 8 anni, dal Dr. Reinhard Heerkloss. La catena alimentare di questa comunità planctonica è costituita da batteri, diverse specie di fitoplancton, zooplancton erbivoro e carnivoro e specie detritivore. Nonostante le condizioni costanti di laboratorio, le specie fluttuavano in modo irregolare esibendo oscillazioni di parecchi ordini di grandezza. Diverse tecniche statistiche sono state applicate con lo scopo di caratterizzare le dinamiche planctoniche. In particolare si è osservato che tutte le specie nella catena alimentare erano caratterizzate da un esponente di Lyapunov positivo (indice della caoticità delle dinamiche di un sistema). Inoltre si è visto che l'andamento delle specie poteva essere previsto per un periodo compreso tra i 15 e i 30 giorni, un tempo leggermente più alto delle previsioni del tempo locali. Questi risultati rappresentano la prima prova sperimentale della presenza di caos nelle dinamiche di una catena alimentare complessa.

Nonostante nel **capitolo 2** sia stato mostrato come meccanismi di interazione tra le specie fossero alla base delle dinamiche di una comunità planctonica sperimentale, l'approccio seguito non aveva permesso di identificare quali precisamente fossero questi meccanismi. Per rispondere a questa domanda sono state applicate tecniche di analisi wavelet e cross-wavelet (**capitolo 3**). Da queste analisi è risultato che le fluttuazioni delle specie fossero causate da due cicli preda-predatore, che oscillavano in gran parte in anti-fase. Secondo studi teorici questa differenza fasica indica la presenza di un forte meccanismo di competizione tra le due specie di fitoplancton e un debole meccanismo di competizione tra le due specie di zooplancton. Questo risultato è in pieno accordo con le dimensioni e le preferenze alimentari delle specie di

plancton presenti nella nostra catena alimentare. Quindi sembra altamente probabile che le dinamiche caotiche osservate in questa catena alimentare sperimentale siano generate dall'interazione di queste due oscillazioni preda-predatore.

Nel **capitolo 4** viene investigata la possibilità che le variazioni stagionali nelle condizioni ambientali possano sopprimere il caos nelle comunità planctoniche naturali. A questo scopo è stato studiato un modello preda-predatore costituito da svariate specie di fitoplancton e zooplancton in interazione tra di loro e sottoposte a condizioni ambientali variabili stagionalmente. I risultati delle simulazioni effettuate usando il modello sopra descritto hanno mostrato che le variazioni ambientali stagionali aumentano la probabilità di osservare dinamiche caotiche nel plancton, ma che le dinamiche di popolazione hanno la peculiare caratteristica di seguire un ciclo stagionale. Guardando attentamente si osserva però che la composizione e la successione delle specie presentano delle notevoli variazioni annuali. Questo risultato ha delle conseguenze molto importanti perché suggerisce che il variare delle specie di anno in anno possa essere una caratteristica intrinseca delle comunità caratterizzate dalla presenza di molte specie e che non richieda in linea di principio il variare di anno in anno delle condizioni meteorologiche.

Tuttavia, in aggiunta alle regolari variazioni stagionali, gli ecosistemi sono sottoposti anche a variazioni ambientali stocastiche come ad esempio a variazioni giornaliere di temperatura. Nel **capitolo 5** viene utilizzato un semplice modello preda-predatore con lo scopo di esaminare come e in che misura le dinamiche planctoniche rispondano a questa stocasticità nelle condizioni ambientali. Fluttuazioni nelle condizioni ambientali, come ad esempio nella temperatura dell'acqua di laghi e oceani, può essere descritta come "red noise", nel caso in cui queste fluttuazioni siano correlate temporalmente. In linea con il nostro lavoro precedente, i risultati ottenuti dall'applicazione di questo modello mostrano che il "red noise" ha un effetto particolarmente forte nel caso in cui le dinamiche preda-predatore siano al limite della stabilità. In questa situazione, anche minime fluttuazioni di temperatura sono amplificate dalla intrinseca natura oscillatoria delle interazioni tra predatore e preda. Nello specifico questo studio dimostra che sistemi che hanno un'intrinseca tendenza ad oscillare con un certo periodo T sono particolarmente sensibili a fluttuazioni ambientali stocastiche caratterizzate da una scala temporale uguale a $t = \frac{T}{2\pi}$. In aggiunta, ulteriori analisi statistiche applicate a dati di temperatura dell'acqua di diversi laghi e oceani dimostrano che le caratteristiche scale temporali delle fluttuazioni di temperatura osservate in natura corrispondono ampiamente al range di valori in cui le comunità di plancton mostrano di essere maggiormente sensibili.

In conclusione, questa tesi dimostra sia dal punto di vista teorico che da quello sperimentale, che le specie planctoniche possono fluttuare in modo caotico. Questo comporta la possibilità di predire le dinamiche planctoniche per un corto intervallo di tempo, ma l'impossibilità di poter fare previsioni a lungo termine: è possibile infatti indicare solamente entro quali limiti le specie fluttueranno. Tenuto conto che molte altre catene alimentari hanno una struttura simile alla nostra catena alimentare planctonica è molto allettante ipotizzare che altri ecosistemi possano esibire delle

dinamiche caotiche. I risultati presentati in questa tesi hanno conseguenze molto importanti perchè mettono in crisi la tradizionale idea che la natura sia in equilibrio e che solamente processi esterni siano in grado di spostarla da questo equilibrio. Spero che questa tesi abbia fatto un po' di luce sul complicato tema delle fluttuazioni delle specie in natura e che possa stimolare future ricerche indirizzate allo studio delle complesse dinamiche di popolazione in altri ecosistemi.

Acknowledgments

It seems still incredible to me that I'm finally at the stage of writing my last pages of my PhD thesis. Looking back at the many years spent on this project I feel the need to thank many people that helped me in many ways to reach this achievement.

First I would like to thank my two supervisors Jef Huisman and Marten Scheffer: for me it has been a wonderful opportunity to have the possibility to work with such good scientists. Jef, you have been a great supervisor: thanks for your guidance and your crucial help during the entire period of my PhD, for the very stimulating scientific discussions and the very valuable advices. I have learned a lot from you and I'm very proud of all the publications we have done together. Marten, thanks for your guidance and your help in many phases of my PhD. I always enjoyed your ability of building bridges between different scientific, artistic and social disciplines and your way of explaining things. In moments while I was confused, it was enough discussing with you in the "Pensatorium" with a good cup of Gaggia espresso and everything was clear again!

Next, I would like to thank my two co-supervisors: Klaus Jöhnk and Egbert van Nes. Klaus (my scientific guru), your help was really essential especially in the first phase of my PhD thesis. Your door was always open for me: even in moments when you were clearly busy, you always found the time for discussions and for helping me with the analysis. Thanks also for the big support you gave to me in the difficult situations: a cup of (sometimes too light) coffee and a couple of Lebkuchen were always ready for cheering me up! An other special thank is for Egbert, for the always interesting scientific discussions and for the precious help with programming.

A big part of this thesis would have never existed without the fundamental work of Reinhard Heerkloss. Reinhard, you ran a mesocosm experiment for more than eight years and you patiently counted twice a week the abundances of species present in there. This is really exceptional and I'm so grateful to you that I could work with your data. Thanks and I wish you all the best.

An other special thank goes to Prof. Steve Ellner for his crucial help in part of the analysis performed in this thesis. Steve, having the possibility to collaborate with you and to learn from you was a great opportunity for me.

I would also like to acknowledge Wolf Mooij and Lisette de Senerpont Domis: although the project we started took a different direction than in the original plans, thanks for the interesting and stimulating work meetings.

I would then like to thank my paranymphs Olja and Vasilis for sharing with me this important day. Olja, thanks to both you and Hans for the help and the big support, for taking care of my kids and for always coming to Amsterdam because I was too stressed and tired to move. In other words: thanks for your friendship! Vasilis working with you with you was a very pleasant experience: our conversations, scientific and not, and your very Mediterranean way to do, always made me feel at home. I'm real glad that our project that was supposed to be ready in one year, ended up, though after three years, as a very nice publication. We had some difficult time then, but with mutual help we overcame the obstacles. Thanks!

In the years of my PhD I had a great time, thanks to the always nice atmosphere created by my colleagues at the Aquatic Microbiology Group in Amsterdam. Thanks to Anouk, Barbara, Corrien, Fleur, Hans, Jolanda, Joost, Michael, Pascale, Pedro, Petra, Pieter, Suzanne, Vladimir. In particular, I would like to thank Maayke ("my twin") with whom I shared my office room for four years. I enjoyed a lot the time we spent together and in particular I still remember with big pleasure our trip in Michigan, Wisconsin and Illinois: we had a lot of fun! Next I would like to thank Verena for the big support in the difficult moments. We shared many things but the most important was for sure being pregnant at the same time. Thanks also to Anouk, Jolanda and Petra for the always "gezellige" coffee moments. A big thank is also for Pedro: you have been my first student and really a good one. The work you started ended up as a very nice publication, you can really be proud of it! A special thank goes also to Michael (my new room mate!), for the interesting conversations and for helping me with L^AT_EX. Thanks also to Hans for the very useful advices and the suggestions concerning the printing of the thesis.

I would also like to thank former people who worked or studied at the Aquatic Microbiology Group in Amsterdam: Dedmer, Edwin, Eneas, Floris, Linda, Jutta, Martina, Michele, Miriam, Natasha, Nona, Suzanne. Among these a special thank is for Dedmer with whom I always had a lot of fun. Dedmer, your enthusiasm and your cheerful smile always made me feel happy. In particular I enjoyed so much our trip in New Foundland: thanks for all your support in that difficult journey on the boat and sorry for not believing you when you said that you saw a moose!

A big thank is also for the people of the Aquatic Ecology and Water Quality Management Group in Wageningen: Andrea, Annalies, Bart, Betania, Edwin, Giselle, Ingrid, Jeroen, John, Marijke, Miquel, Nika, Sarian. I know, I didn't come very often to Wageningen in these years and I could almost never take part in your social activities, but thanks anyway for having always involved me.

During the years spent at the UvA I met many other people that I would like to thank. In particular Petra, that together with Olja was a constant weekly appointment for the mommy's lunch breaks and the Italian friends working at the UvA with whom I shared many "pranzi and pause caffè": Filippo, Mauro, Alessandro e Fabrizio. Mauro, finalmente la storia di "Addolorato" sta per avere una fine anche per me! Filippo, mi dispiace moltissimo che tu non possa essere qui a Dicembre, ma ti auguro Buona Fortuna in Cina!

Hartelijk dank aan mijn Apeldoornse guru Michiel. Jij was èèn van de eerste personen die ik leerde kennen toen ik in Nederland kwam. Ik heb met jou zes maanden op dezelfde kantoor gezeten en dat was erg leuk! “Prima stukje!”.

Ik wil ook Frans Pieter nog bedanken voor een hele avond L^AT_EX problemen oplossen.

Haartelijk dank ook aan mijn schoonouders en schoonzusjes voor de steun. Klaas bedankt voor jouw suggesties: ik vond het altijd erg leuk om met jou te praten.

Un ringraziamento va anche a Massimo per avermi aiutato com la traduzione. Un altro ringraziamento è per Koen per avermi aiutato quando sono venuta in Olanda e per aver tradotto pagine e pagine di noiosissima legislatura italiana. Grazie anche anche a Elena per aver sopportato più volte l’argomento “Dottorato”.

Grazie anche a tutti i miei amici in Italia che mi sono venuti a trovare qui in Olanda e a tutti quelli che ci sono sempre quando torno a Genova. In particolare, grazie Simo per aver “scrupolosamente” controllato la mia frase latina!

Un ringraziamento speciale va poi ai miei genitori e ai miei nonni, che mi hanno sempre capito, sostenuto e incitato ad andare avanti. Se sono arrivata a questo punto è anche grazie a voi che mi avete sempre dato la forza per affrontare le difficoltà che mi si sono presentate. Grazie anche per essere venuti innumerevoli volte dall’Italia a tenere i miei bambini e avermi permesso così di partecipare a simposi e conferenze. Un enorme grazie va anche alla mia sorellina Erica: che ha affrontato un lunghissimo viaggio dal Giappone per poter essere presente al mio dottorato.

Un enorme grazie va a Guido e ai miei bambini, Alessio e Aurora, che hanno dovuto sopportare una mamma spesso assente. Grazie Guido per avermi sempre sostenuta, incoraggiata e aiutata: se sono riuscita in questa impresa lo devo in gran parte anche a te. Nell’ultimo anno hai dovuto sentire molte volte i miei “Sorry, Ik ben laat”, o “Sorry, Ik moet werken” e non ti sei mai lamentato. Nog bedankt!